Analysis of the central carbon metabolism of the unicellular cyanobacterium *Synechocystis* sp. PCC 6803 in photomixotrophic and heterotrophic growth mode using ^{13}C metabolic flux analysis

Dissertation

zur Erlangung des Grades

des Doktors der Ingenieurwissenschaft

der Naturwissenschaftlich-Technischen Fakultät

der Universität des Saarlandes

von

Dennis Schulze

Saarbrücken

2021

Tag des Kolloquiums:	14.04.2022
Dekan:	Prof. Dr. Jörn Erik Walter
Berichterstatter:	Prof. Dr. Christoph Wittmann
	Prof. Dr. Elmar Heinzle
Vorsitz:	Prof. Dr. Uli Kazmaier
Akad. Mitglied:	Dr. Ruth Kiefer

Summary

Cyanobacteria are a promising host for sustainable production of a wide variety of biotechnological products. One of these specimens is the unicellular cyanobacterium *Synechocystis* sp. PCC 6803 that has been extensively studied and became a model organism for photosynthesis. Recently two novel pathways have been identified: Gens for two phosphoketolases and the Entner-Doudoroff pathway (ED).

Resolution of the core metabolism of *Synechocystis* sp. PCC 6803 was encumbered by model topology and the unique demands for cultivation techniques. Identification of optimum tracer and analysis setups for generation of a data basis with sufficient resolution power was achieved by *in silico* experiments and aided by detailed analysis of cultivation methods.

All optimization efforts were finalised in complete and precise resolution of the core metabolism of *Synechocystis* sp. PCC 6803 under photomixotrophic and heterotrophic growth regime. Photomixotrophic growth is dominated by high Calvin-Benson-Basham cycle activity that is boosted with glucose from medium, whereas heterotrophic metabolism is dominated by the oxidative branch of the pentose phosphate pathway. Tricarboxylic acid cycle was providing biomass building blocks in both growth modes. Novel pathways were found inactive during both tested conditions. This work demonstrated the impact of cultivation parameters and experimental setup on physiology.

Zusammenfassung

Cyanobakterien sind eine vielversprechende Gruppe von Organismen, die für eine diverse Palette biotechnologischer Produkte genutzt werden könnten. Kürzlich wurden zwei neue Stoffwechselwege identifiziert: Zwei Phosphoketolasen und der Entner-Doudoroff-Weg.

Die Auflösung des Zentralstoffwechsels wurde maßgebliche durch die einzigartigen Anforderungen an Kultivierungsmethoden und Modellierung erschwert. Detaillierte Analyse der Kultivierungssystemen und *in silico* basiertes experimentelles Design hat schlussendlich ermöglicht qualitativ hochwertige Markierungsdaten für metabolischen Steady-State zu generieren.

Alle Optimierungs-Anstrengungen erlaubten die detaillierte Auflösung des Zentralstoffwechsel von *Synechocystis* sp. PCC 6803 unter photomixotrophen und heterotrophen Wachstumsbedingungen. Dabei war photomixotrophischer Metabolismus vom Calvin-Benson-Basham-Zyklus dominiert, in den Glucose aus dem Medium als zusätzliches Substrat eingeflossen ist. Unter heterotrophen Bedingungen war vor allem der oxidative Teil des Pentosephosphatweg aktiv. Unter beiden Bedingungen stellte der Tricarbonsäurezyklus Biomasse-Bausteine bereit. Neue Stoffwechselwege waren inaktiv, unabhängig vom Wachstumsregime. Diese Arbeit demonstriert den Einfluss von Kultivierungsparametern auf die Physiologie von Mikroorganismen.

Partial results of this work have been published in advance. This was authorised by the Institute of Systems Biotechnology of the Saarland University by Prof. Dr. Christoph Wittmann.

Peer reviewed journals

- GC/MS-based ^{13}C metabolic flux analysis resolves the parallel and cyclic photomixotrophic metabolism of *Synechocystis* sp. PCC 6803 and selected deletion mutants including the Entner-Doudoroff and phosphoketolase pathways. Schulze *et al.*; Microb Cell Fact 21, 69 (2022). doi.org/10.1186/s12934-022-01790-9
- Glycolytic Shunts Replenish the Calvin-Benson-Bassham Cycle as Anaplerotic Reactions in Cyanobacteria. Makowka *et al.*; Mol Plant. 2020 Mar 2;13(3):471-482. doi:10.1016/j.molp.2020.02.002. 2

Conference contributions

- Metabolic network analysis of the unicellular cyanobacterium *Synechocystis* sp. PCC 6803 using ^{13}C isotope experiments; Poster presentation; “Metabolic Pathway Analysis” conference Riga, Latvia 12.08.19 – 16.08.19

Danksagung

Zuallererst möchte ich Prof. Dr. Christoph Wittmann dafür danken, dass er mir die Möglichkeit gegeben hat als Teil des Teams am iSBio diese Arbeit zu erstellen. Ich bin dankbar für die Unterstützung und das Vertrauen, ohne die ich nicht bis zur Fertigstellung meiner Dissertation gekommen wäre. Mir wurde durch Ihn ein Umfeld gegeben, in dem ich mich weiterentwickeln konnte und ich durfte mich auf verschiedenen Gebieten ausprobieren und hatte immer das Gefühl seinen vollen Rückhalt zu genießen.

Mein Dank gilt auch Dr. Judith Becker, die immer unterstützend hinter mir gestanden hat. Sie zu verlieren war schmerzhaft. Ein Teil von ihr steckt auch in dieser Arbeit und ich möchte dieses hiermit ausdrücklich würdigen. Ich bedauere sehr, dass Sie in diesen Tagen bei der Fertigstellung dieses Projektes nicht dabei ist; sie fehlt mir sehr.

Großer Dank kommt meiner Lebensgefährtin Linda zu. Sie hat immer zu mir gestanden und war mein Ruhepol in stürmischen Zeiten. Sie konnte mich immer auf den Boden der Tatsachen zurückholen, wenn meine Gedanken ein ums andere Mal um Kleinigkeiten gekreist sind oder ich Selbstzweifel hatte. Zusätzlich bin ich dankbar für ihr Verständnis, wenn Nachtschichten geschoben werden mussten und ich dementsprechend launisch war.

Ich danke meinen Geschwistern Tim und Sally für ihre Unterstützung in jeglicher Hinsicht. Ich freue mich sehr über unser gutes Verhältnis und hoffe, dass es so bleibt.

Niko, Patrick, Steffen und Raphael, die ich durch Studium und Promotion in Saarbrücken kennen gelernt habe möchte ich auch für ihre Geduld und Unterstützung danken. Natürlich gilt mein Dank auch meinen drei „Bielefeldern“ Julian, Simon und Eddi.

Zu guter Letzt möchte ich mich beim ganzen iSBio Team für die vergangenen fast 6 Jahre bedanken. Vorweg: ich weiß das es mit mir nicht immer leicht war. Danke, dass ihr mich trotzdem so angenommen habt wie ich bin. Namentlich erwähnen möchte ich meine Büro-Genossen Lars, Martin und Peng, die die meiste Zeit das Arbeiten erleichtert haben. Leider war die Zeit mit Sabrina, Roxane und Felix viel zu kurz. Ich hätte mit ihnen gerne noch länger zusammengearbeitet. Ich möchte mich auch bei Michel für seine Unterstützung bedanken. Das Fachsimpeln über Motoren und Motorräder/Dreiräder werde ich vermissen. Ich wünsche Julian, den „Jugo-Chicks“ und allen anderen Doktoranden, dass sie ihre Dissertationen erfolgreich abschließen und alle Ziele in ihrem Leben erreichen die sie sich vornehmen.

Table of contents

1. Introduction and aim of this work

The photosynthetic microorganism *Synechocystis* sp. PCC 6803 has become one of the model organisms for the understanding of photosynthesis in general. Due to the change in climate, induced by constantly increasing carbon emissions since the industrial revolution [1, 2], it has become a major objective to use carbon dioxide as a substrate for biotechnological production. The major use of carbon dioxide in biotechnology is done indirectly by using plants. They are used as substrates for bioprocesses or modified to produce biotechnological products [3, 4]. Besides being used for food production, plants are currently used for production of biofuels on large scale [5]. The generation of biofuels from crop plants has come with major drawbacks regarding the use of fertile soil and environmental destruction [6]. To avoid the intensification of competition of feed vs food, it is necessary to develop methods for the use of non-food dependent processes for biotechnology [7-9]. A possibility to achieve this goal is the use of waste streams from a variety of industries as substrates for bio processes [10]. Alternatively, the use of carbon dioxide from atmosphere or exhaust streams could be used. The fixation of carbon dioxide is an ability not solely present in photosynthetically active organisms. Nevertheless, carbon fixation is energy demanding [11] and thus needs the supply of additional substrates. To overcome the mentioned competition for resources, photosynthesis appears to be a promising solution, to provide the energy needed for carbon fixation coupled with bioprocessing. The biotechnological use of microorganisms that can perform photosynthesis is an opportunity to combine the gained knowledge in strain development and the need for environmentally friendly production of chemicals.

The aim of this thesis is the elucidation of the contribution of novel pathways to the central carbon metabolism of *Synechocystis* sp. PCC 6803 using ^{13}C metabolic flux analysis. Special focus is placed on the Entner-Doudoroff (ED) pathway. Recent literature [12, 13] stated, that deletion of key genes associated with the oxidative pentose phosphate (PP) pathway cause alteration of growth behaviour in different growth modes. Especially, deletion of 2-keto-3-deoxy-6-phosphogluconate (KDPG) aldolase (Δ*eda*) and both isoforms of phosphofructokinase (Δ*pfkA/pfkB*) caused changes in phenotype. This led to the conclusion, that the ED pathway must play a crucial role for photomixotrophic metabolism of *Synechocystis* sp. PCC 6803. To verify this hypothesis, metabolic flux analysis is the method of choice since it is capable to estimate in vivo fluxes with high precision from labelling patterns. Apart from ED pathway, phosphoketolase (PK) pathway was identified for *Synechocystis* sp. PCC 6803 [14], present with two phosphoketolase genes (Δ*xfp1*/*xfp2*). Like the ED pathway, the phosphoketolase pathway can bypass the PP pathway and may act as a regulatory mechanism for the pentose phosphate pool. Resolving the metabolic network as it is known to

this point to its full extent will aid in the further implementation of cyanobacteria into next generation CO_2 neutral bioprocesses. Apart from answering physiological questions, performing ^{13}C tracer studies supplies vast data sets, that can aid in future research and the identification of other pathways, yet unknown. High quality experimental data is very valuable for training of bioinformatics software and testing of complex whole genome models. The complexity of the cyanobacterial metabolism makes the demand for high quality and consistent data even more important.

2. Theoretical background

Synechocystis sp. PCC 6803

Blue green cyanobacteria differ in their ability to perform oxygenic photosynthesis in the group of photosynthetically active bacteria. They share the structure of their electron transport chain and photosystems with chloroplasts from prokaryotic photosynthesis performing organisms. Cyanobacteria are used for long periods as food and natural fertilizers by humans [15]. Especially their ability to assimilate and in some cases fix nitrogen makes them suitable for fertilization of e.g. rice fields [15]. The strain *Synechocystis* sp. PCC 6803 was first isolated from a sweet water lake in 1968 and deposited in the Pasteur culture collection (PCC). The oxygenic photosynthesis performing cyanobacteria are one of the oldest genus of bacteria, still in existence [16]. Fossil founds suggest, that cyanobacteria type organisms were in existence 2.4 billion years ago [17]. The long period cyanobacteria are present in different forms show their high versatility and robustness, allowing them to survive rough environmental conditions. In the genus of cyanobacteria, *Synechocystis* sp. PCC 6803 is one of the most investigated organisms. Its genome is sequenced and was published in 1996 [18], enabling rational strain development of this organism. The genome analysis revealed metabolically outstanding, compared to e.g., *Escherichia coli*. For more than 50 years, the tricarboxylic acid cycle (TCA) of *Synechocystis* was considered to be incomplete due to the lack of alpha-ketoglutarate dehydrogenase [19] thus, this organism was considered unable to convert alpha-ketoglutarate into succinyl-CoA. In 2011 Zhang *et al.* published the identification of two novel enzymes, catalysing the decarboxylation of alpha-ketoglutarate (2-oxoglutarate decarboxylase) and the conversation of succinate-semialdehyde to succinyl-CoA (succinyl-CoA synthetase) [20]. Regarding the structure of *Synechocystis* sp. PCC 6803, vast differences to other bacteria are given by the existence of membrane divided compartmentation. As in chloroplasts, *Synechocystis* sp. PCC 6803 cells contain stacks of membranes that inhabit protein complexes for photosynthesis.

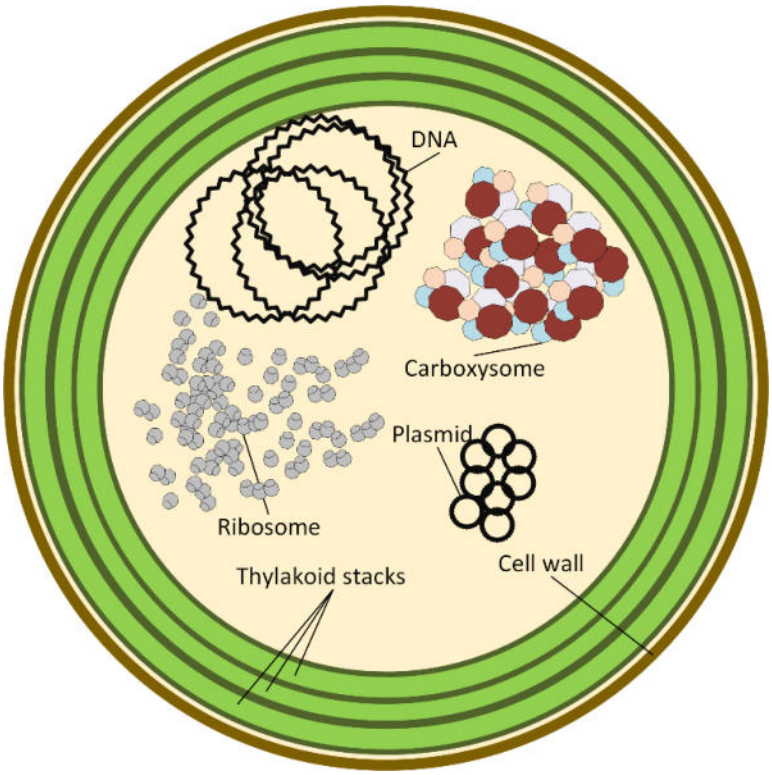

Figure 2.1: Schematic view of a *Synechocystis* sp. PCC 6803 cell including important cell components.

As in the thylakoid stacks of plant plastids, the photosystems (PS) I and II contain chlorophyll for the activation of electrons [21]. For better light harvesting efficiency, cyanobacteria evolved so called phycobillisomes that inhabit a large variety of chromophores that aid light absorption and energy transmission towards the photosystems [22]. An additional difference between chloroplasts and cyanobacteria is the ratio of photosystems. In cyanobacteria the ratio of PSI to PSII is about 5 [23], whereas in plants it ranges at around 0.5 to 0.7 [24]. It is believed that the high ratio of PSI to PSII is connected to succinate dehydrogenase that is located on the thylakoid membrane. This enzyme transfers electrons from succinate to plastoquinone (Q) [25].

The mode of action of the photosystems in *Synechocystis* sp. PCC 6803 is the same as in plants. At the photosystem II light driven lysis of water to protons and O_2 is catalysed [25]. The protons are transported to the thylakoid lumen, where they participate in maintaining an electro chemical gradient. For each split water molecule, two electrons are transferred onto plastoquinone, which is thereby reduce to plastoquinol (QH_2). This redox reaction takes place in the photosystem II [26] and presupposes the incorporations of two protons form the cytoplasm into plastoquinol. The reduced plastoquinol diffuses in the following step through the thylakoid membrane towards the cytochrome b_6f complex, where it is oxidized and deprotonated. One electron of each electron pair, supplied by plastoquinol (QH_2) is transferred onto another plastoquinone. The remaining electron is used to reduce one copper atom of plastocyanin. This process needs to be cycled two times, to transfer both electrons from one

water molecule to two plastocyanines. During two cycles in the cytochrome bf6 complex both protons from plastoquinol and two additional protons form the cytosol are translocated to the thylakoid lumen [27]. PSI operates differently compared to PSII. Common in each photosystem is the activation of an electron of chlorophyll-a by light. In the case of PSI, the activated electrons are replaced by electrons from reduced plastocyanin. After electrons are activated in PSI, they are used to reduce ferredoxin. Ferredoxin is an electron donor that participates in a variety of reactions. Most important is the transition of electrons onto the flavo-protein $NADP^+$ reductase. This enzyme inhabits flavin adenine dinucleotide (FAD) as prosthetic group and transfers two electrons from two molecules of ferredoxin do regenerate nicotinamide adenine dinucleotide phosphate (NADPH). Protons that are transported across the membrane into the lumen of the thylakoids cause the formation of a high proton motoric driving force. As it is the case for the generation of adenosine triphosphate (ATP) during oxidative phosphorylation, ATP-synthase is using the proton gradient to fuse one phosphate and adenosine diphosphate (ADP). To maintain the constant supply of ATP, cyclic electron transfer can be performed. In this mode of operation electrons are transferred from PSI onto plastoquinone, which is then again interacting with the cytochrome b_6f complex, as described before. By this cyclic electron flow, the absorbed sunlight is solely used to maintain the proton gradient across thylakoid membranes [25]. The ability of *Synechocystis* sp. PCC 6803 to perform photosynthesis enables the generation of reduction equivalents in form of quinol and NADPH/NADH and regeneration of ATP. Thus, the organism can grow under autotrophic condition, in which it fixes carbon in form of carbon dioxide. This implies, that the presence of CO_2 or carbonate is a necessity for autotrophic growth. Besides sole autotrophic growth, *Synechocystis* sp. PCC6803 can grow in mixotrophic conditions, which is characterized by the additional presence of an organic carbon source like glucose. Under this condition *Synechocystis* sp. PCC6803 is simultaneously performing photosynthesis and respiration. The ability to grow on organic compounds enables heterotrophic growth and survival under anaerobic conditions.

Use of cyanobacteria in biotechnology

The ability of cyanobacteria to perform oxygenic photosynthesis has drawn the attention of many researchers for different reasons. Together with the shortage of fossil fuels and increasing pollutions by their use, alternatives to petrochemistry become essential. A promising opportunity is the combination of carbon fixation from atmosphere and the production of valuable products. As a major benefit, substrate costs are (during the day) basically limited to medium. Since most autotrophs are not depending on addition of vitamins or other cofactors, costs for chemically defined media are low. Apart from medium and sunlight, carbon dioxide is the main substrate for cultivation of phototrophs. Implementing bioprocesses that draw CO_2 from the atmosphere may benefit from policies implemented by different states

and e.g the european union. Here, special focus can be placed on carbon trading [28], where scenarios can be created in which using CO_2 as substrate is subsidized. Different approaches have been taken to transform cyanobacteria into production hosts for different biotechnological products. Most cyanobacteria species produce small amounts of ethanol, when grown under autotrophic conditions [29]. Thus, it is obvious to try to enhance ethanol production with cyanobacteria to enable bioethanol production from CO_2. Different work groups have reported modifications of cyanobacteria to produce ethanol with moderate yields [30]. One easy way to produce ethanol was shown to be realisable by the overexpression of two enzymes, leading to redirection of carbon in form of pyruvate towards ethanol [31]. Nevertheless, effective fuel production is hindered by high costs for downstream processing and the physical properties of ethanol. The production of a more suitable alcohol has been proven to be possible. Isobutanol has better combustion and storage properties in comparison to ethanol. It is easy to derive isobutyraldehyde or isobutanol directly from valine biosynthesis [32]. The first compound can also be used in chemical synthesis, which makes this approach to biofuel production more appealing. Apart from fuels used in Otto-type engines, the production of long chain combustible hydrocarbons was realised. As in the production of bio-diesel from plant oils, triglycerides produced with cyanobacteria can be used for transesterification [33]. A drawback for the use of lipids for biofuel production are high costs and afford for product extraction from biomass, but the energy density of lipid-based biofuels is much higher in comparison to alcohols. Alternatively, long chain fatty acids are produced and directly secreted to the medium [34]. Compared to other potential biofuel production approaches, the production of long chain fatty acids enables simple separation of the product from the culture broth. Further promising molecules usable for biofuel production are long chain alkanes which are naturally produced by cyanobacteria species. These alkanes are part of the plasma membrane of the corresponding organisms and can make up to 0.14 % of the biomass dry weight [29, 35]. The exploitation of the native production routes for these compounds lead to an increase up to 1.10 % of cell dry weight [35]. Again, in the case of membrane compounds the downstream process can become too expensive to stay in economically reasonable ranges for large scale fuel production. Biofuels from cyanobacteria and other microalgae must compete with their fossil counterparts and are currently not economically feasible [36]. Furthermore, other alternatives like synthetic fuels may render biofuels production with microalgae obsolete in the long term. Still, biofuels from microalgae are considered an important building stone in the transition towards a carbon neutral future [37]. On the product range regarding fine chemicals for chemical synthesis, polhydroxybutyrates (PHB) could be used as a substituent for chemical synthesis. Some cyanobacteria accumulate PHBs when under nitrogen and phosphor starvation [29, 38]. It was shown, that PHB in *Synechocystis* sp. PCC 6803 can be improved by over expression of the σ factor SigE in combination with nitrogen starvation [39]. The feature

of some cyanobacteria to use CO_2 and organic substrates during photomixotrophic growth mode [40, 41] opens an opportunity to use waste streams from multiple origins. Coupling generation of cyanobacteria biomass with waste water treatment [42, 43] is just one example for use of photomixotrophic growth. Thereby carbon capturing via photosynthesis may be incorporated into e.g., municipal wastewater treatment plants, and thereby help achieving a carbon neutral future.

Constraints and limitations for the cultivation of phototrophs

Cultivation of microalgae is commonly performed in cultivation systems that allow illumination. Light driven carbon fixation is the main feature making this group of organisms interesting and outstanding in the context of biotechnology. The supply of a culture of microalgae with a sufficient amount of photons with the proper light spectrum is challenging [44, 45]. Two extremes for cultivation of phototrophic microorganisms were established. On the one extreme side of the spectrum are open culture systems [46]. They are characterized by cultivation in large basins or ponds that are agitated for mixing. Open cultivation systems have the benefit of low process cost, but are limited by atmospheric carbon dioxide concentration, maximum light passage for sufficient supply of light, exposure to environmental conditions and easy contamination. On the other side of the cultivation spectrum are photo bioreactors (PBR). They enable precise control of cultivation parameters, whilst increasing costs. Off gas from e.g., power plants can be directed into PBRs for cultivation with high CO_2 concentrations. Photo bioreactors can overcome limitations regarding light passages by introducing light sources into the reactor, allowing for higher yields compared to open cultivation systems or illumination from sun light. The additional energy costs in connection with the current dominant use of fossil fuels for electricity generation make this approach unfeasible for production of biofuels or commodity chemicals.

Central Metabolism of *Synechocystis* sp. PCC 6803

As discussed above, *Synechocystis* sp. PCC6803 can grow on glucose as sole or additional carbon source. Glycolysis is present with the same enzymes as compared to e.g. *Escherichia coli*. Glycolytic enzymes play a double role when photosynthesis is active. Glucose is not only converted into C3-compounds but can be synthesised via gluconeogenic reactions. Gluconeogenesis plays an important role for replenishing energy deposits in form of glycogen. The ability to build reserves enables photosynthetically active organisms to survive during night times, when no photosynthesis can be performed. The pathways that are discussed in the following section of this work are annotated according to the KEGG database [47-49] and recent literature [50].

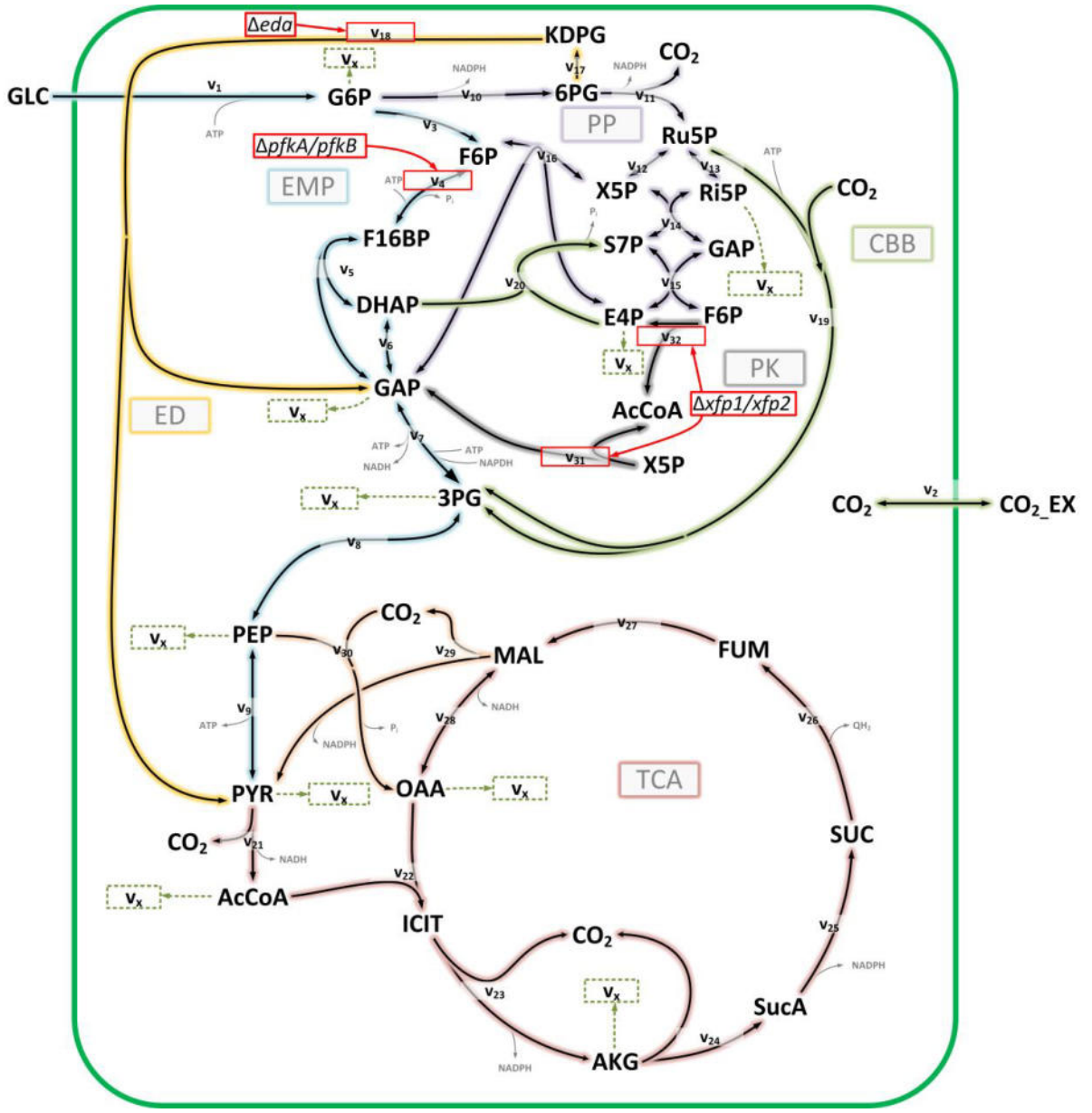

Figure 2.2: Core metabolism of *Synechocystis* sp. PCC 6803 as used for metabolic flux analysis. Abbreviations: Glucose (GLC), glucose 6-phosphate (G6P), fructose 6-phosphate (F6P), dihydroxyacetone phosphate (DHAP), glyceraldehyde 3-phosphate (GAP), 3-phosphoglycerate (3PG), phosphoenolpyruvate (PEP), pyruvate (PYR), acetyl coenzyme A (AcCOA), isocitrate (iCIT), α-ketoglutarate (AKG), succinate-semialdehyde (SucA), succinate (SUC), fumarate (FUM), malate (MAL), oxaloacetate (OAA), 6-phosphogluconate (6PG), 2-keto-3-deoxy-6-phosphogluconate (KDPG), xylose 5-phosphate (X5P), ribose 5-phosphate (Ri5P), ribulose 5-phosphate (Ru5P) sedoheptulose 7-phosphate (S7P), erythrose 4-phosphate (E4P), extracellular carbon dioxide (CO2_EX), intracellular carbon dioxide (CO2). Anabolic fluxes into biomass are represented as v_x. Colour code for pathways: blue: EMP pathway (v_3-v_9), yellow: ED pathway (v_{17} and v_{18}), dark red: TCA cycle (v_{21} – v_{28}), green: CBB cycle (v_{19} and v_{20}), lilac: PP pathway (v_{10} to v_{16}), grey: PK pathway (v_{31} and v_{32}), orange: PYR/PEP node reactions (v_{29} and v_{30}). Deletion mutants and their corresponding reaction numbers are highlighted with red arrows and boxes.

Embden-Meyerhof-Parnas pathway

Synechocystis sp. PCC 6803 possesses genes for the import of glucose from its surrounding medium. It is imported via a glucose H^+ symporter system (*glcP*, sll0771, TC:2.A.1.1) and phosphorylated via a glucokinase to glucose-6-phosphate (G6P) under the consumption of equimolar amounts of ATP (*glk*, sll0593, EC 2.7.1.2). G6P sits at one of the major metabolic branch points of *Synechocystis* sp. PCC 6803. It is either used to replenish carbon deposits in

form of glycogen or is taking glycolytic routs. Glycolysis is started by additional phosphorylation of F6P to fructose 1-6-bisphosphate (F16BP) by phosphofructokinase (*pfk*, sll0745 EC2.7.1.11). The phosphate group is transferred from ATP to the C6 atom of F6P. Fructosediphosphatase (*fba*, sll0018, EC4.1.2.13) is splitting F16BP into two molecules with three carbon atoms each. These molecules are di-hydroxy-acetone phosphate (DHAP) and glycerine-aldehyde-3-phophate (GAP). Both molecules are interconverted by triosephosphate isomerase (*tpi*, slr0783, EC5.3.1.1). The trioses resulting from G16PB cleavage can either enter pentose phosphate pathway or continue glycolytic routes. Glycolysis continues with NAD^+ dependent oxidation and direct phosphotransferation of GAP with inorganic phosphate to 3-phosphoglycerate (3PG) by glyceraldehyde 3-phosphate dehydrogenase (*gap1*, EC1.2.1.12 slr0884; *gap2* (NADP dependent), sll1342, EC:1.2.1.59) and phosphoglycerate kinase (*pgk,* slr0394, EC2.7.2.3). The second step involves phosphorylation of ADP to ATP. Both steps are reversible and have 1,3–bisphosphoglycerate as intermediate. Resulting 3PG is first isomerized into 2-phosphoglycerate (2PG) by reversible reaction mediated by phosphoglycerate mutase (*yibO*, slr1945, EC5.4.2.12). 2PG is reversibly dehydrated to phosphoenolpyruvate (PEP) by enolase (*eno*, sll0395, EC 5.4.2.1). Final step of glycolysis is the dephosphorylation of PEP to pyruvate, involving another direct phosphorylation of ADP to ATP. This final step is catalysed by pyruvate kinase (*pyk*, sll0587, EC2.7.1.40).

Gluconeogenesis

Gluconeogenesis uses in most parts enzymes of the EMP pathway. They catalyse the reverse reaction of their glycolytic mode of action. Only for some reactions an additional set of enzymes is present. Thus, gluconeogenesis is not only regulated via substrate pools, but by levels of gluconeogenic enzymes. Starting from pyruvate, the final product of glycolysis, its conversion to PEP is catalysed by posphoenolpyruvate synthase (*ppsA*, slr0301, EC2.7.9.2). All enzymes from F16BP to PEP are reversible. Dephosphorylation step of F16BP to F6P can be catalysed by either fructose bisphosphatase (*fpb*, slr0952, EC3.1.3.11) or by phosphofructokinase A (*pfkA*, sll0745, EC2.7.1.90). The latter is reversible. At this point of metabolism, the high metabolic robustness of *Synechocystis* sp. PCC6803 is observable. The redundancy of enzymes and their ability to use either $NADP^+$ or NAD^+ as cofactor at key points of central carbon conversion is common for *Synechocystis* sp. PCC6803.

Pentose phosphate pathway

Pentose phosphate pathway (PPP) reaction can be divided into redox reactions and isomerization/carbon transfer reactions. The oxidative part of PPP starts with the $NADP^+$ dependent oxidation of G6P to gluconate-6-phosphate via the intermediate glucono-delta-lacton-6-phosphate. The reactions are catalysed by glucose-6-phosphate dehydrogenase (*zwf*, slr1843, EC1.1.1.49/1.1.1.363) and 6-phosphogluconolatonase (*devB*, sll1479,

EC3.1.1.31). Last reaction of oxidative PPP is decarboxylation of gluconate-6-phosphate by 6-phosphogluconate dehydrogenase to ribulose-5-phosphate (*gnd*, sll0329, EC1.1.1.44), a pentose. In case of *Synechocystis* sp. PCC6803 this enzyme can transfer electrons from gluconate-6-phosphate to $NADP^+$ and NAD^+. Non-oxidative reactions of PPP involve isomerization of pentoses by an isomerase (*rpiA*, slr0194, EC5.3.1.6) and epimerase (*cfxE*, sll0807, EC 5.1.3.1). Two other major enzymes participate in the non-oxidative PPP. They are transaldolase (*talB*, slr1793, EC2.2.1.2) and transketolase (*tktA*, sll1070, EC 2.2.1.1). Transaldolase transfers C1 units between sugar phosphates, whereas transketolase transfers C2 units from one sugar phosphate to another.

Light reactions of photosynthesis

The unique ability of cyanobacteria to fixate carbon is based on direct use of light energy to regenerate ATP and NADPH. All necessary enzymes for photosynthesis in *Synechocystis* sp. PCC 6803 are in and on the cell's thylakoid membranes. Photosynthesis is based on photochemical reaction of chlorophyll. This molecule is a conjugated polyene with a high density of delocalized π electrons. Delocalized electrons are easily excited by light; thus, the molar extinction coefficient of chlorophyll A is in the range of 10^5 mol L^{-1} cm^{-1}. Excited electrons either reduce their potential energy by heat emission or are transferred to acceptor molecules. Chlorophylls are embedded into protein complexes that enable transfer of excited electrons onto acceptor molecules. All participating enzymes together with their cofactors are shown in Figure 2.3.

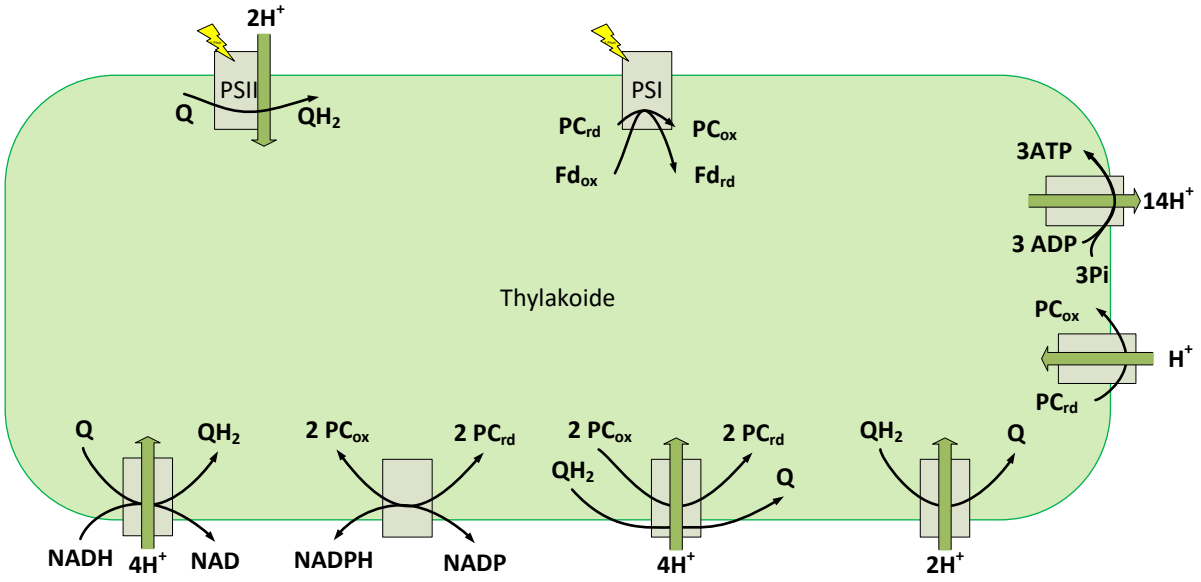

Figure 2.3: Schematic overview of electron transport for photosynthesis and proton transport for thylakoids of *Synechocystis* sp. PCC 6803. Abbreviations: Plastoquinone (Q), plastoquinole (QH_2), phycocyanin (PC), ferredoxin (Fd). Subscripts indicate reduces (rd) and oxidised (ox) status of reactants.

In *Synechocystis* sp. PCC6803 photosynthesis starts with the excitation of a specific pair of chlorophyll that is embedded in photosystem II (PSII). The high proximity of those two chlorophylls to each other changes their physical properties. The absorbance maximum of the specific pair is at 680 nm (thus P680). Photosystem II is a protein complex assembled from multiple polypeptides (D1 (*psbA* sll1867), D2(*psbD* sll0849), CP43(*psbC*, sll0851), CP47 (*psbB*, slr0906), PsbO (*psbO*, sll0427)). D1 and D2 consist of five transmembrane helices each spanning the total width of thylakoid membrane. They are associated with four chlorophyll molecules, two pheophytines, two quinones and one ferrous iron molecule. The transmembrane helices are flanked by CP43 and CP47. On the lumen side of thylakoids, a Mn_4CaO_5-cluster is associated and stabilized with the peptide PsbO.

Structurally outstanding for cyanobacteria is the presence of light harvesting antenna called phycobilisomes that are located on the cytosolic side of thylakoid membranes. Phycobilisomes are large protein complexes that contain chromophores which are specific for cyanobacteria. The presence of the chromophores phycocyanin (PC) (*cpcA* sll1578, *cpcB* sll1577) and phycoerythrocyanine enables funnelling of energy to the specific pair of P6870 from light with wavelength not covered by chlorophyll (green gap).

Mode of action of PS II is transfer of exited electrons onto plastoquinone (becoming thus plastochinol) and replenishing of missing electrons from water molecules. In the centre of photosynthesis is the specific pair. By excitement it becomes P608*, a very potent oxidation agent (less then – 0.7 V). This oxidative power causes the transfer of one electron from P680* to pheophytine (chlorophyll with two protons instead of Mg^{2+}). The specific pair thereby become positively charged (+1.15 V). $P680^*$ only prevails for milliseconds, before it is oxidized back to P680. The electron necessary for oxidation of $P680^*$ is gained from splitting water into protons and molecular oxygen. The net reaction is depicted in reaction equation RXN. 1. Extraction of electrons from water is enabled by the Mn_4CaO_5 Cluster that is contained in PsbO and is located on the lumen side of thylakoid membrane.

$$2\,H_2O \overset{h\nu}{\rightarrow} O_2 + 4H^+_{lumen} \qquad \text{RXN. 1}$$

The reactions catalysed in PSII in total is the conversion of light energy into chemical energy in form of electrochemical potentials. Approximately half of the energy contained in the light quanta absorbed by P680 is transformed into reductive power. The final reaction of PSII is reduction of plastoquinone with electrons from reduced pheophytines.

The plastoquinol pool in cyanobacteria is of large importance because of its connective function between photosynthetic and respiratory electron flow. Both respiration and photosynthesis are located in thylakoid membranes. In both cases plastoquinol is migrating through the membrane until encountering the cytochrome b_6f complex (*petB* slr0342, *petD*

slr0343, *petA* sll1317, *petC* sll1182, *petM* smr0003, *petN* sml0004, *petG* smr0010). This complex contains three subunits that are cytochrome b_6 (associated with two cytochrome b), cytochrome f (one cytochrome f), the Rieske-protein (2Fe-2S-protein) and the subunit IV. In the cytochrome b_6f complex, one electron from two plastoquinols is transferred via the iron sulphur cluster of the Rieske-protein to the copper containing protein plastocyanine. The electron of the second quinol is transferred onto another quinone that re-enters the quinone pool. The latter reaction is catalysed by the cytochrome part of the enzyme complex. Plastocyanine is located in the lumen of the thylakoid stack and moves freely. Alternatively, depending on the type of cyanobacterium, plastocyanine is substituted with cytochrome c_{553}. The electrochemical potential of the electrons that are transferred to plastocyanine is slightly decreasing. The potential difference is used in the cytochrome p_6/f complex to translocate one proton per processed electron.

$$2\ H^+_{cyt}\ QH_2 + Pc(Cu^{2+}) \rightarrow Q + 2\ Pc(Cu^{+}) + 4\ H^+_{lumen} \qquad \text{RXN. 2}$$

In total, per molecule plastoquinol four protons are translocated to the lumen. The electrochemical energy preserved in quinone is used to build up an electrochemical gradient across the thylakoide membrane system. Photosynthetic electron flow continues with the migration of plastocyanine through the lumen. It passes its electron to the photosystem I (PSI). PSI is a transmembrane protein build from two polypeptides: PsaA (*psaA*, slr1834) and PsaB (*psaB*, slr1834). The photosystem has, comparable to PSII, a specific pair of chlorophylls. Absorbance maximum of PSI specific pair is at 700 nm (P700). In its light induced exited form $P700^*$ is not as potent of a reducing agent as $P680^*$ (+0.45 eV). Excited electrons are channelled via a series of chinones from the specific pair to a Fe_4-S_4 cluster. Resulting electron gap is refilled with an electron donated from plastocyanine. From the PSI iron-sulphur-cluster the electron is transferred onto ferredoxin. One of the ferric iron atoms of the Fe_4S_4 cluster contained in ferredoxin (Fd) can be reduced to ferrous iron (compare RXN. 3). In general, PSI is a light driven plastocyanine-ferredoxin-oxidoreductase.

$$Pc(Cu^{+}) + Fd(2\ Fe^{3+}, 2\ Fe^{2+}) \overset{h\nu}{\rightarrow} Pc(Cu^{2+}) + Fd(1\ Fe^{3+}, 3\ Fe^{2+}) \qquad \text{RXN. 3}$$

In its reduced state the iron-sulphur cluster of ferredoxin has a reducing potential high enough to reduce $NADP^+$ to NADPH. Regeneration of NADPH is mediated by ferredoxin-$NADP^+$-oxidoreductase (FNR, *petH*, slr1643, EC1.18.1.2) that is located in the cytosol. FNR is a flavoprotein with a flavin-adenine-dinucleotide (FAD) as cofactor. Two ferredoxins are needed to regenerate one molecule of NADPH. FNR is iteratively accepting one electron from reduced ferredoxin. As intermediate, FAD with a single additional electron is present. The overall reaction stoichiometry is shown in RXN.4.

$$2\,Fd(1\,Fe^{3+}, 3\,Fe^{2+}) + NADP^{+} \leftrightarrow 2\,Fd(2\,Fe^{3+}, 2\,Fe^{2+}) + NADPH \qquad \text{RXN. 4}$$

Summing all processes involved into light dependent reactions of photosynthesis, a total reaction equation as shown in RXN. 5 can be formulated. The generation of two NADPH molecules and twelve protons translocated into the thylakoid lumen demands absorption of eight light quanta.

$$2H_2O + 2\,NADP^{+} + 10\,H^{+}_{cyt} \xrightarrow{8h\nu} O_2 + 2\,NADPH + 12\,H^{+}_{lumen} \qquad \text{RXN. 5}$$

The membrane potential builds up by translocation of protons into the lumen and is used by ATP-synthetase (*atpI*, EC7.1.2.2, sll1322) to regenerate ATP.

Dark reaction of photosynthesis

Molecules of NADPH and ATP generated by light driven reduction and exploit of electrochemical gradients are used in *Synechocystis* sp. PCC 6803 to fix carbon dioxide. Carbon fixation starts with the conversion of ribose 5-phosphate into ribulose 5-phosphate by ribose 5-phosphate isomerase (*rpiA*, slr0194, EC5.3.1.6). Under the consumption of equimolar amounts of ATP phosphoribulokinase (*pek*, sll1525, EC2.7.1.19) phosphorylates ribulose 5-hosphate to form ribulose 1,5-bisphosphate. The enzyme catalysing the carbon fixation reaction is ribulose-1,5-bisphosphate carboxylase/ oxygenase (rubisco) (*rbcL*, slr0009, EC4.1.1.39). A molecule of ribulose 1,5-bisphosphate that is binding to rubisco is changing into an enediol form by dissociation of one proton. The unstable enediol then reacts with one molecule of carbon dioxide that is pushed into proximity by rubisco, resulting in the fission of the fusion product into two molecules of 3-phospoglycerate. Besides carboxylation, rubisco can also catalyse oxygenation of the enediol form of ribulose 1,5-bisphosphate. The result of this second rubisco activity is one molecule of 3-phospoglycerate and one molecule of phosphoglycolate. The latter needs to be recycled under the use of reductions equivalents. Rubisco catalyses either of the reactions depending on the ambient concentration of both gases in the cytosol. To avoid the oxygenation reaction, cyanobacteria form so called carboxysomes consisting of rubisco and carbonic anhydrase (*icfA*, slr0051, EC4.2.1.1). In the carboxysome the CO_2 concentration is kept at high levels by conversion of carbonate by carbonic anhydrase. 3-phospoglycerate from rubisco activity is entering either glycolysis or gluconeogenesis depending on the metabolic state of the cell. To replenish the pentose phosphate pool for maintaining high activity of carbon fixation by rubisco *Synechocystis* sp. PCC6803 fuses erythrose 4-phosphate and dihydroxyacetone phosphate to synthesize sedoheptulose 1,7-bisphosphate. This is mediated by fructose-bisphosphate aldolase (*cbbA*, slloo18, EC4.1.2.13), which is having an additional activity apart from lysis of fructose 1,6-bisphosphate. The sedoheptulose 1,7-bisphosphate is dephosphorylated (*plgX*, slr2094, fructose-1,6-bisphosphatase II / sedoheptulose-1,7-bisphosphatase, EC3.1.3.11/3.1.3.37) and

enters the PP pathway as sedoheptulose 7-phosphate in which it is converted together with other gluconeogenic products to form pentose phosphates. The phosphate group initially transferred to ribulose 5-phosphate is released as phosphate.

Photorespiration

Rubisco does not use carbon dioxide as sole reactant together with ribulose 1,5 bisphosphate. It also catalyses the split of R15BP into 3PG and phosphoglycolate by incorporation of oxygen. This oxygenase reaction is competing with the carboxylation reaction. The ratio of oxygenation to carboxylation is depending on the concentrations of oxygen and carbon dioxide surrounding rubisco. Phosphoglycolate is dephosphorylated to form glycolate. The phosphate transfer energy of phosphoglycolate is too low to be harnessed for regeneration of ATP and the phosphate is released into the pool of free organic phosphates. Glycolate is further oxidised with oxygen under the formation of hydrogen peroxide. Two molecules of glyoxylate are fused to form 3PG. This conversion into 3PG demands one molecule of NAD^+ and includes the loss of carbon in form of CO_2. Since the oxygenase reaction of rubisco means a net loss of energy for the cell, cyanobacteria inhibit carboxysomes that include rubisco and carbonic anhydrase. The latter catalyses the formation of carbon dioxide from carbonate and causes a CO_2 rich environment for rubisco to minimize the rate of oxygenase reaction.

Respiration

Respiration in cyanobacteria in general shares most of the enzymes and electron carriers described in the photosynthesis section of this chapter. Since ferredoxin $NADP^+$ oxidoreductase operates bidirectional, NADPH from catabolic activity can be fed into the electron transport chain to regenerate ATP. Additionally, NADH can be reduced by NADH plastoquinone oxidoreductase (*ndh*, slr1279, EC7.1.1.2) to replenish the QH_2 pool. The NADH plastoquinone oxidoreductase in cyanobacteria shares a particularity with the enzyme present in plants: it can transfer electrons from NADPH as well, making NADPH a catabolic reducing equivalent, which can be used for regeneration of ATP. As final electron acceptor, oxygen is used by a cytochrome c oxidase (*cta*, sll0813, EC7.1.1.9)

Tricarboxylic acid cycle

The tricarboxylic acid cycle in cyanobacteria was thought to be incomplete, since the enzymes converting 2-oxoglutarate into succinate were missing. Only recently genes were identified that closed this gap [20]. Genes encoding for 2-oxoglutarate decarboxylase (*OgdA,* EC4.1.1.71) and succinic semialdehyde dehydrogenase (*SsaD* EC1.2.1.79). The latter is $NADP^+$ dependent and converts succinic semialdehyde as the unique intermediate of the cyanobacterial TCA cycle into succinate. Other enzymes are shared with common bacteria. Acetyl Coenzyme A is fused with oxaloacetate by citrate synthase (*gltA*, sll0401, EC2.3.3.1) to form citrate, with is then isomerized to isocitrate via cis-aconitate using hydratse (slr0665,

EC4.2.1.3). Isocitrate is subsequently decarboxylated yielding 2-oxoglutarate (*icd*, slr1289, EC1.1.1.42) under the regeneration of NADPH. Succinate resulting from decarboxylation and oxidation of 2-oxoglutatrete is further oxidised by succinate dehydrogenase that is located on the thylakoid membrane (*sdhB*, all0823, EC1.3.5.1). This enzyme complex directly transfers electrons from succinate onto a quinone and *vis versa*. Resulting fumarate is hydrated via fumarate hydratase (*fumC*, slr0018, EC4.2.1.2) giving malate, that is subsequently oxidised by malate dehydrogenase (*citH*, sll0891, EC1.1.1.37) (NAD^+ dependent). This reaction returns one molecule of oxaloacetate, completing the TCA cycle.

Entner Doudoroff Pathway

The Entner-Doudoroff-Pathway is a bypass for the oxidative part of the PP pathway and yields two C3 molecules from 6-phosphogluconate. It is known to be operated by a vast variety of organisms and provides metabolic flexibility [51-53]. The enzyme 6PG dehydrates (*edd*, slr0452, EC4.2.1.12) draws one molecule of water from 6-phospho gluconate resulting in the formation of 2-keto 3-deoxy 6-phosphogluconate (KDPG). This molecule is cleaved by KDPG aldolase (*eda*, sll0107, EC4.1.2.14). This pathway was discovered for cyanobacteria just recently [12]. The role of this pathway for the complex metabolic construct of *Synechocystis* sp. PCC 6803 is unclear to this point. Genetic perturbations and cultivation experiments suggested that this pathway plays a key role for photomixotrophic growth, since strains lacking KDPG aldolase showed impaired growth under said growth regime.

Phosphoketolase Pathway

Another bypass reaction that surpasses PP pathway and EMP pathway is the phosphoketolase pathway. It is composed of two reactions catalysed by the same enzyme. Phosphoketolase in *Synechocystis* sp. PCC 6803 (*xfp1*, *xfp2*, EC4.1.2.9 and EC4.1.2.22, slr0453) can split either X5P into GAP and acetyl phosphate or F6P into E4P and acetyl phosphate. Splitting the substrates requires phosphate during phosphate acetylation reaction. Acetyl phosphate is entering the Acetyl-CoA pool under the release of phosphate. As is the case for ED pathway, the PK pathway was annotated recently and its role for the metabolism of cyanobacteria is unclear [14].

Pyruvate node

Synechocystis sp. PCC 6803 has enzymes that connect PEP, pyruvate, and malate. The malic enzyme (*me*, slr0721, EC1.1.1.38) is NADPH dependent and oxidises malate into pyruvate under the loss of carbon in form of CO_2. Apart from carbon fixation via rubisco, CO_2 can be used to replenish oxaloacetate from PEP via phosphoenolpyruvate carboxylase (*ppc*, sll0920, EC4.1.1.31). The necessary rection energy is obtained from the phosphate group of PEP that is subsequently released as free organic phosphate.

Metabolic flux analysis

For biotechnological production it is essential to know as much as possible about a production host and a process. This knowledge provides the basis for any directed optimization [54]. Besides process parameters like growth rate, yields and product formation kinetics, metabolic flux distribution has become a key for bioprocess optimisation [54-56]. With the knowledge about metabolism, it has become possible to perform target directed manipulation of microorganisms.

Metabolic fluxes in general describe the routes and ratios in which carbon flows through an organism's metabolism. Carbon is the predominant atom of interest for the elucidation of metabolic flows, because it is the main participant in metabolic reactions. An organism's metabolism, in its core, is the rearrangement and maintenance of compounds containing carbon. The elucidation of intracellular metabolite conversions was firstly approached by calculating metabolic fluxes according to substrate uptake and product formation e.g. the maximum yields for antibiotic production [57]. Known enzymatic reactions were therefore organized in networks. The conversion rates of the molecules participating in this network were calculated according to the amount of substrates consumed and products secreted to the medium [58]. Additional to the knowledge about the metabolic reaction it is necessary to know the exact biomass composition to be able to calculate the net flux of biomass precursors [58].

Flux calculation in its core is balancing of reactions participating in an objective network. Therefore, the task of every algorithm is to solve the linear equation systems defined by the mass balances of the metabolic network. In constraint based modelling a metabolic network is represented in form of a matrix in contrast to kinetic modelling, that uses a series of differential equations including kinetics to resolve the contributions of individual reactions [59]. In a so-called stoichiometric matrix (*S*) biochemical reactions are organized by representing reaction stoichiometry in form of reaction numbers. In stoichiometric matrix columns represent metabolites and rows represent stoichiometric coefficients. Because reaction balances are differential equations that are characterized by rate terms, the change of reaction rates over time needs to be eliminated. This is achieved by assuming metabolic steady state in which the cross product of stoichiometric matrix (*A*) and flux vector becomes 0 (compare equation 1)

$$S\,v = 0 \qquad \text{Eq. 1}$$

Dimensions of stoichiometric matrix and flux vector determines the type of network. When *n* is representing the number of reactions and *m* is the number of fluxes, networks can be assigned into three groups:

Square system: m=n

Underdetermined system: m<n

Overdetermined system: m>n

Using measured external fluxes (*r*) and the stoichiometric matrix for said reactions (S_{meas}), the rate vector (*v*) can be calculated. In a biological system not all reaction rates are accessible without experimental data. Separating measurable vector and matrix elements from stoichiometric matrix and rate vector yields one matrix containing the stoichiometry for reactions with measurable rates (S_{meas}) and a second matrix that is representing reactions with rates to be calculated (S_{calc}). In equation 2 the stoichiometric matrix is combining measurable rates like substrate uptake, biomass, and product formation.

$$S_{meas}\, r = 0 \qquad \text{Eq. 2}$$

The combination of the equations 1 and 2 enables the calculation of all vector elements of the flux vector. In an overdetermined system (m>n), solving the equation is achieved by a square regression during which calculated fluxes and determined fluxes are the objectives (r = calculated rates, r_m = measured rates or rates resulting from measurements).

$$v = S_{meas} S^{-1} r \qquad \text{Eq. 3}$$

The problem shown in equation 3 is solved by linear programming to minimize the deviation between measured rates and those simulated according to the model. Optimization is performed for an objective function like maximum biomass formation. Analysis of stationary metabolic flux distributions based on extracellular measurable compounds is limited by the number of rates and compounds measurable by product and substrate analysis.

The addition of further metabolic limitations and knowledge about constrains for certain fluxes can be used to perform so called flux balance analysis [58]. This method is used when the model is underdetermined. Metabolic constraints that are used are e.g., limitations of flux barriers, growth rate or maximum production of certain metabolites. This results in final fluxes that are represented by solution spaces, rather than absolute values. Both presented methods for metabolic flux analysis lack direct measurement of intracellular metabolites. Even though, intracellular metabolite pools are measurable, it is difficult to draw conclusions on conversion rates from such measurements, since conversion rates are depending on enzyme kinetics and

underly complex regulatory networks [60, 61]. A solution for this problem is the use of isotope based stationary metabolic flux analysis. This method uses isotopic distribution of carbon in different metabolites to calculated intracellular fluxes.

^{13}C metabolic flux analysis

Isotope based metabolic flux analysis is a powerful tool to investigate the activity of pathways in the central metabolism of an organism [62-64]. This method is well established and has been used to determine intracellular rates for the metabolism of e.g. *Escherichia coli* [65], *Corynebacterium glutamicum* [56], *Basfia succiniciproducens* [66], *Bacillus subtilis* [67] or *Pseudomonas putida* [51]. In ^{13}C metabolic flux analysis, *in vivo* enzymatic rates are estimated according to isotopic enrichments in cellular components of an organism cultivated on labelled substrates. Determination of isotopic enrichments can be carried out by mass spectrometry or by NMR, resulting in different labelling information [68]. Isotopic distributions are obtained from MS measurements of different analytes, whereas NMR is enabling determination of position specific isotopic enrichment [69]. The information density of data interpreted with a stoichiometric model can be increased by using differently labelled tracer substrates in parallel experiments [70].

Atom species occur in different isotopic states that is defined by the presence of additional neutrons in the atom nucleaus. Every atom type has its own distribution of naturally occurring isotopes. For example, naturally 1.07 % of all carbon atoms carry a further neutron. A molecule´s isotopic distribution is the sum of contributions by all its atom´s isotopic distributions. The distributions are presented as vectors, so-called mass distribution vectors (MDV), that encode an isotopic distribution as shown in equation 4. Each entry represents the molar fraction (*X*) of molecule´s corresponding to the number of additional neutrons in the core, starting at zero at positions one.

$$MDV = \begin{pmatrix} m+0 \\ m+1 \\ m+2 \end{pmatrix} = \begin{pmatrix} X_{m+0} \\ X_{m+1} \\ X_{m+2} \end{pmatrix} \qquad \text{Eq. 4}$$

The sum of all vector elements of an MDV is 1 since the MDV is representing the basic totality of molecules. The isotopic distribution of a molecule is calculated by iterative convolution of MDVs of atoms contained in the molecule. For each atom of a molecule, one convolution step is necessary. Vector convolution is defined by equation 5 (the convolution of vectors *a* and *b* results a vector *c*).

$$\mathrm{a} * \mathrm{b} = \mathrm{c}$$
$$with$$
$$c_n = \sum_{k=0}^{n} a_k \cdot b_{n-k} \qquad \text{Eq. 5}$$

The presence of isotopes in metabolites can be used for metabolic flux analysis by feeding substrates that have a known isotopic enrichment at a given atom (position specific labelling). In case of ^{13}C metabolic flux analysis, one or more carbon atoms of a substrate are labelled. Tracking the path of this labelled carbon through the metabolism is possible by using mass spectrometry or nuclear magnetic resonance spectroscopy (NMR) [58]. Incorporation of labelled carbon from substrates into products of any reaction is depending on stoichiometry and reaction rates. It is assumed that enzymes do not distinguish between labelled and unlabelled substrates, regarding reaction rates [62].

When considering different types of reactions, isotopic distributions of products and educts are depending on the position of labelling. In Figure 2.4 an example for the cleavage of a molecule is presented, that consists of four atoms. It is split into two molecules. The isotopic distribution of the molecule containing atom a and b from the parent molecule is bearing 100 % of the labelling, whereas the molecule composed of c and d is not carrying labelling at all. The hypothetic MDVs are shown in equation 5 where *E* is representing the substrate and *A* and *B* are giving the product MDVs.

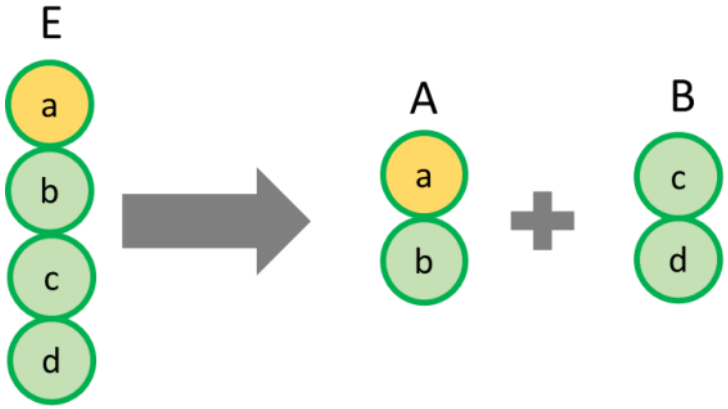

Figure 2.4: Scheme for a molecule (E) being split to yield two new molecules (A and B). Atoms are marked with small letters (a to c). Yellow indicates an atom with an additional atom mass unit.

$$\mathrm{E} \rightarrow \mathrm{A} + \mathrm{B}$$
$$\begin{pmatrix} 0 \\ 100 \\ 0 \\ 0 \\ 0 \end{pmatrix} \rightarrow \begin{pmatrix} 0 \\ 100 \\ 0 \end{pmatrix} + \begin{pmatrix} 100 \\ 0 \\ 0 \end{pmatrix} \qquad \text{Eq. 6}$$

When adding further conversion reactions to the scheme presented in Figure 2.4, it becomes obvious, that the ratio of reaction speeds is determining isotopic distributions of molecules A(ab) and B(cd). Such an addition of reactions is shown in Figure 2.5. In this scheme a further reaction is added that consist of the cleavage of a three-atom molecule into the same product as the previous reaction.

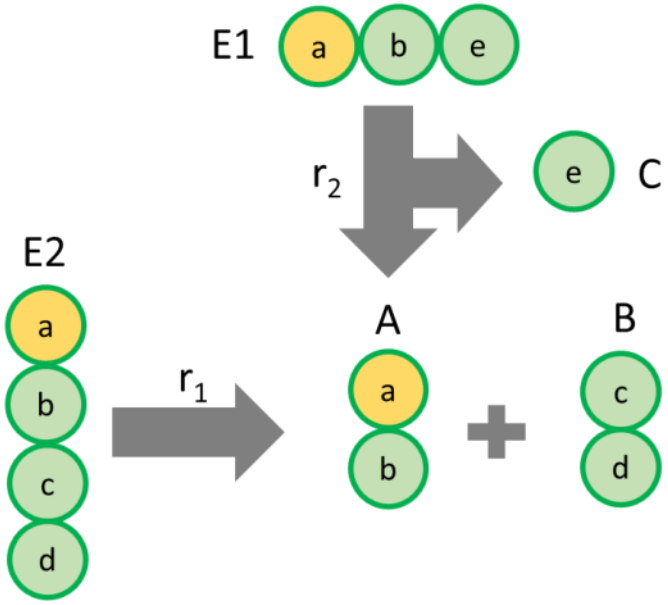

Figure 2.5: Addition of a second reaction to the previous scheme. Both reaction share the molecule A as a product and contribute to its isotopic enrichment.

The resulting isotopic distribution will be depending on the rates *r1* and *r2*. Mass balances for the reactions in Figure 2.5 are listed in Eq. 7. The formation of compound *A* over time is given by the sum of rates *r1* and *r2*.

$$\frac{d[E1]}{dt} = -r_2$$
$$\frac{d[E2]}{dt} = -r_1$$
$$\frac{d[A]}{dt} = r_1 + r_2$$
$$\frac{d[B]}{dt} = r_1$$
$$\frac{d[C]}{dt} = r_2$$

Eq. 7

The incorporation ratio of labelling information from *E1* and *E2* into molecule a is determined by the ratio of *r1* to *r2*. When knowing the exact isotopic composition of substrates that enter a metabolic network, isotopic distributions for all participating metabolites can be calculated

from a set of rates. *Vice versa*, reaction rates are accessible through isotopic distributions of metabolites in a network.

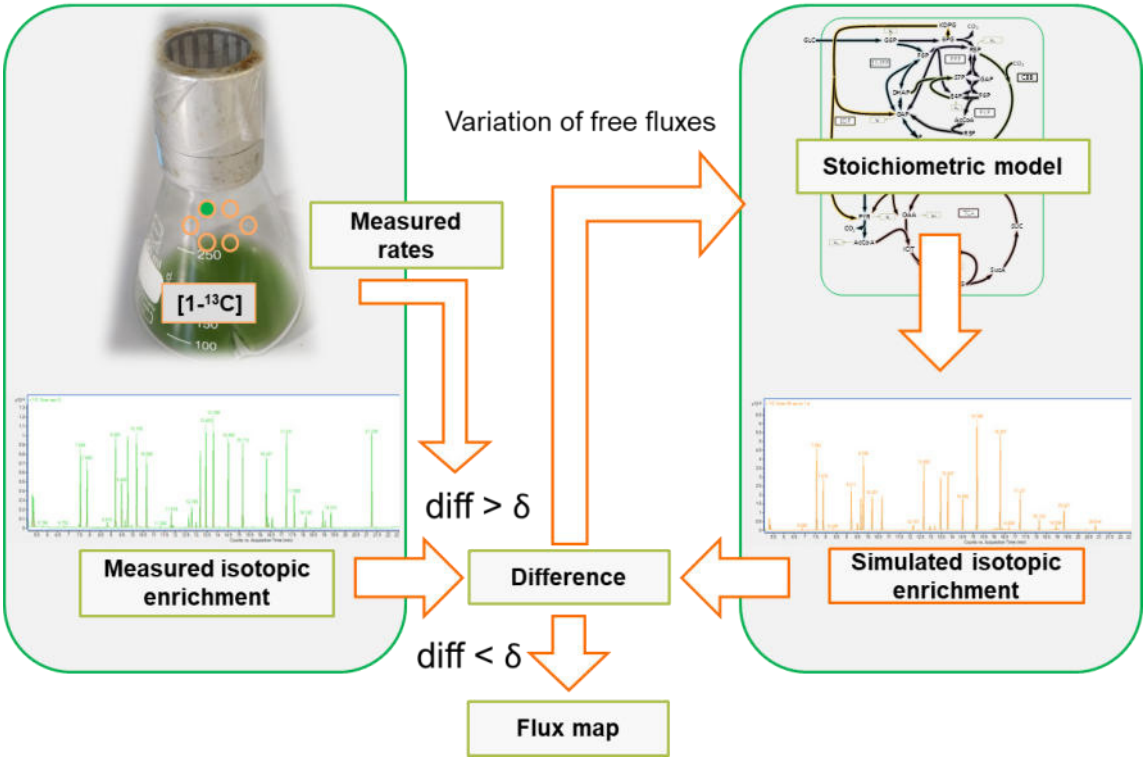

Figure 2.6: Graphic representation of the flux estimation algorithm for ^{13}C metabolic flux analysis.

For the estimation of metabolic fluxes from labelling data, a stoichiometric model is used to simulate isotopic distributions from a random set of free fluxes [71]. These simulated distributions are then compared to the measured distributions via difference analysis using a sum of squares weighted residuals approach that considers measured rates and labelling information. If the margin of error is exceeding a defined threshold, the free fluxes are altered, until a statistical criterion is met.

$$\min SSR = \sum \frac{(x - x_m)^2}{\sigma_x^2} + \sum \frac{(r - r_m)^2}{\sigma_r^2} \qquad \text{Eq. 8}$$

In Eq. 8 this nonlinear regression for ^{13}C stationary metabolic flux analysis is presented. The objective function consists of two variance weighted sum of square residuals (SSR) [68]. One is calculated for measured mass isotopic distributions x and for measured distributions x_m with the variance for isotopic distributions σ_x. The second SSR calculation is based on comparison of measured rate r_m and calculated rates r. Because most metabolites do not accumulate in detectable amounts, isotopic distribution determination is limited to metabolic end products that are incorporated into cell compounds. With the assumption, that isotopic distributions are dependent on reaction rates, the incorporation of labelling information into the measured cellular components follows the same rule. To assure that the discussed estimation of fluxes

is possible metabolic and isotopic steady state need to be present. Only if the rate of labelling incorporation into measured biomass constituents is constant, it is possible to estimate fluxes that are connected to the analyte [72].

Biomass composition

For metabolic flux analysis of any kind, biomass plays an essential role [73]. Biomass is one of the measurable fluxes that was described above. The simplest way to implement kinetics for biomass formation (or decrease) is to find a mathematical expression, describing experimental data. Using an exponential function with a specific growth rate defined for exponential growth is the most common approach. If the growth rate is constant over time, it can be assumed, that the metabolism is also in a constant state (metabolic steady state). Biomass is composed of different building block that are derived from the central metabolism. Growth is thus characterized by the rates at which biomass building block are drawn from the metabolism and are incorporated into biomass [74]. If the growth rate is constant, rates for synthesis of building blocks will also be constant and thus it can be assumed that the whole metabolism is in a state in which all metabolic rates are constant. This metabolic steady state thus allows estimation of fluxes based on biomass compositions and growth rate since these are fluxes with known rates. Table 1 gives an overview on the central precursor metabolites used for the synthesis of biomass constituents.

Table 1: List of precursors and their corresponding metabolites.

Precursor	Final compound
Pyruvate	Alanine, Valine, Leucine, Coenzyme A, Fatty acids
Oxoglutarate	Glutamate, Proline, Purines, Chlorophyll
Oxaloacetate	Aspartate, Lysine, Threonine, Isoleucine, Methionine, Meso-Diaminopimelate
Phosphoenolpyruvate	Tryptophan, Phenylalanine, Tyrosine
3-Phosphoglycerate	Serine, Glycine, Cysteine
Ribose-5 Phosphate	Pyrimidines, Histidine, Nucleotides
Erytrose-4-Phosphate	Phenylalanine, Tyrosine, Tryptophan
Glucose-6-Phosphate	Glycogen
Fructose-6-Phosphate	Cell wall
Acetyl-CoA	Fatty acids, Leucine
Succinyl-CoA	Methionine, Lysine
Glyceraldehyde-3-phosphate	Quinones

The biomass equation can be expressed in form of mmol of precursor and reducing equivalents needed per gram of biomass formed. It can be implemented with varying degrees of complexity

[73]. Assembly reactions for macromolecules can be implemented as an additional step. This can bring the benefit of easier calculation of multiple models for the same organism with different macromolecular composition. By supplying the model with reactions with known rates via the biomass formation, the solution space for a stoichiometric network becomes easier to resolve and supplies a physiological framework for a mathematical operation.

Elementary flux modes

As discussed before, in constraint based metabolic flux analysis, *in vivo* fluxes are estimated according to measured external fluxes, the biomass composition and the stoichiometry of the network´s reactions. Since the mathematical problem described in Eq. 3 is characterised by a series of differential equations, its result is given by a solution space [58]. To minimize the computational effort and time for the estimation of metabolic fluxes, Zanghellini et al. [75] introduces the concept of elementary flux modes (EFM). According to their definition: Elementary flux modes are thermodynamically and stoichiometrically possible pathways reducing the complex metabolism into all, unique, non-decomposable biochemical pathways, which connect the supplied substrates with the corresponding end products [75]. Using this approach, a metabolic network can be analysed for the possible contributions of metabolic pathways. Still, it must be considered, that the complexity of the underlying model is defining the number of resulting EFMs. For the network shown in Figure 2.2 the analysis can yield important aprioristic information.

3. Methods

Strains.

The wildtype strain of *Synechocystis* sp. PCC 6803 was obtained from the Pasteur Culture Collection of Cyanobacteria (PCC, Paris, France). Deletion mutants, missing 2-keto 3-deoxy 6-phosphogluconate aldolase (*eda,* EC4.1.2.14), phosphofructokinase A and B (*pfk*A, EC 2.7.1.11, sll0745; *pfk*B, EC 2.7.1.90, sll0745) and phosphoketolase A and B (xfp A/B EC:4.1.2.9 4.1.2.22, slr0453) were obtained from recent works [12, 76].

Medium.

Cultivations were carried out in liquid BG11 medium [40]. It contained the salts that are listed with their concentration in Table 2. The medium was buffered using 5 mL per 1 L medium of 1 mol L^{-1} N-Tris(hydroxymethyl)methyl-2-aminoethanesulfonic acid (TES) that was adjusted to pH 8.0. For cultivation in photomixotrophic and heterotrophic growth mode the medium was supplemented with 10 mM glucose. For cultivation of strains on plates the BG11 medium was solidified using 15 g L^{-1} agar (Becton Dickinson, Franklin Lakes, NJ, USA). Additionally, 1 mM thiosulfate was added to avoid oxidation of iron during sterilization.

Table 2: Concentrations of salts used for the preparation of BG11 medium.

Compound	Concentration [mg L^{-1}]
$NaNO_3$	1,500.00
$MgSO_2$* 6 H_2O	69.00
$CaCl_2$* 2 H_2O	36.00
citric acid	6.00
Na_2EDTA	10.40
H_2BO_3	2.86
$MnCl_2$* 4 H_2O	1.81
$ZnSO_4$* 7 H_2O	0.22
$NaMoO_4$* 2 H_2O	0.39
$CuSO_4$* 5 H_2O	0.079
$Co(NO_3)_2$* 6 H_2O	0.0494
K_2HPO_4	4.00
Na_2CO_3	2.00
ammonium ferric citrate	6.00

Light intensity measurement and simulation of light profiles

Illuminance was measured using an illuminometer (Tack Life LM01, Shenzen Temine Technology, Guandong, China). Values were determined as maximum read outs after 20 s of light exposure with constant white light at 50 µE m^{-2} s^{-1} (Infors Multitron, Infors, Basel, Switzerland). To determine the illuminance after any given layer thickness and optical density of a cell suspension of *Synechocystis* sp. PCC 6803 in BG11 medium a series of measurements was conducted. Therefore, a culture of *Synechocystis* sp. PCC 6803 was grown, concentrated by centrifugation (8,000 x*g*, 3 min, room temperature), and diluted with BG11 medium to yield accurate optical densities ranging from OD_{750} 0.5 to 5.0. Each cell suspension was used to measure the illuminance after light passages ranging from 0.0 cm to 1.0 cm. Lambert-Beers law was used to generate a matrix representing illuminance according to optical density and light passage.

Quantification of cell concentration

Cell growth was monitored by measuring the optical density (OD) at a wavelength of 750 nm (UV-1600 PC, VWR International, Darmstadt, Germany). Additionally, cell dry mass (CDM) was quantified gravimetrically by filtering a known volume of culture (0.2 µm, regenerated cellulose, 47 mm, Sartorius, Göttingen, Germany), washing it once with deionized water, and drying it at 80°C until constant weight. The resulting correlation factor determined was CDM [g L^{-1}] = 0.261 * OD_{750}.

Cultivation

Shake flask cultivation was carried out with 250 mL baffled flasks with 10 % (V/V) filling volume equipped with self-made translucent caps consisting of aluminium caps with a 3 cm hole that was covered with translucent foil (PCR adhesive film, Axon Labortechnik, Kaiserslautern, Germany) for better illumination. They were incubated on a rotary shaker (28 °C, 100 rpm, 25 mm, Infors Multitron, Infors, Basel, Switzerland). For experiments with bubble columns, tubular bioreactors with a diameter of 3.5 cm and filled with 250 mL medium (aeration rate 10 sL h^{-1}) were used. For inoculation, a plate culture was used that was incubated for 5 days at 28 °C and, 50 µE m^{-2} s^{-1}. Biomass (about 10 mg mL^{-1}) from the plate was resuspended in BG11 medium and used to adjust the starting optical density to OD_{750} 0.1. Photomixotrophic cultures were exposed to constant illumination of 50 µE m^{-2} s^{-1}, whereas heterotrophic cultures were only exposed to day light for 5 min per day. Flasks were illuminated from the top, tubular bioreactors from opposing sides.

Quantification of glucose

Glucose was quantified in culture supernatant using a biochemical analyser (Biochemical Analyzer 2950D, YSI, Yellow Springs, Ohio, USA).

Elemental analysis of biomass

Biomass was harvested by centrifugation (8,000 x*g*, 3 min, 4 °C), washed twice with deionized water, freeze dried and analysed for the content of carbon, hydrogen, and nitrogen (Vario Micro Cube, Elementar, Hanau, Germany).

Network for metabolic flux analysis

The core metabolism of *Synechocystis* sp. PCC 6803 as seen in Figure 2.2 was translated into a stoichiometric model for elementary flux mode analysis and for flux estimation from ^{13}C labelling patterns. The reactions and their reactants were defined according to genome annotation [47] and recent literature [50]. Pathways included into the model were: Embden Meyerhof Parnas pathway (EMP), the Entner-Doudoroff (ED) pathway [12], the tricarboxylic acid cycle (TCA) containing succinate semialdehyde as intermediate [20], the pentose phosphate (PP) pathway, the Calvin-Benson-Basham (CBB) cycle, the phosphoketolase (PK) pathway [14], and reactions of the pyruvate/phosphoenolpyruvate node. Macromolecular biomass composition for photomixotrophic growth was obtained from literature [77]. The macromolecular composition was used to calculate a precise biomass equation [78] including synthesis pathways for amino acids. Since no formation of by-products was observed for photomixotrophic growth, pathways for formation of by products were not implemented. The metabolic network is shown in Figure 2.2. For heterotrophic growth biomass formation was adopted as found in literature [79].

Elementary flux mode analysis

The model as shown in Figure 2.2 was implemented using the EFM tool [80]. Therefore, the core metabolism was implemented using all reactants, including energy metabolites (see appendix). To account for the energy metabolism of *Synechocystis* sp. PCC 6803, reactions of the respiratory chain and photosynthesis were also considered. Biomass formation was implemented according to literature, including photon yields [77].

Isotopic tracer studies

For mixotrophic ^{13}C tracer studies, instead of naturally labelled glucose either (i) 99.9 % [1-^{13}C] glucose (Sigma-Aldrich, Steinheim, Germany), (ii) 99.9 % [3-^{13}C] glucose (Cambridge Isotope Laboratories, Tewksbury, MA, USA), (iii) 99.9 % [6-^{13}C] glucose (Omicron Biochemicals, Southbend, IN, USA), and (iv) 99.9 % [$^{13}C_6$] glucose (Eurisotop, Saarbrücken, Germany),

respectively were used. For heterotrophic tracer experiments, naturally labelled glucose was replaced by (i) 99.9 % [1-^{13}C] glucose, (ii) 99.9 % [6-^{13}C] glucose (Omicron Biochemicals, Southbend, IN, USA), and an equimolar mixture of [$^{13}C_6$] (Eurisotop, Saarbrücken, Germany) and naturally labelled glucose [51].

For tracer experiments a two-step consecutive cultivation setup was used. The first labelled culture was grown from OD_{750} 0.1 to an OD_{750} higher than 1.0. This culture was then used to inoculate the second labelled culture starting from OD_{750} 0.1. Biomass for flux estimation was harvested at OD_{750} values higher than 1.0. Thus, the naturally labelled carbon from the first inoculum was diluted to less than 1 % (mol/mol) in harvested biomass used for flux estimation. The molar fraction of naturally labelled carbon from the inoculum was thus neglected for parameter estimation [81]. For each glucose isoform an individual two-step consecutive cultivation was performed.

GC-MS labelling analysis of amino acids

Amino acids were released from cell protein by hydrolysis. Therefore 2 mg CDM were incubated with 250 µL 6 mol L^{-1} HCl for 18 h at 100 °C. Insoluble fractions of the resulting hydrolysate were removed by filtration (0.2 µm, Ultrafree-MC, Merck Millipore, Darmstadt, Germany). The hydrolysate was dried with constant nitrogen flow. The dry residues were solved in 50 µL N,N-dimethylformamide (1 % (v/v) in pyridine). Derivatization of amino acids into their *t*-butyl-dimethyl-silyl derivatives was started by addition of 50 µL N-methyl-*t*-butyldimethylsilyl-trifluoroacetamide (MBDSTFA, Macherey-Nagel, Düren, Germany). The mixture was incubated for 30 min at 80° C [66]. After incubation, the samples were subjected to measurement of mass isotopomer distributions using GC-MS (Agilent 7890A, Quadrupole Mass Selective Detector 5975C, Agilent Technologies, Santa Clara, California, USA) Separation of the analytes was achieved using a constant flow of helium (5.0) as mobile phase with a flow rate of 1.7 mL min^{-1} and an HP-5MS column as stationary phase (30 m, 250 × 0.25 µm, Agilent Technologies) [66]. The temperature profile used was: 0-2 min, 120 °C; 2-12 min, 8 °C min^{-1}; 12-24.5 min, 10 °C min^{-1}; 24.5 – 27 min, 325 °C. Other controlled parameters were inlet (250 °C), transfer liner (280 °C), ion source (230 °C), and quadrupole temperature (150 °C). A total number of 17 isotopomer distributions originating from amino acids were measured and are listed in Table 3. Same fragments were used in previous studies on *Synechocystis* sp. PCC 6803 [82] and other bacteria [51, 66]. Fragments of lysine, histidine, and tyrosine were not used for flux estimation due to insufficient quality of resulting peaks. The basic amino acids glutamine and asparagine, as well as the sulphur containing amino acids cysteine and methionine were not detectable in the hydrolysate due to chemical degradation during acid catalysed hydrolysis [81]. The same occurred for tryptophane. Isotopic distributions of every fragment listed in Table 3 were first measured in scan mode to detect potential isobaric

interference with other sample compounds. After confirming optimum separation of analytes, each fragment was measured in single ion monitoring mode in duplicates to obtain maximum accuracy [66].

Table 3: Amino acid fragments measured with GC-MS and used in flux estimation.

Amino acid of fragment origin	Fragments
alanine	*m/z* 260, *m/z* 232
glycine	*m/z* 218, *m/z* 246
valine	*m/z* 288, *m/z* 260
leucine	*m/z* 274
isoleucine	*m/z* 274
serine	*m/z* 390, *m/z* 362
threonine	*m/z* 404, *m/z* 376
phenylalanine	*m/z* 336
aspartate	*m/z* 418, *m/z* 390
glutamate	*m/z* 432
arginine	*m/z* 442

GC-MS labelling analysis of sugars

To obtain trimethylsilyl derivatives of biomass sugars, 2 mg of biomass was first hydrolysed by addition of 250 µL 2 mol L^{-1} HCl and subsequent incubation for 2 h at 100 °C. The insoluble fraction of the hydrolysate was removed by filtration (0.2 µm, Ultrafree-MC, Merck Millipore, Germany) [51]. The filtrate was then dried under constant nitrogen flow. To avoid formation of cyclic sugars during derivatization, an oximation step was performed by dissolving the dry hydrolysate in 100 µL methoxylamine (2 % (m/V) in pyridine) and subsequent incubation at 80 °C for 1 h. The oximated sugars were then derivatised by addition of 50 µL N-methyl-N-(trimethylsilyl) trifluoracetamid (MSTFA, Macherey-Nagel, Germany) and incubation for 30 min at 80 °C. The resulting sugar derivatives were subsequently subtracted to analysis of their mass isotopomer distributions using GC-MS (Agilent 7890A, Quadrupole Mass Selective Detector 5975C, Agilent Technologies). Separation of the analytes was achieved using a constant flow of helium (5.0) as mobile phase with a flow rate of 1.7 mL min^{-1} and an HP-5MS column as stationary phase (30 m, 250 × 0.25 µm, Agilent Technologies) [66]. The temperature profile used was: 0 min, 100°C; 0-26 min, 5 °C min^{-1}; 26– 29.8 min, 25 °C min^{-1}. Further temperature settings controlled the inlet (250 °C), the transfer liner (280 °C), the ion source (230 °C), and the quadrupole temperature (150 °C). Isotopic distributions for the following sugars and fragments were measured: glucose (*m/z* = 319), glucosamine (*m/z* = 319) and ribose (*m/z* = 307) [51]. The fragments were fist measured in scan mode to avoid isobaric

interference with other sample compounds. After confirming optimum separation, each fragment was measured in single ion monitoring mode.

NMR measurement

Biomass was harvested (5 mg) and hydrolysed with 6 M HCl by incubation for 12 h at 110 °C. After drying and washing twice with D_2O (with drying in between the steps), the hydrolysate was dried a final time and resuspended in 200 µL DCl (0.1 % (v/v) in D_2O). The sample was subsequently transferred into 3 mm NMR tubes and subjected to 1D ^{1}H NMR, 1D ^{13}C NMR, 2D ZQF-TOCSY NMR and 2D HSQC measurements [83]. For the analysis, a spectrometer Bruker Ascend™ 800 MHz (Bruker, Billerica, Massachusetts, USA) equipped with a 5 mm CQPI (1H, 13C, 31P, 15N) cryoprobe and a Sample Jet auto sampler (Bruker, Billerica, Massachusetts, USA) were used.

Flux estimation from ^{13}C labelling data

The network depicted in Figure 2.2 was implemented in the modelling software OpenFlux [84]. Reactions were implemented together with information of atom transitions for the carbon backbone all metabolites and reactions (Table A 3). The files of the modelling software were modified to compile labelling data from multiple parallel experiments [66]. For flux estimation in photomixotrophic growth mode labelling data from GC-MS measurements of amino acids and sugars were combined with NMR data for amino acids [83]. For estimation of fluxes in photomixotrophic growth mode, GC-MS data for was use with an error of ± 0.006 for amino acids and ± 0.01. For NMR data an error of ± 0.025 was used. In heterotrophic growth mode, the error for GC-MS data for amino acids and sugars was ± 0.01 due to low stability of derivatized samples. Biomass formation for photomixotrophic growth was implemented according to recent literature [13, 77, 78] and experimental data for biomass yields and uptake rates (compare Table 4). For heterotrophic growth, biomass formation was derived from literature [79] and experimental data (compare Table 6). For anabolic fluxes an error of 15 % was used. This deviation was implemented using the pre-solver function of OpenFlux [84].

Flux estimation was performed by iterative comparison of experimental and simulated labelling data (compare Figure 2.6). Calculated deviations were minimized by adjusting of free fluxes, until no further minimisation was achieved. The set of metabolic fluxes with the smallest deviation was considered the best results to represent *in vivo* fluxes [85]. Due to the nonlinear nature of the underlying differential equations of the model 250 runs of random starting point simulation were performed to verify that the calculated set of fluxes represents the global minimum regarding the deviation between measured and simulated labelling data [86]. The resulting global minimum was tested for its statistical probability by performing 250 runs of Monte-Carlo simulation with a confidence interval of 95 % for resulting metabolic fluxes [87].

Enzyme assays.

Cells were harvested by centrifugation (8,000 ×*g*, 3 min, 4 °C), washed twice (100 mM Tris-HCl, pH 7.8), and resuspended (100 mM Tris-HCl, 10 mM dithiothreitol). Cells were mixed with lysing matrix in form of 0.1 mm silica beads (Lysing Matrix B, MP Biomedicals, Santa Ana, CA, USA) and disrupted (3x 30 s, 6000 s^{-1}, Precellys, PeqLab, Erlangen, Germany) with 30 s cooling breaks on ice in between runs. Cell debris was removed by centrifugation (8,000 ×*g*, 3 min, 4 °C). The resulting supernatant was used for determination of enzyme activities.

Phosphofructokinase was assayed using coupling to pyruvate kinase and lactate dehydrogenase [88]. The reaction mix (1 mL) contained 100 mM Tris-HCl (pH 7.8), 5 mM ATP, 20 mM PEP, 20 mM F6P, 1 mM NADH, 5 mM $MgCl_2$, 1 U pyruvate kinase, 1 U lactate dehydrogenase, and 100 µL cell extract. Malic enzyme activity was assayed using a reaction mix (1 mL) that contained 100 mM Tris-HCl (pH 7.8), 1 mM $NADP^+$, 40 mM sodium malate, 5 mM $MgCl_2$, and 100 µL cell extract [89]. In a parallel set-up, $NADP^+$ was replaced by an equimolar amount of NAD^+. Isocitrate dehydrogenase activity was determined using a reaction mix (1 mL) that contained 100 mM Tris-HCl (pH 7.8), 1 mM $NADP^+$, 5 mM $MgCl_2$, 40 mM isocitrate, and 100 µL cell extract [90]. Fructose 1,6-bisphosphatase activity was coupled to glucose 6-phosphate isomerase and glucose 6-phophate oxidase. The reaction mix (1 mL) contained 100 mM Tris-HCl (pH 7.8), 1 mM $NADP^+$, 5 mM $MgCl_2$, 20 mM Fructose 1,6-bisphospahte, 10 U glucose 6-phosphate isomerase, 10 U glucose 6-phophate oxidase and 100 µL cell extract. Enzyme activity was monitored at 28 °C via the change of absorbance at 340 nm. Phosphoketolase activity was assayed by transforming acetyl phosphate into its corresponding hydroxamic acid form. The hydroxamate was quantified by using complex formation with ferrous iron [91]. Reactions were carried out in 200 µL aliquots of reaction mix containing 100 mM Tris-HCl (pH 7.8), 20 mM F6P, or F6P and GAP, 0.5 mM thiamine pyrophosphate, 5 mM $MgCl_2$ and 20 µL cell extract. Aliquots were incubated at 28°C. After each time interval one aliquot was mixed with 100 µL 2 M hydroxylamine solution (pH 7.0) and subsequently incubated for 10 min at room temperature. After incubation 600 µL of 50 % (V/V) mixture of 2.5 % (m/V) $FeCl_3$ in 2 M HCl and 10 % (m/V) trichloroacetic acid was added. Absorption was measured at 540 nm and concentrations were calculated according to calibration with synthetic acetyl phosphate treated equal to reaction mixtures. KDPG aldolase was assayed by coupling its activity with lactate dehydrogenase [12]. The reaction mix (1 mL) contained 100 mM Tris-HCl (pH 7.8), 1 mM NADH, 5 mM $MgCl_2$, 20 mM KDPG, 10 U lactate dehydrogenase and 100 µL cell extract. Enzyme activity was monitored at 28 °C via the change of absorbance at 340 nm.

The protein concentration in the cell extract was measured using a colorimetric kit (Pierce BCA Protein Assay Kit, Thermo Fisher, Rockford, IL, USA).

Quantification of KDPG.

Metabolite extraction and sampling was performed according to Gläser *et al.*[92]. Prior to metabolite extraction cells were quenched by transferring a culture aliquot of known volume and biomass concentration to a quenching solution (25 mM formic acid in 95 % (V/V) acetonitrile in water) that was kept at -30 °C. The aliquot was added to the quenching solution in a ratio of one part cell suspension and three parts quenching liquid. Subsequently, the quenching mixture was frozen using liquid nitrogen and freeze dried. The dry extract was resuspended in 500 µL 5 mM ammonium carbonate solution that was adjusted to pH 9.2. The insoluble fraction was removed by filtration (0.2 µm, Ultrafree-MC, Merck Millipore, Germany) and the filtrate was used for analysis with LC-MS.

For separation of metabolites a pHILIC column (SeQuant® ZIC®-pHILIC 5µm polymer 150 x 2.1 mm, Merk, Darmstadt, Germany) was used with a gradient of two eluents: Eluent A was composed of 5 mM ammonium carbonate adjusted to pH 9.2. For eluent B acetonitrile was used. The following gradient was applied at a flow rate of 0.3 ml min^{-1} and a column temperature of 25 °C: 0 min 80 % of eluent B, 20 min 20 % eluent B, 21 min to 25 min 5 % eluent B, 28 min to 30 min 80 % eluent B. MS parameters were set to values acquired for synthetic KDPG prior to measurement (KDPG: M1 = 257 , M2 = 97, DP= -4.64 kV, CE= -20.63 kV, CXP= -9.9 kV). For quantification, each measurement batch was run with standards containing known concentrations of synthetic KDPG.

4. Results and discussion

Establishing a cultivation system for ^{13}C metabolic flux analysis.

The basis for flux estimation from labelling data is metabolic steady state of the analysed bacterium. The organisms must be in metabolic and isotopic steady state to obtain labelling data that can be used for computation of metabolic fluxes [72]. Therefore, cultivation of the organisms that is subjected to ^{13}C metabolic flux analysis must fulfil said requirements. Different methods to grow cyanobacteria were tested for their applicability for ^{13}C labelling experiments. A common method to cultivate phototrophs is the use of tubular bioreactors that are operated as bubble columns [45, 93, 94]. Tubular bioreactors with a diameter of 35 mm, filling volume of 250 ml and a gassing rate of 10 sL h^{-1} were tested, since identical dimensions were used by Chen *et al.* [12], being the major reference for the behaviour of the tested strains. Illumination of the tubes was done from opposing sides with 50 µE m^{-2} h^{-1} white light. Cultivation was performed with wildtype and deletion mutant with an interrupted ED pathway (Δ*eda*).

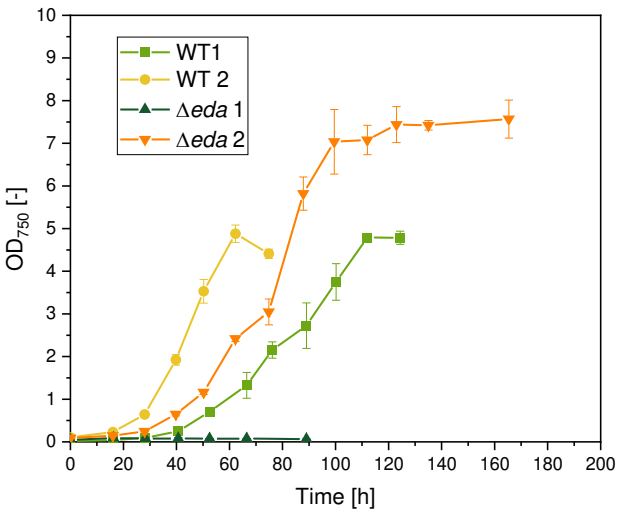

Figure 4.1: Cultivation profile for four different cultivations. Experiments were carried out with two strains grown in tubular bioreactors with a diameter of 3.5 cm, illumination of 50 µE m-2 s-1 and gassing rate of 10 sL h-1 in triplicates.

The resulting cultivation profiles depicted in Figure 4.1 showed poor performance regarding reproducibility. In one case, no growth was observable at all. Most notably, for both strains a dent in the cultivation profile at an OD_{750} of 3.0 was observed, dividing the cultivation into two separate growth phases. Since no differences in preparation of pre cultures or medium were present, performance of cultivation with tubular reactors appeared to cause ambiguous results regarding the overall performance. Alternatively, cultivation was carried out in non-baffled shake flask. For this cultivation system reproducibility higher and deviations between replicates

were smaller in comparison to bubble columns. Still, growth of *Synechocystis* sp. PCC 6803 appeared to be dividable into different sections. As indicated by a green area Figure 4.2, stable growth was between OD_{750} of 0.2 and 5.0.

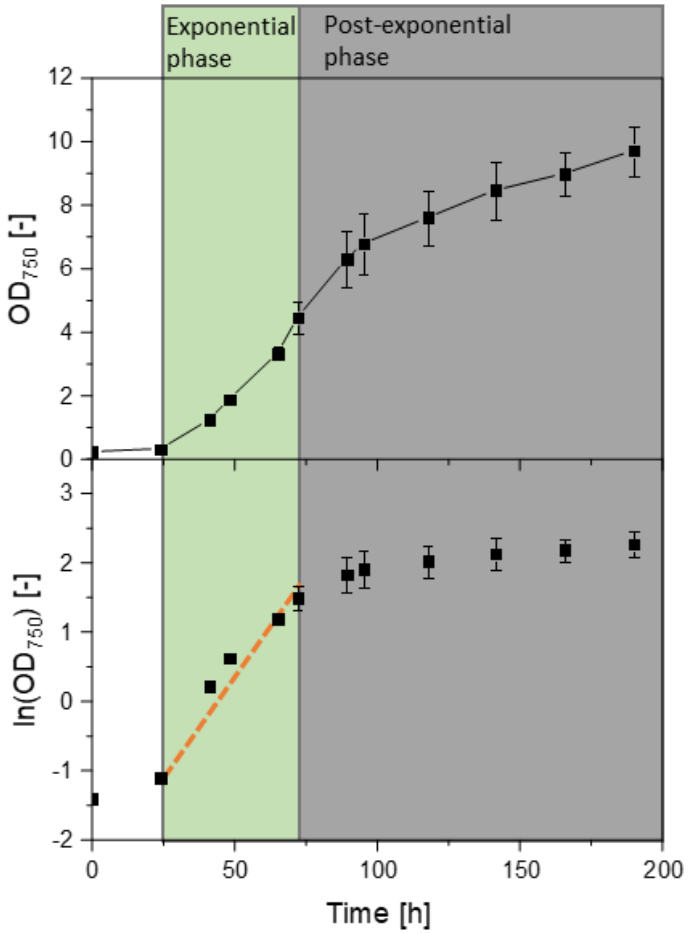

Figure 4.2: Example of a cultivation profile of *Synechocystis* PCC 6803 grown under photomixotrophic conditions. The upper part depicts optical densities. The bottom part shows a semi logarithmic plot with a dashed orange line as reference (μ= 0.052 h^{-1} ± 0.006 h^{-1}). Growth phases are indicated by the following colours and areas: Green= exponential phase, grey= post exponential phase. Depicted are mean values for triplicates.

The semilogarithmic plot indicates the presence of separate growth modes. The change in growth after the culture reaches OD_{750} is obvious and lead to an in-depth analysis of the cultures supply with light.

Light transmission measurements in cultures of *Synechocystis* sp. PCC 6803

To investigate the lighting conditions and thus light supply during cultivation, a series of light intensity measurements was performed. Varying optical densities and light passages were tested for the fraction of light passing through the liquid. Lambert-Beers law as presented in equation 9 gives a correlating for transmission (τ), as function of wavelength (λ) and concentration (c), with concentration of given substance (c), proportionality constant (k) and thickness of light passage (d).

$$\ln(\tau(\lambda, c)) = k * c * d \qquad \text{Eq. 9}$$

Since concentration can be assumed as constant for measurements with known optical density, correlation was performed for transmission and varying layer thickness. Series were measured for optical densities ranging from 0.5 to 5.0 in 0.5 increments (see Figure 4.3 A and B). Measurements yielded slopes that are listed in Table A 1. Correlations for each optical density showed very high statistical probability, thus confirming, that Lamber-Beer´s is a valid model to describe light distributions in the cultivation equipment discussed here. The slopes listed in Table A 1 each describe the nondimensional dependency of light intensity and passage. Introducing a correlation for space dependent slopes and optical densities resulted in a correlation with excellent fit (Figure 4.3 C). Using these correlations, a matrix was derived that depicts light fractions passing through a given layer thickness (from 0 cm to 1 cm) and optical density (from OD_{750} 0.0 to 5.0) (Figure 4.3 D).

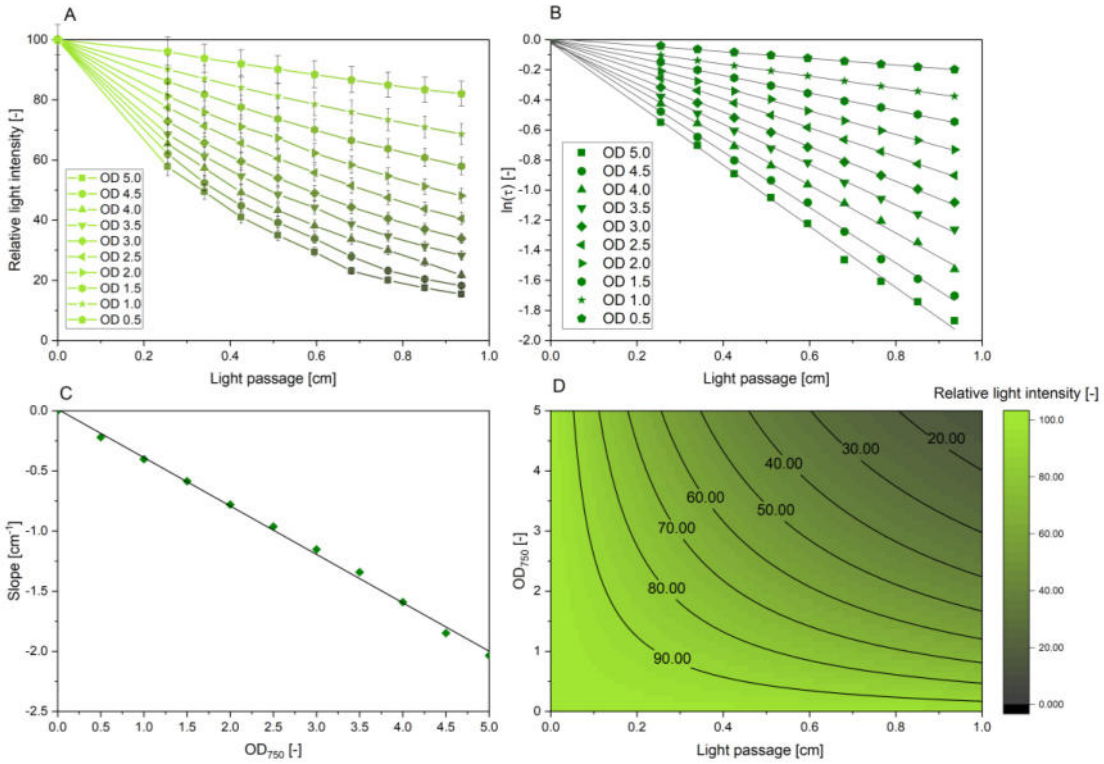

Figure 4.3: Evaluation of optical properties for suspensions of *Synechocystis* sp. PCC 6803 in BG 11 medium: decreasing relative light intensities depending on light passage for cell suspension of *Synechocystis* sp. PCC 6803 in BG11 medium with varying optical densities. B: logarithmic plot of the transmission values obtained from the data depicted in A. Black lines represent linear regressions. The resulting slopes are used in C: Correlation between slopes and optical densities obtained from B. D: Calculated matrix from the combined slopes of B and C. Relative light intensities are encoded in different shades of green, ranging from bright green (100 %) to black (0 %).

Based on transmission measurements, tubular bioreactors and shake flasks were compared for their optical properties and ability to supply cultures with light. The maximum light passage for a 250 mL shake flask with small baffles and a filling volume of 10 % (V/V) as adopted for cultivation was measured with 0.86 cm. The liquid in the flask was treated as a slab of liquid

that is illuminated from the top, translating directly into a one-dimensional decrease of light intensity as presented in Figure 4.3. With a maximum light passage of 0.86 cm, the mean light intensity for the cells is depicted in Figure 4.4 as indicated by an orange line (assuming optimal mixing).

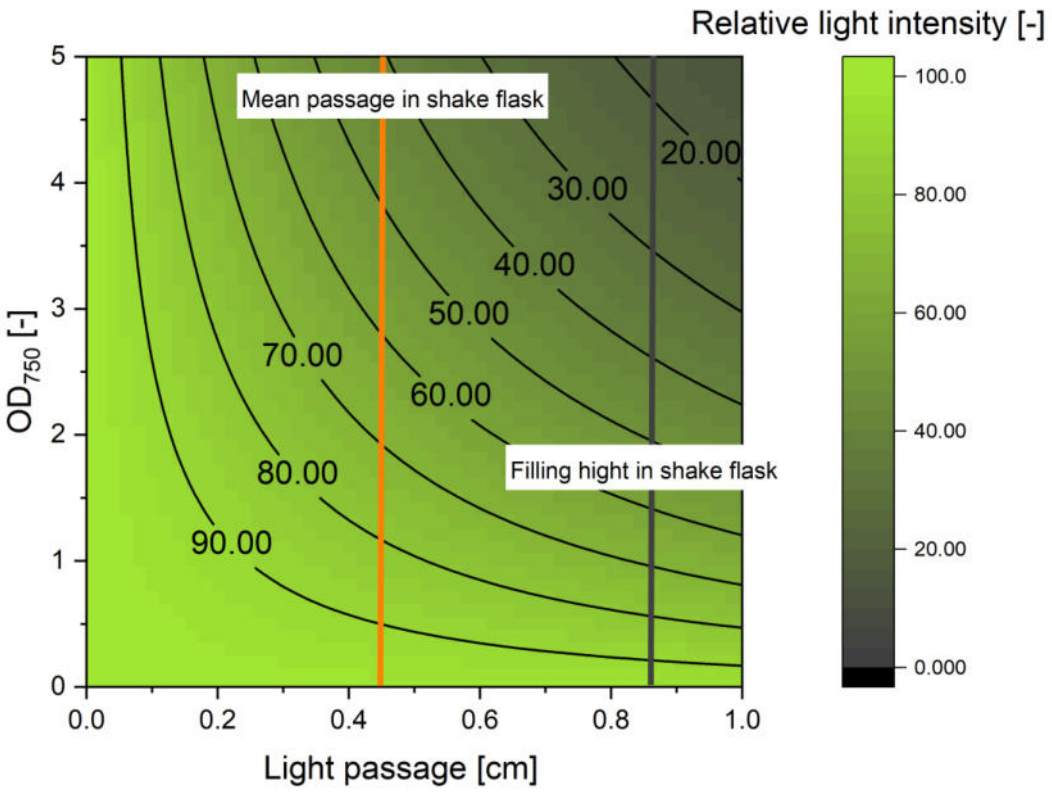

Figure 4.4: Correlation between light intensity, layer thickness and optical density for a cell suspension of *Synechocystis* sp. PCC 6803 in BG11 medium. The orange line indicated the mean light intensity for cultivation using shake flasks with a filling hight of 0.86 cm (grey line).

As indicated by the orange line in Figure 4.4 the relative light intensity that cells encounter in shake flask during cultivation falls below 60 % of the initial light intensity when culture surpass OD_{750} 3.0. Based on this observation, cultivation in shake flasks was limited to optical densities below OD_{750} 3.0, to assure that cells were always encountering light intensities above 60 % of surface lighting intensity. For flux estimation, sampling was further limited to OD_{750} values below 2.0 to assure, that cells were in a state with more than 70 % of initial light intensity. To further minimize any effect on the metabolic state of cells. For direct comparison with tubular bioreactors, slopes obtained from data depicted in Figure 4.3 A and B were used to calculate relative light intensities for a circle with a diameter of 3.5 cm that is illuminated from two sides. The resulting light profiles are depicted in Figure 4.5 and were used as a model for tubular bioreactors.

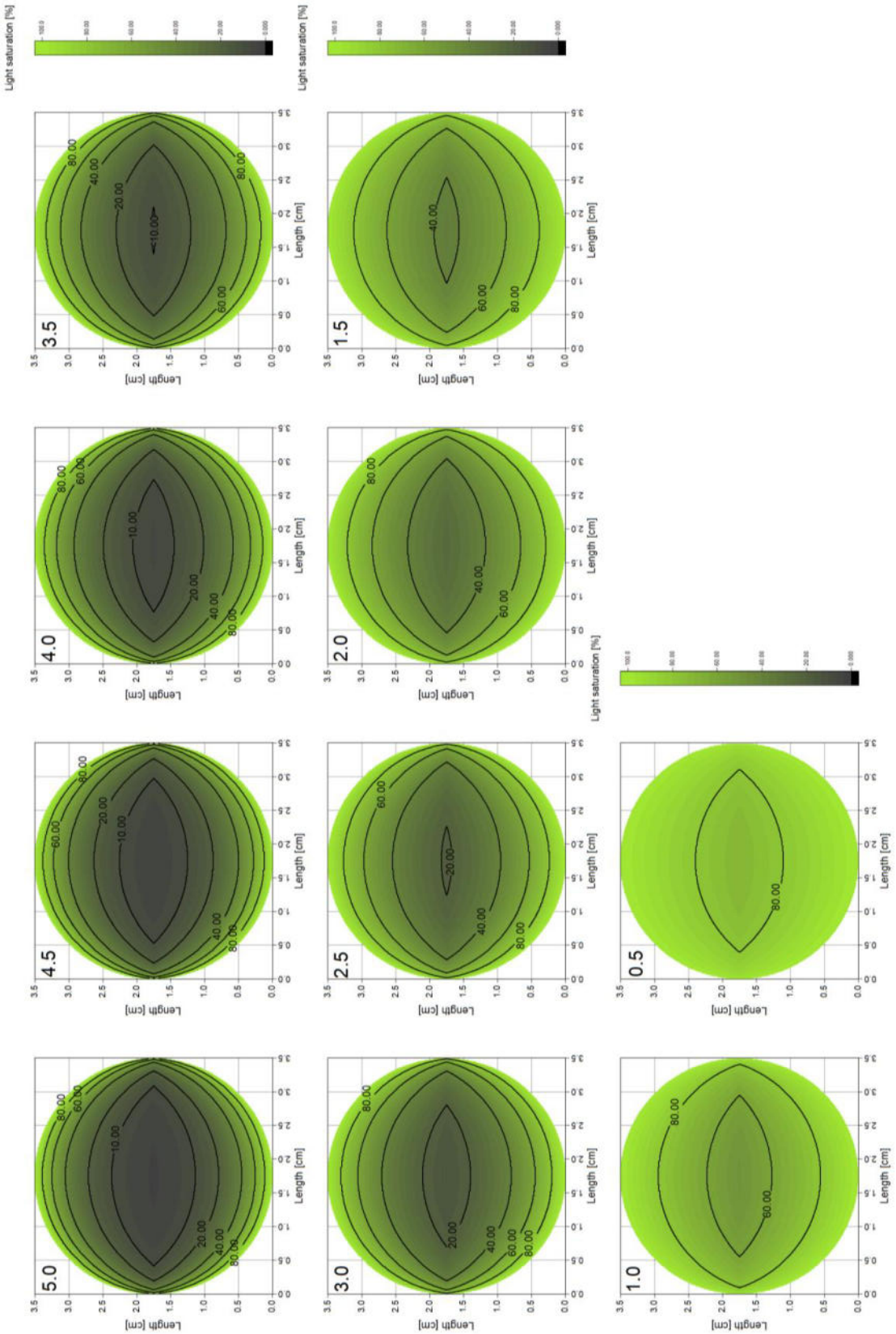

Figure 4.5: Relative light intensity profiles in tubular bioreactors illuminated from two sides. Profiles are given for different optical densities ranging from 0.5 to 5.0. Relative light intensities are encoded in different shades of green, ranging from bright green (100 %) to black (0 %). Values were calculated to a resolution of 0.1 mm.

Resulting profiles show elliptical volume parts with decreasing light intensities inside the tubes. When cultures reach OD_{750} 2.0 parts of the liquid already provide less than 40 % of the initial light intensity to the cells. After further increase of cell concentration to OD_{750} 2.5, inner parts of the liquid have less than 20 % of initial light intensity. For better comparison, the light profiles depicted in Figure 4.5 were used to calculate mean relative light intensity for each cross-section.

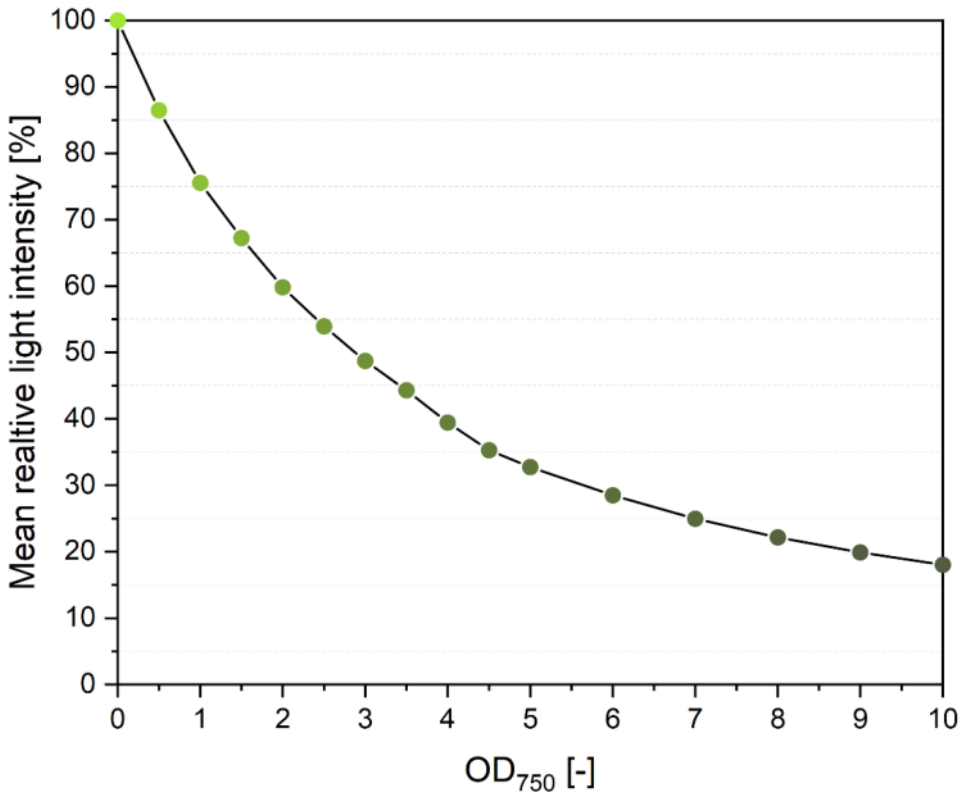

Figure 4.6: Mean values for relative light intensities for dissections of a tubular airlift bioreactor with a diameter of 3.5 cm for different optical densities ranging from 0.0 to 5.0. In 0.5 increments. Mean values were extrapolated to OD 10.0 in 1.0 increments

Mean light intensities for cultures in tubular bioreactors show worse characteristics in comparison to shake flasks. Already at an OD_{750} of 2.0, cells encounter less than 60 % of initial illumination. Not only the optical properties govern the exposure of cells to light, but fluid dynamics must also be considered. The effect of light intensity, mixing or angle of illumination on the growth of phototrophs has been studied extensively [95, 96]. Regarding the results for modelling of light intensities presented here, cultivation in shake flasks showed better characteristics regarding light supply and overall reproducibility. Thus, shake flask cultivation was considered superior to bubble column reactors for conducting tracer experiments and subsequent ^{13}C metabolic flux analysis.

Shake flask geometry.

Besides investigating the physical properties of a cell suspension to absorb light, shake flask geometry and the use of baffled or non-baffled shake flasks was investigated. Time laps videos of particles in different shake flasks showed two-fold short comings of non-baffled smooth walled flasks. First, mixing is insufficient, and second radial laminar flow was observed. In Figure 4.7 the consequence of this laminar flow is depicted. In said figure, illumination of different parts of the liquid is encoded in different shades of green ranging from high light intensity (bright green) to low intensity (dark green). In said figure, beam paths and intensities are not depicting measured values.

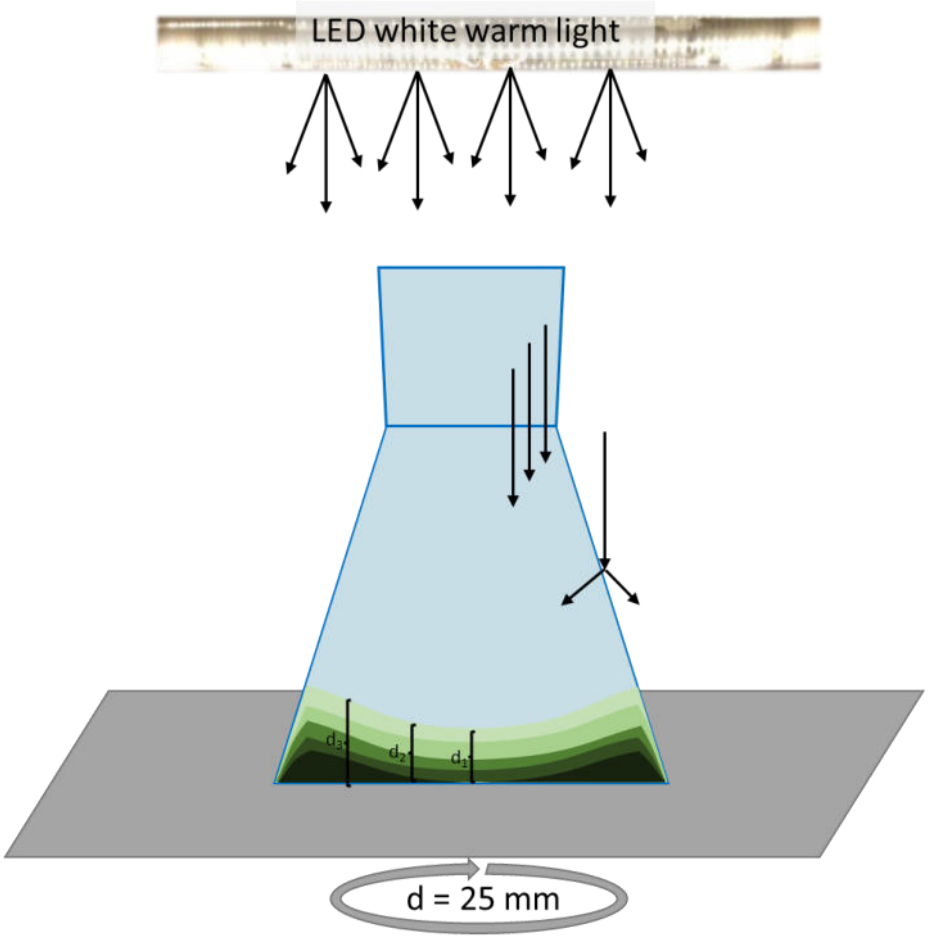

Figure 4.7: Schematic of lighting conditions for cultivation with illumination using shake flasks. The flasks are illuminated from the top with white warm light. Black arrows indicate a selection of beam paths. A cross section of a shake flask is shown that is in the incubator and is shaken with a rotation diameter of 25 mm. Different shades of green indicate parts of the medium with decreasing light intensities. The intensities range from light green = high light intensity to dark green = low intensity. The small numerals $d_{1\text{-}3}$ mark different thickness of the liquid.

Due to the laminar flow, the liquid is forming a concave flow pattern. As indicated by d_1 to d_3 the thickness of the liquid is increasing toward the walls of the flasks. With this increase in layer thickness, it can be assumed that volume parts that are close to the bottom and walls show low light intensity in comparison to other volume parts. Introduction of small baffles on the bottom of the flask showed good mixing and avoiding of laminar flow at moderate shaking

frequency (100 rpm with a diameter of 25 mm). According to literature [97] oxygen transfer rates in baffled shake are superior in comparison to their non-baffled counter parts. With the assumption that carbon dioxide supply is limited by the same underlying kinetics as oxygen, adoption of baffled shake flask also contributed to better supply of cultures with CO_2. Preliminary experiments showed that shake flasks with large baffles that are generated by indentation into the flasks side walls lead to worse growth profiles compared to their non-baffled equivalents (data not shown). The introduction of indentations into the surface of the flasks adds additional complexity to the beam paths during cultivation with light. This is due to additional scattering, refraction, and reflection by introduction of multiple differently angled surfaces. The resulting beam paths are difficult to quantify and describe [95]. For this reason, Figure 4.7 is only giving a schematic overview and is not depicting absolute values. Because of the better performance of the smooth surfaced flasks with baffles on the bottom, this type of flasks was adopted for cultivation. Further improvements to cultivation with these flasks was achieved by opting for transparent lids instead of solid aluminium caps, that caused measurable differences in light intensities inside the flasks, as seen in Figure 4.8. The measurements of local light intensity with different cap configuration confirmed, that the transparent lid allows for better light supply in comparison to solid metal caps.

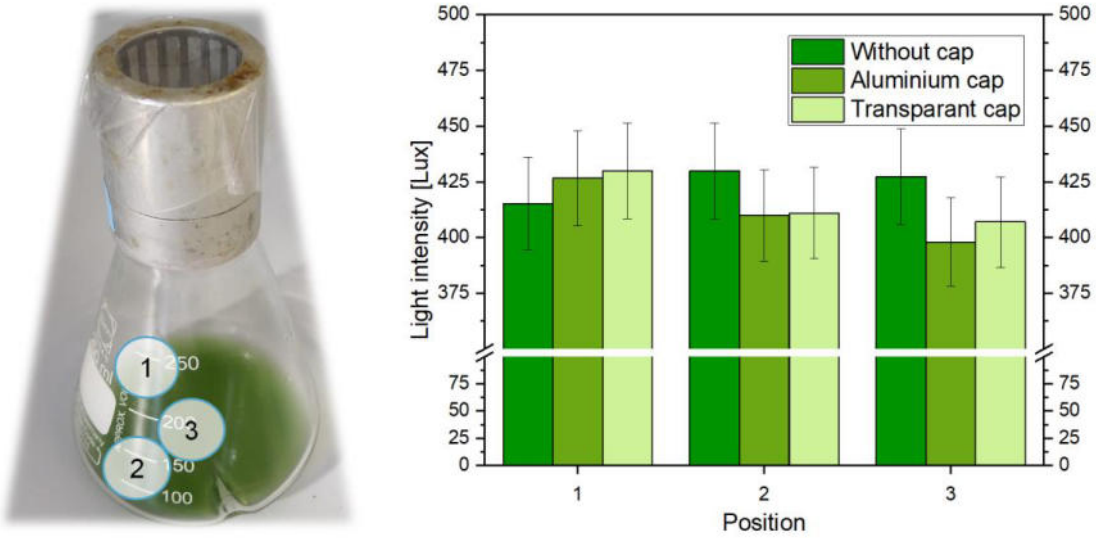

Figure 4.8: Comparison of light intensities for different areas of a shake flask covered without an aluminium cap, with an aluminium cap and with an aluminium cap with a translucent foil. For each position 10 replicates were measured.

The adoption of a transparent lid even improved the light intensity on the outer parts of the cultivation liquid in comparison to no lid. Again, the alteration in beam path by the transparent lid is difficult to quantify and thus the values depicted in Figure 4.8 are the sum of multiple effects. All efforts to optimise light supply and mixing allowed for stable exponential growth

with high reproducibility for cultivation of *Synechocystis* sp. PCC 6803. An example for a cultivation profile with this set up is depicted in Figure 4.9. The optical density is encoded in the colour code used for relative light intensity data.

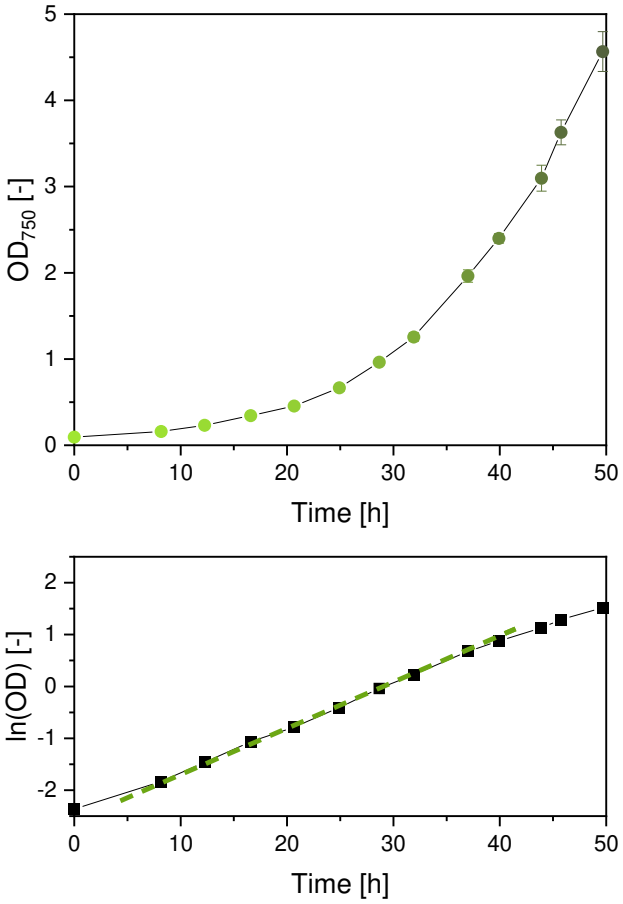

Figure 4.9: Cultivation of *Synechocystis* sp. PCC 6803 in photomixotrophic growth mode with the optimized cultivation setup using smooth walled shake flasks with small baffles and transparent lids. Depicted are triplicates. For this example, the growth rate given by the slope of the green dashed line in the semi-logarithmic plot is 0.085 h^{-1} ± 0.002 h^{-1}.

Exponential phase using this cultivation setup ranged from OD_{750} 0.1 to 3.5, as indicated by the green dashed line in the semi logarithmic plot in Figure 4.9. According to the measurement of light intensities the cultivation window was limited to OD_{750} values below 3.0. Thus, this cultivation setup was used to determine physiological data for different strains of *Synechocystis* sp. PCC 68003 in photomixotrophic and hetero trophic growth mode.

Isotopic steady state

For high precision ^{13}C metabolic flux analysis it must be assured that measured fluxes are obtained from labelling data that solely includes information on the incorporation rate of labelled substrates into biomass constituents. For this reason, the amount of naturally labelled carbon from an initial population of cells used for inoculation needs to be kept at a

minimum [81]. Inoculation with low initial optical densities (below OD_{750} 0.02) resulted in poor reproducibility of physiological parameters. Notably, limiting the maximum optical density of cultivation to below DO_{750} 3.0 limits the maximum "dilution" of initial carbon to 1/30 when cultivation was started with DO_{750} 0.1. Therefore, a two-step cultivation system was designed that was composed of two consecutive cultivations with labelled substrates. In Figure 4.10 the system is represented as a simple scheme.

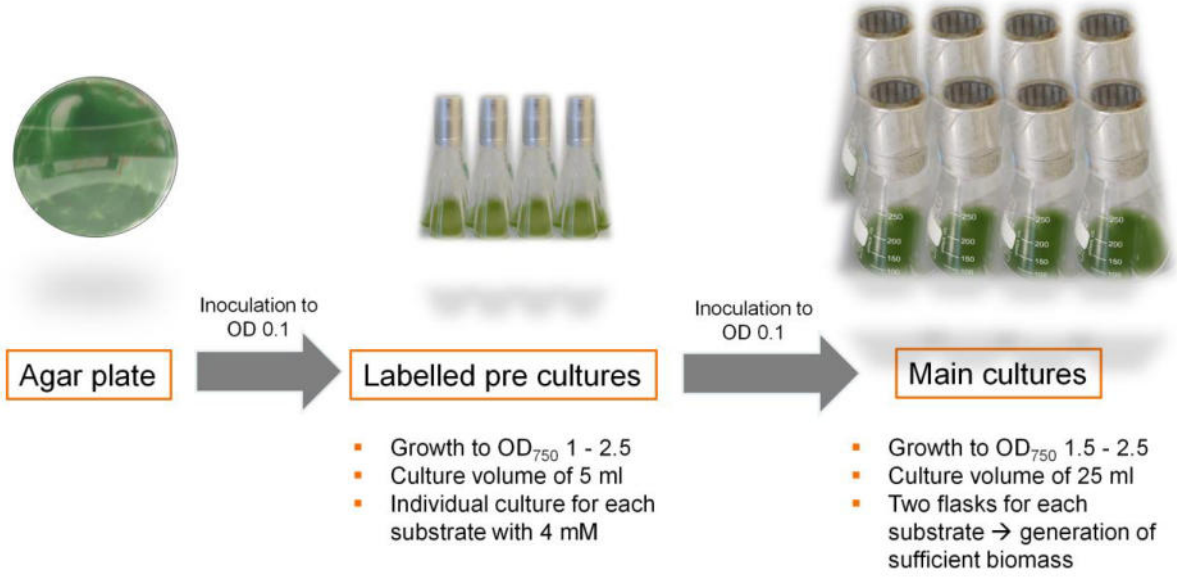

Figure 4.10: Schematic overview on the two-step consecutive cultivation system.

By repeating cultivation with labelled substrates from OD_{750}= 0.1 to OD_{750} > 1.5 the fraction of carbon originating from the initial inoculum of the first cultivation is limited to less than 1 % (mol/mol). Said cultivation system was tested for isotopic steady state. Resulting isotopic fractions for the m+1 fragment of six amino acids is shown in Figure 4.11. Isotopic steady state was confirmed for OD_{750} values ranging from 1.0 to 2.5, fulfilling cultivation range set according to light intensity measurements. Therefore, biomass samples for flux analysis were taken in between these values.

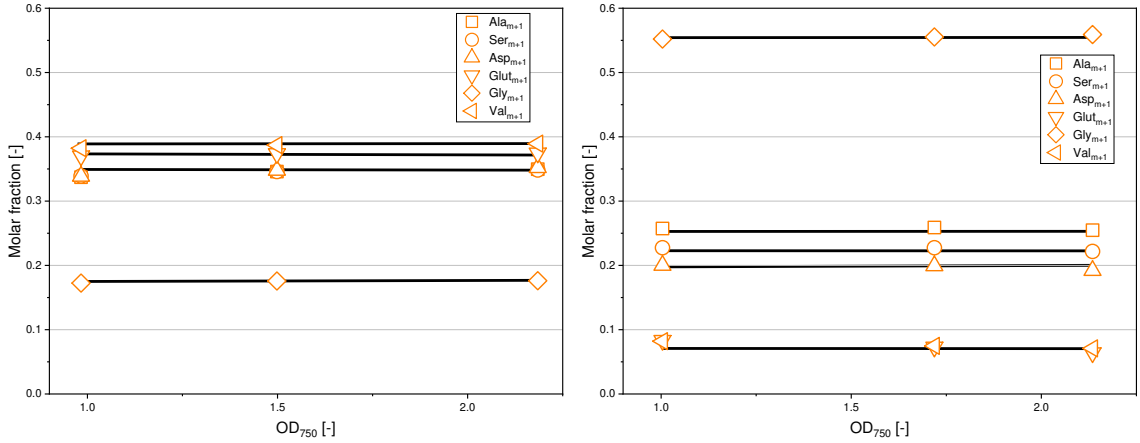

Figure 4.11: Isotopic distributions of different amnio acid fragments for different optical densities of two cultures of *Synechocystis* sp. PCC 6803 grown on [1-^{13}C]-glucose (left) and [$^{13}C_6$]-glucose (right) in photomixotrophic growth mode.

Since light is the limiting factor for the cultivation of *Synechocystis* sp. PCC 6803 in photomixotrophic growth mode, generation of labelled biomass in heterotrophic growth mode was done with the same consecutive labelling experimental setup. Isotopic steady state was confirmed for heterotrophic growth mode, as well.

Photomixotrophic growth of wildtype and mutant strains

After a suitable cultivation system was established that allows for generation of labelled biomass, cultivation of *Synechocystis* sp. PCC 6803 was carried out with this optimised setup. Cultivations were performed for the wildtype (WT), Δ*eda*, Δ*pfk1*/*pfk2* and Δ*xfp1*/*xfp2* in photomixotrophic growth mode. The resulting cultivation profiles are depicted in Figure 4.12.

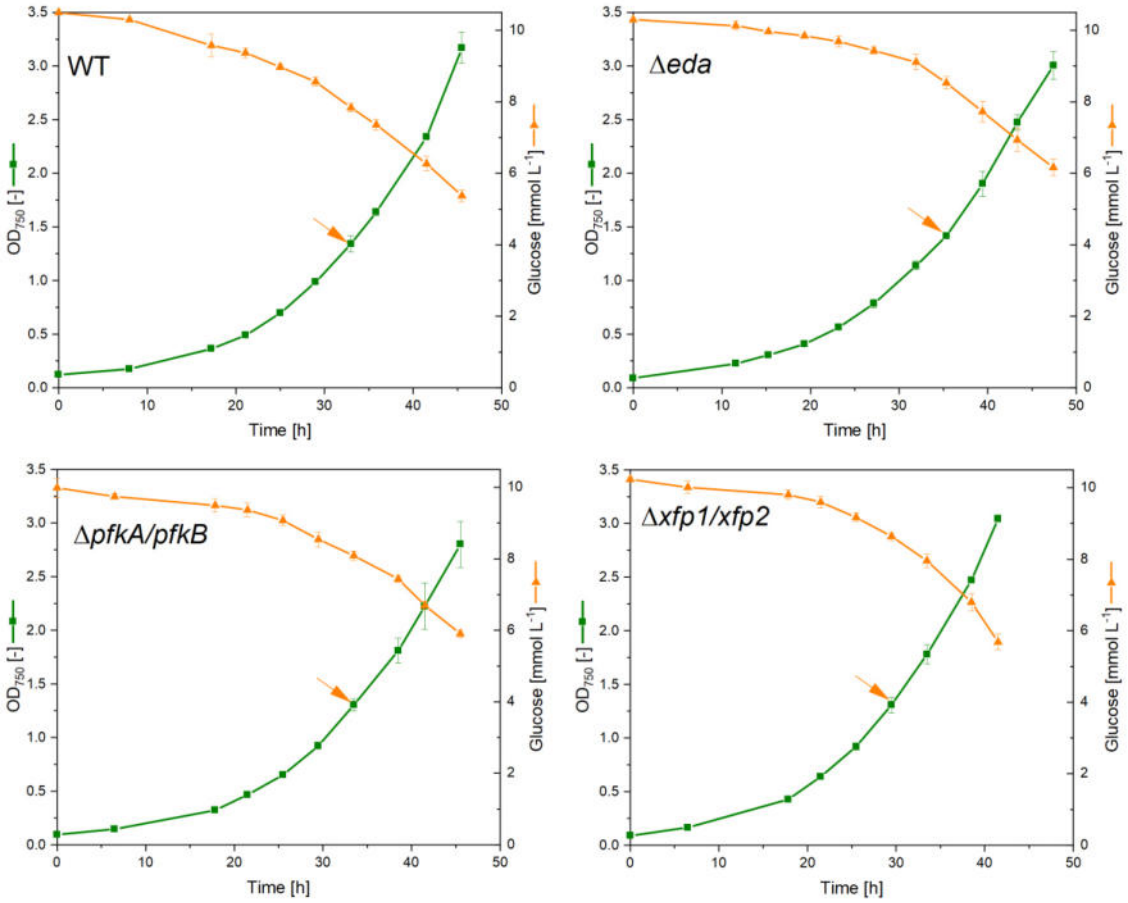

Figure 4.12: Cultivation profiles for *Synechocystis* sp. PCC 6803, Δ*eda*, Δ*pfk1*/*pfk2* and Δ*xfp1*/*xfp* cultivated in photomixotrophic growth mode with 50 µE s^{-1} m^{-2} illumination and atmospheric carbon dioxide supply. Strains were grown as triplicates in shake flasks with small baffles. Depicted are optical density (green squares) and glucose concentration (orange triangles). Orange arrows indicate sampling time points for flux estimation. Resulting growth rates are listed in Table 4.

As seen in Figure 4.12 all four strains showed exponential growth in the optical density range set according to light intensity measurements. None of the strains consumed all the glucose present in the medium and no formation of by-products was detected. In all four cases no prolonged lag phase was present. For all four experiments growth rates, biomass yields, and specific uptake rates were determined. Correlations for determination of biomass yields are shown in Figure 4.13.

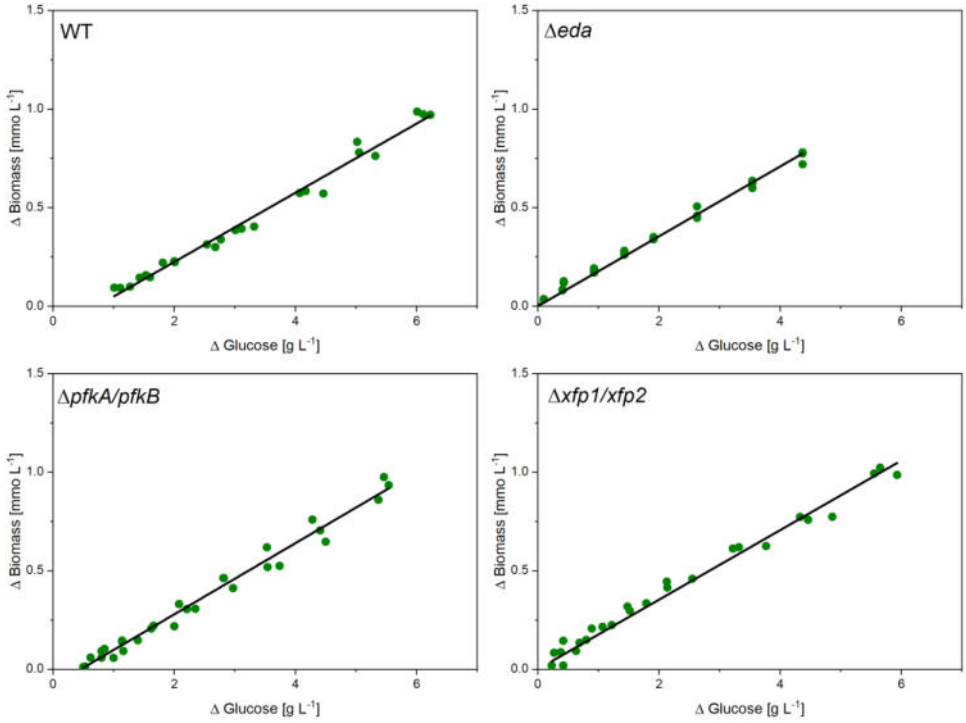

Figure 4.13: Correlations for the determination of biomass yields for *Synechocystis* sp. PCC 6803, Δ*eda*, Δ*pfk1*/*pfk2* and Δ*xfp1*/*xfp2* grown in photomixotrophic growth mode with 50 µE s^{-1} m^{-2} illumination and atmospheric carbon dioxide supply. Cultivations were carried out in triplicates using shake flasks with small baffles.

Figure 4.13 demonstrates for all four strains metabolic steady state. None of the strains showed largely deviating behaviour from wildtype. Obtained yields and rates are summed in Table 4. The listed values represent the part of cultivation in which constant growth was observed.

Table 4: Physiological parameters for four strains of *Synechocystis* sp. PCC 6803 cultivated as triplicates in photomixotrophic growth mode with 50 µE s^{-1} m^{-2} illumination in shake flasks.

Strain	$Y_{X/S}$ [g mol^{-1}]	$Y_{X/S}$ [Cmol $Cmol^{-1}$]	µ [h^{-1}]	q_s [mmol g^{-1} h^{-1}]
Wildtype	183 ± 8	1.171 ± 0.053	0.077 ± 0.002	0.421 ± 0.012
Δ*eda*	177 ± 8	1.129 ± 0.053	0.076 ± 0.002	0.429 ± 0.017
Δ*pfkA/pfkB*	181 ± 8	1.181 ± 0.053	0.077 ± 0.001	0.425 ± 0.011
Δ*xfp1/xfp2*	177 ± 8	1.167 ± 0.054	0.083 ± 0.002	0.468 ± 0.012

Physiological parameters listed in Table 4 show that the cultivated strains did not differ on a large scale from wildtype. Only deletion of both isoforms of phosphoketolase increased growth rate and specific glucose uptake rate. These results contradict observations made for comparative cultivation of wildtype, Δ*eda* and Δ*pfkA*/*pfkA* by Chen *et al.* [12]. They stated that alterations of growth behaviour were present when said strains were cultivated in tubular

bioreactors. These differences may be rooted in the way, cultivation was carried out. During cultivation in shake flask, as the data presented here demonstrates, cells are in metabolic steady state. Sufficient supply with light and gases during the adopted cultivation period was assured and contributes to the absence of large differences in growth behaviour. Cultivation in tubular bioreactor subjects the cells to changes in light intensity that are larger and prevail longer due to worse mixing in comparison to shake flask, as discussed above. To investigate, if genetic perturbations altered the overall composition of the individual strains, elemental composition analysis was carried out. Elemental contents were determined for carbon, hydrogen, and nitrogen. Results are listed in Table 5.

Table 5: Elemental composition for biomass of four different strains of *Synechocystis* sp. PCC 6803 cultivated in photomixotrophic growth mode with 50 µE s^{-1} m^{-2} illumination in shake flasks. Errors were calculated from nine biological replicates for each strain.

Strain	C [% (g/g)]	H [% (g/g)]	N [% (g/g)]
Wildtype	46.1 ± 0.5	7.3 ± 0.2	10.5 ± 0.3
Δ*eda*	45.9 ± 0.5	6.6 ± 0.2	9.4 ± 0.8
Δ*pfkA/pfkB*	47.0 ± 0.5	6.7 ± 0.2	9.6 ± 0.4
Δ*xfp1/xfp2*	47.5 ± 0.5	6.6 ± 0.2	9.6 ± 0.4

The determination of elemental composition confirmed the observation made for other physiological parameters, that deletion mutants do not differ on a large scale in their physiology from wildtype under the tested conditions. Determining elemental compositions allowed for calculation of carbon yields. They indicate that photomixotrophic growth combines simultaneous incorporation of glucose and CO_2, because carbon yields exceed values of one mole cellular carbon per carbon mole of glucose. Carbon yields did not differ from wildtype either. Cultivation experiments performed for photomixotrophic growth demonstrate the high reproducibility and consistency of the cultivation system described above. In general, deviations for each data set are lower in comparison to cultivation in bubble columns and assure a high quality of labelling data.

Heterotrophic growth of wildtype and mutant strains

Since *Synechocystis* sp. PCC6803 can grow in heterotrophic growth mode [98] the optimised cultivation setup was used to investigate growth characteristics of *Synechocystis* sp. PCC 6803 and deletion mutants Δ*eda*, Δ*pfkA*/*pfkB* and Δ*xfp1*/*xfp2* under heterotrophic conditions [40]. During heterotrophic growth of *Synechocystis* sp. PCC 6803 glucose was supplied in the medium and cultivation was carried out without illumination except for exposure to light for 5 min per day. It is stated in the literature that cells need to be illuminated with blue light once per day to maintain growth [98]. Cultivation of *Synechocystis* sp. PCC 6803 and deletion mutants Δ*eda*, Δ*pfkA*/*pfkB* and Δ*xfp1*/*xfp2* resulted in the profiles depicted in Figure 4.14. In

comparison to cultivation in photomixotrophic growth mode, growth rates were lower, and the cultivation window was not limited due to the absence of light and all its implications. Still, optical densities did not exceed values above OD_{750} 2.5. Cultivation time was prolonged, deviations for triplicates also increased.

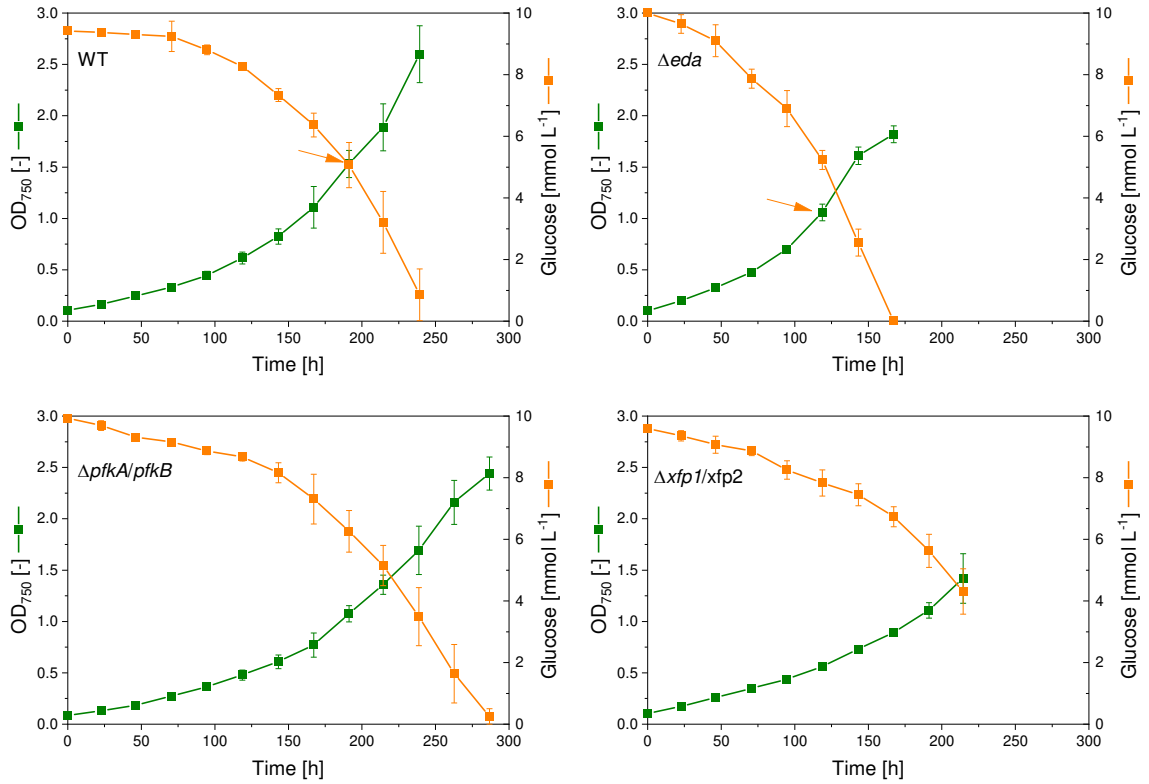

Figure 4.14: Cultivation profiles for *Synechocystis* sp. PCC 6803, Δ*eda*, Δ*pfk1*/*pfk2* and Δ*xfp1*/*xfp* in heterotrophic growth mode. Depicted are optical density (green squares) and glucose concentration (orange triangles). Profiles were obtained from triplicates cultivated using baffled shake flasks. Resulting growth rates are listed in Table 6. Orange arrows indicate sampling time points for flux estimation.

Opposite to cultivation in photomixotrophic growth mode, differences between mutant strains and wildtype *Synechocystis* sp. PCC 6803 were observed. None of the genetic permutations disabled growth under heterotrophic growth regime. Physiological parameters were determined for the cultivation profiles obtained for heterotrophic growth. Correlations for determination of biomass yield are shown in Figure 4.15.

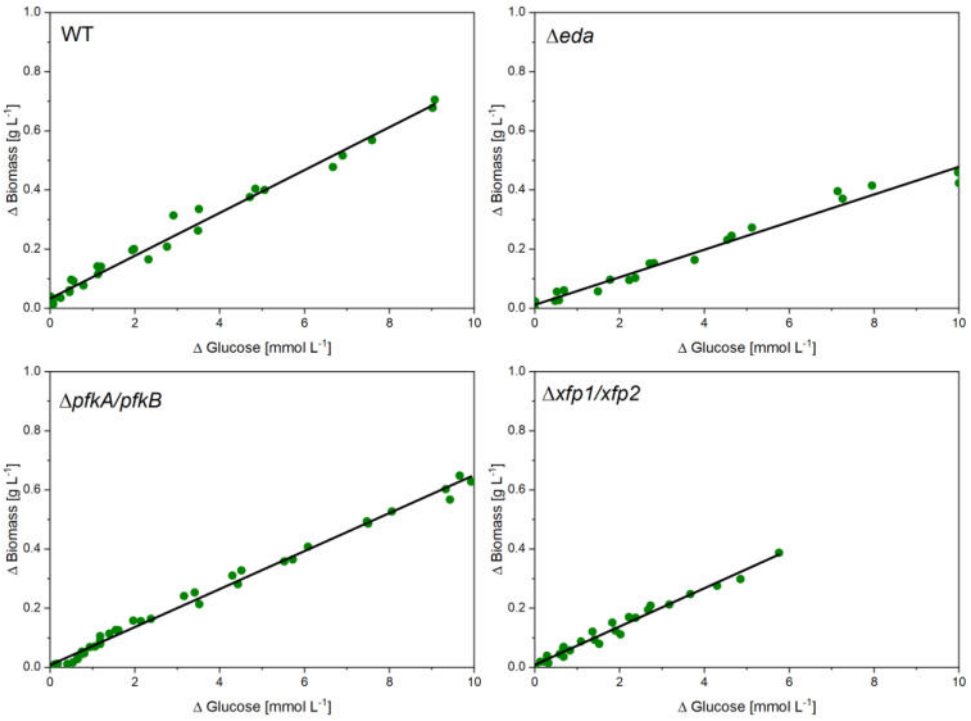

Figure 4.15: Correlations for the determination of biomass yields for *Synechocystis* sp. PCC 6803, Δ*eda*, Δ*pfk1*/*pfk2* and Δ*xfp1*/*xfp* grown in heterotrophic growth mode. Cultivations were carried out in triplicates using baffled shake flasks.

Figure 4.15 shows, as in case of cultivations for photomixotrophic growth, that metabolic steady state was present between OD_{750} 0.1 to 1.5. The resulting physiological parameters are listed in Table 6. Listed are biomass yields, growth rates and specific rates for glucose uptake.

Not only growth rates are smaller in comparison to experiments performed for photomixotrophic growth, but biomass yields decreased as well. The latter already indicates that under the absence of light, carbon dioxide is not fixed on a major scale. Comparing mutants to wildtype strain of *Synechocystis* sp. PCC 6803, major differences can be observed. Interruption of the ED pathway by deletion of KDPG aldolase (Δ*eda*) caused alteration of growth behaviour. Growth rate was increased and a drop in biomass yield was observed. This may indicate a contribution of the ED pathway to heterotrophic growth. Most notably, deletion of phosphofructokinase caused no macroscopic alteration of physiology at all. At first glance, this is surprising, since this enzyme contributes to the EMP pathway that can be expected to be one of the major contributors to heterotrophic metabolism, as it is the case for other heterotrophs [55, 56, 66].

Table 6: Kinetics and stoichiometry of wildtype and deletion mutants of Synechocystis sp. PCC 6803 grown as triplicates in heterotrophic growth mode. The table lists biomass yield ($Y_{X/S}$), specific growth rate (μ) and specific glucose uptake rate (q_s) obtained from parallel experiments (n= 3).

Strain	$Y_{X/S}$ [g mol^{-1}]	μ [h^{-1}]	q_s [mmol g^{-1} h^{-1}]
Wildtype	64.1 ± 2.1	0.013 ± 0.001	0.203 ± 0.007
Δ*eda*	49.3 ± 1.4	0.017 ± 0.001	0.345 ± 0.010
Δ*pfkA/pfkB*	64.1 ± 0.4	0.013 ± 0.001	0.203 ± 0.002
Δ*xfp1/xfp2*	65.9 ± 1.3	0.010 ± 0.001	0.152 ± 0.002

Deletion of phosphoketolase altered growth characteristics during heterotrophic growth. In contrast to Δ*eda* the mutant Δ*xfp1*/*xfp2* showed decreased growth rate but no alteration of biomass yield. Overall, difference between mutants and wildtype showed more diversity in comparison to photomixotrophic growth mode. Analysing wildtype and Δ*eda* for *in vivo* fluxes for this growth mode promised to contribute to the understanding of the role of the ED pathway for the central metabolism of *Synechocystis* sp. PCC 6803.

Model optimisation

Analysis of the metabolic network for possible activity of ED pathway and optimal experimental setup

Before conducting labelling experiments, model topology and experimental setups were subjected to an extended *in silico* analysis. Starting with the metabolic network itself, modelling independent of experimental data was performed by using elementary flux modes. Stoichiometric analysis of the metabolic model was identification of potential pitfalls and a rough estimation if the ED pathway could potentially play a role for the analysed growth modes. A stoichiometric model (see Appendix) representing the core metabolism of *Synechocystis* sp. PCC 6803 as shown in Figure 2.2 was thus implemented into the software tool EFM-tool [80]. Calculation of elementary flux modes (EFMs) allowed for a rough estimation to what extent the ED pathway can contribute to heterotrophic and photomixotrophic growth mode. Since the aim of this work was the resolution of the metabolic network using ^{13}C metabolic flux analysis, hetero trophic and photomixotrophic growth modes were analysed. In both cases, steady state was observed during the consumption of glucose as seen in Figure 4.13 and Figure 4.15.

Processing the model in photomixotrophic growth mode resulted in more than three thousand EFMs, including modes that did not include carbon fixation or glucose uptake. Because the model did not limit photon uptake, EFMs were calculated that describe metabolic states in which only neglectable amounts of glucose are consumed, *de facto* describing autotrophic growth. EFMs with biomass yield exceeding 2.0 g mmol^{-1} were subsequently excluded from further investigation. Resulting fluxes were normalized to glucose uptake to be directly

comparable to flux distributions obtained from ^{13}C metabolic flux analysis. This resulted in a total number of 2400 flux vectors. They are depicted in Figure 4.16 as relative fluxes through the ED pathway in comparison to biomass yields. In this figure the number of EFMs for photomixotrophic growth was further reduced by limiting the maximum biomass yield to less than 0.9 g mmol^{-1}. This limitation was included to further discriminate against EFMs that included glucose uptake rates that were marginal in comparison to carbon fixation. Limiting to biomass yields to 0.9 g mmol^{-1} was still almost 10-fold the value of measured biomass yields from experimental data (compare Table 4).

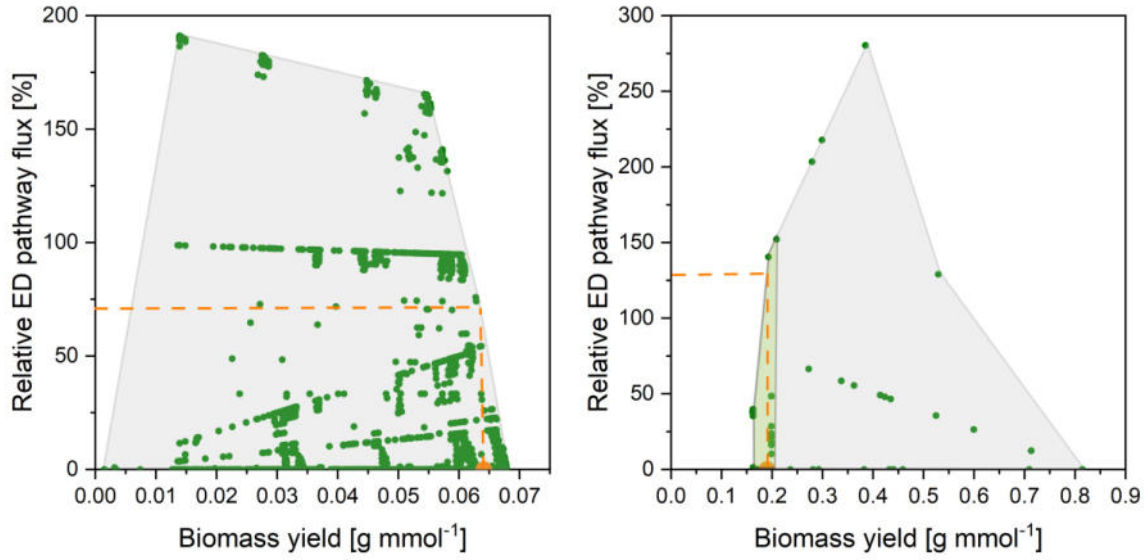

Figure 4.16: Yield space for biomass formation depending on the relative flux through the ED pathway for Synechocystis sp. PCC 6803 in photomixotrophic growth (right) and heterotrophic growth (left). The biomass yield was limited to less than 0.9 g_{CDW} mmol^{-1}. Orange dotted lines indicate experimentally determined biomass yields.

For heterotrophic growth, the number of calculated flux modes yielded about 5500 possible flux distributions. Limiting the biomass yield of these results was not necessary, since the model for heterotrophic growth did not include generation of reducing equivalents from light energy, and thus did not allow for high activity of the CBB cycle.

In both cases flux modes were calculated with high possible activity of the ED pathway. The number of possible flux values for photomixotrophic metabolism was less in comparison to the heterotrophic model. EFMs obtained for photomixotrophic growth that are in the range of experimentally determined biomass yields show that it is stoichiometrically possible, that the ED pathway may be active when the cell is provided with glucose and light. This strongly justified conducting ^{13}C flux analysis to clarify, which one of the metabolic possibilities is present *in vivo* during photomixotrophic growth. For biomass yields that are exceeding experimentally obtainable biomass yields, a negative correlation between biomass yield and

ED pathway activity is present. The stoichiometric model did not account for enzyme and transport kinetics, which is a possible reason why flux modes were calculated that exceed physiologically observable biomass yields for photomixotrophic growth mode. Carbon fixation by photosynthesis in general is slow and a continuous objective for strain improvement strategies [99, 100]. The stoichiometric analysis for photomixotrophic growth presented here demonstrates that the general biochemical potential hidden in the central metabolism of this microbe is far from exploited.

Elementary flux modes obtained for heterotrophic growth yielded a larger variety of possible ED pathway contributions. In general, a negative correlation between biomass yield and ED pathway activity is present. Maximum biomass yields are almost identical to the values obtained from cultivations with the same growth mode. Since experimentally determined biomass yield are close to the stoichiometric maximum it can be expected that the ED pathway contribution to the central metabolism is rather small, as suggested in literature [79]. Again, performing high precision ^{13}C metabolic flux analysis is necessary to resolve the actual *in vivo* flux distribution present in this growth mode.

Resolution power of different tracer setups for photomixotrophic metabolism

The metabolic network as shown in Figure 2.2 contains a high number of interwoven pathways. The consequence for modelling is well demonstrated by the enormous number of EFMs obtained for the described metabolic network. For ^{13}C metabolic flux analysis further imponderabilities are present due to reactions connecting the CBB cycle and the PP pathway. The inclusion of fructose-bisphosphate aldolase activity that forms S7P from E4P and DHAP differentiates the core metabolism of phototrophs from heterotrophic organisms. Because this reaction introduces a new reaction to the PP pathway, it directly contributes to an increase in possible permutations of carbon rearrangement in both pathways. This drastically increases the amount of information needed to resolve these reactions. For flux estimation this means that reactions involving either F6P or S7P are not resolved if insufficient labelling data is used for flux estimation. The metabolic network created for flux estimation was therefore used to investigate the optimal experimental setup regarding the number of parallel tracer experiments and choice of analysis methods. For this purpose, an OpenFlux building function was used to simulate labelling data for several experimental set ups, as demonstrated for *Pseudomonas putida* [51]. Flux distributions used for this simulation was based on physiological data and literature examples [82, 101, 102]. Using the stoichiometric matrix of the model, different scenarios were created with low (5%), medium (25 %) and high (50 %) activity of both, ED pathway and PK pathway. From these scenarios hypothetical labelling data sets were calculated and subsequently used for flux estimation. Simulations were carried out for GC-MS data for amino acids [68, 71], amino acids and sugars [51, 103], GC-MS and NMR [104, 105]

measurements for amino acids , and GC-MS data for amino acids and sugars with inclusion of NMR data for amino acids. The resolution capabilities were tested by flux estimation and 100 runs of Monte-Carlo simulation based on simulated isotopic distributions. Results of the Monte-Carlo simulations are shown in Figure 4.17, Figure 4.18 and Figure 4.19 for six core metabolic pathways of *Synechocystis* sp. PCC 6803.

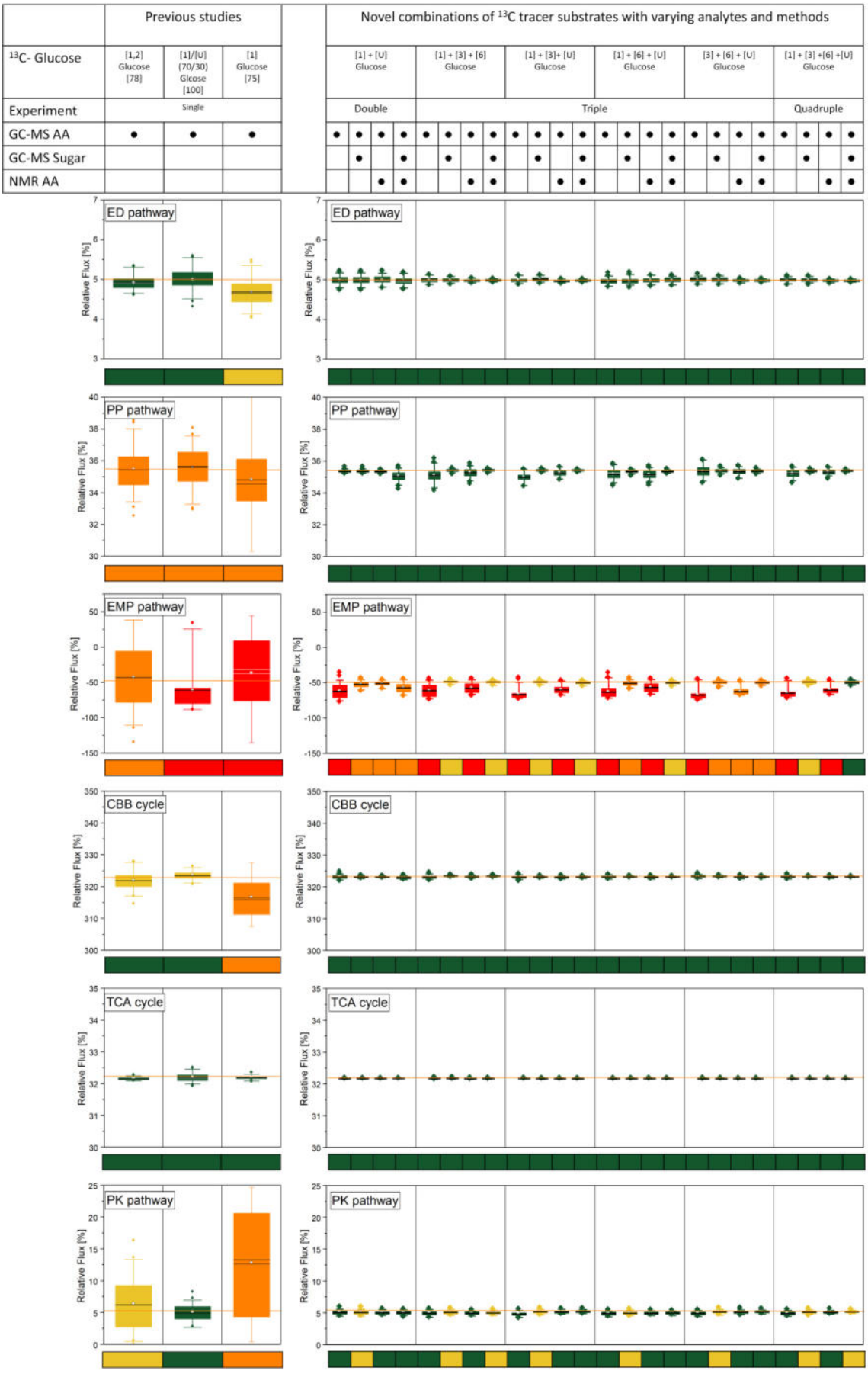

Figure 4.17: Comparison of fluxes for six different pathways of the central carbon metabolism of *Synechocystis* sp. PCC 6803 using different tracer substrate combinations and different analytes. Fluxes were obtained from 100 iterations of Monte-Carlo simulation based on isotopic distributions simulated with a hypothetical flux distribution that assumes ED and PK pathway fluxes of 5 %. Shown are box-whiskers plots for single tracer substrates with [1,2-13C]- glucose ([1,2]), a mixture of [1-^{13}C$_6$] and [^{13}C$_6$] glucose in a ratio of 70:30, [1-^{13}C] glucose, a two substrate experiment with [1-13C] and [U-13C], all possible triplet permutations of [1-^{13}C], [3-^{13}C] , [6-^{13}C] and [^{13}C$_6$], and four parallel tracer experiments with [1-^{13}C], [3-^{13}C] , [6-^{13}C] and [^{13}C$_6$] glucose. Simulations were carried out with information for GC-MS based amino acid labelling (AA), GC-MS based data of amino acid and sugar labelling (AA + Carb), a combination of NMR and GC-MS analysis of amino acids (AA + NMR) and the combination of labelling data obtained with GC-MS data for amino acids and sugars and NMR data for amino acids (Full). Boxes represent the 25 % to 75 % quartiles; whiskers indicate the 1.5 interquartile range and line and circle indicate the mean value of the flux distribution obtained from 100 iteration of Monte-Carlo simulation. Outliners are represented as small rhombuses. Deviation of mean flux from original values are encoded in colours: red: >10 %, orange <10 %, yellow: <1.0%, green: <0.1%

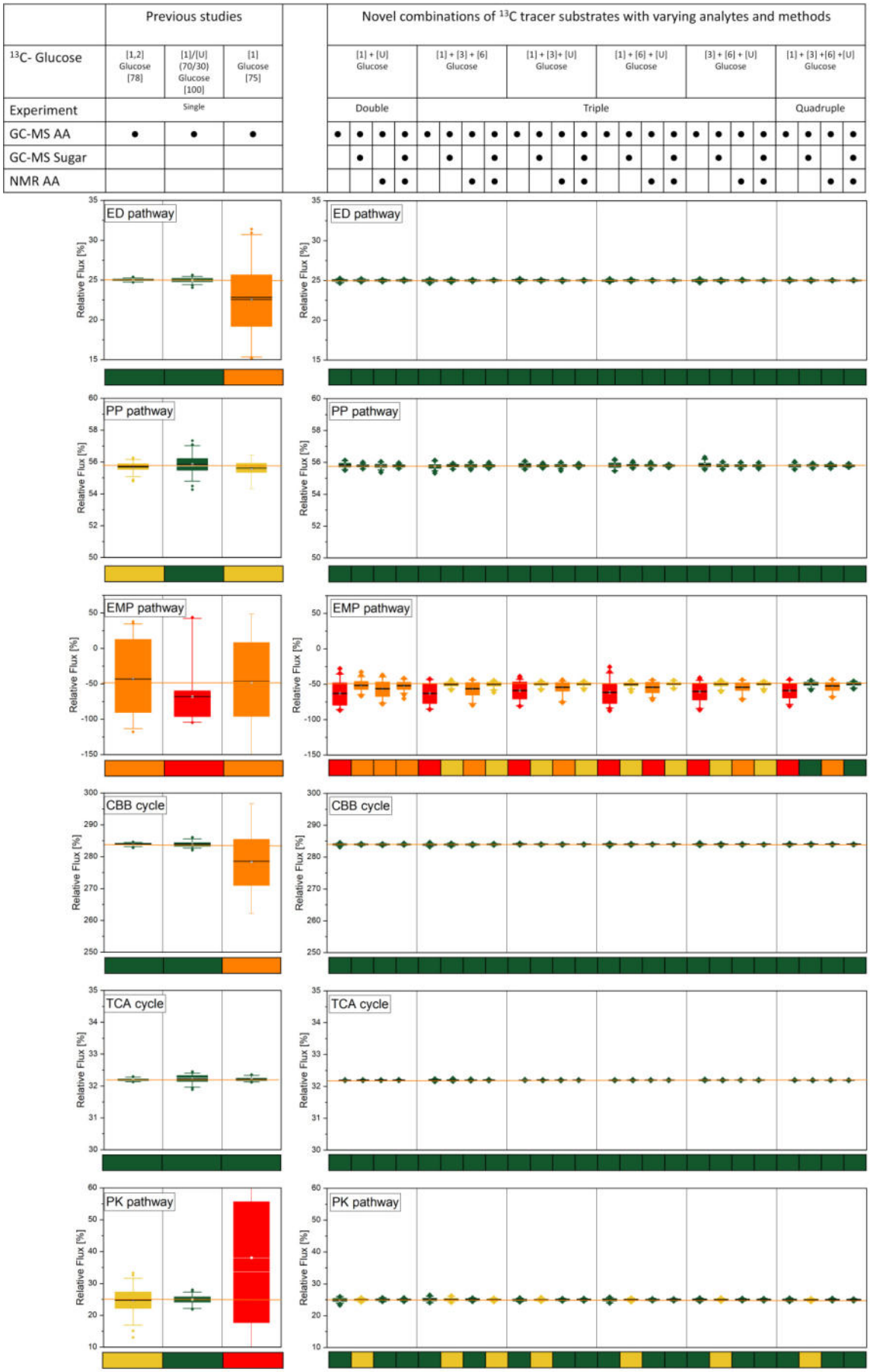

Figure 4.18: Comparison of fluxes for six different pathways of the central carbon metabolism of *Synechocystis* sp. PCC 6803 using different tracer substrate combinations and different analytes. Fluxes were obtained from 100 iterations of Monte-Carlo simulation based on isotopic distributions simulated with a hypothetical flux distribution that assumes ED and PK pathway fluxes of 25 %. Shown are box-whiskers plots for single tracer substrates with [1,2-13C]- glucose, a mixture of [1-^{13}C$_6$] and [^{13}C$_6$] glucose in a ratio of 70:30, [1-^{13}C] glucose, a two substrate experiment with [1-13C] and [U-13C], all possible triplet permutations of [1-^{13}C], [3-^{13}C] , [6-^{13}C] and [^{13}C$_6$], and four parallel tracer experiments with [1-^{13}C], [3-^{13}C] , [6-^{13}C] and [^{13}C$_6$] glucose. Simulations were carried out with information for GC-MS based amino acid labelling (AA), GC-MS based data of amino acid and sugar labelling (AA + Carb), a combination of NMR and GC-MS analysis of amino acids (AA + NMR) and the combination of labelling data obtained with GC-MS data for amino acids and sugars and NMR data for amino acids (Full). Boxes represent the 25 % to 75 % quartiles; whiskers indicate the 1.5 interquartile range and line and circle indicate the mean value of the flux distribution obtained from 100 iteration of Monte-Carlo simulation. Outliners are represented as small rhombuses. Deviation of mean flux from original values are encoded in colours: red: >10 %, orange <10 %, yellow: <1.0%, green: <0.1%

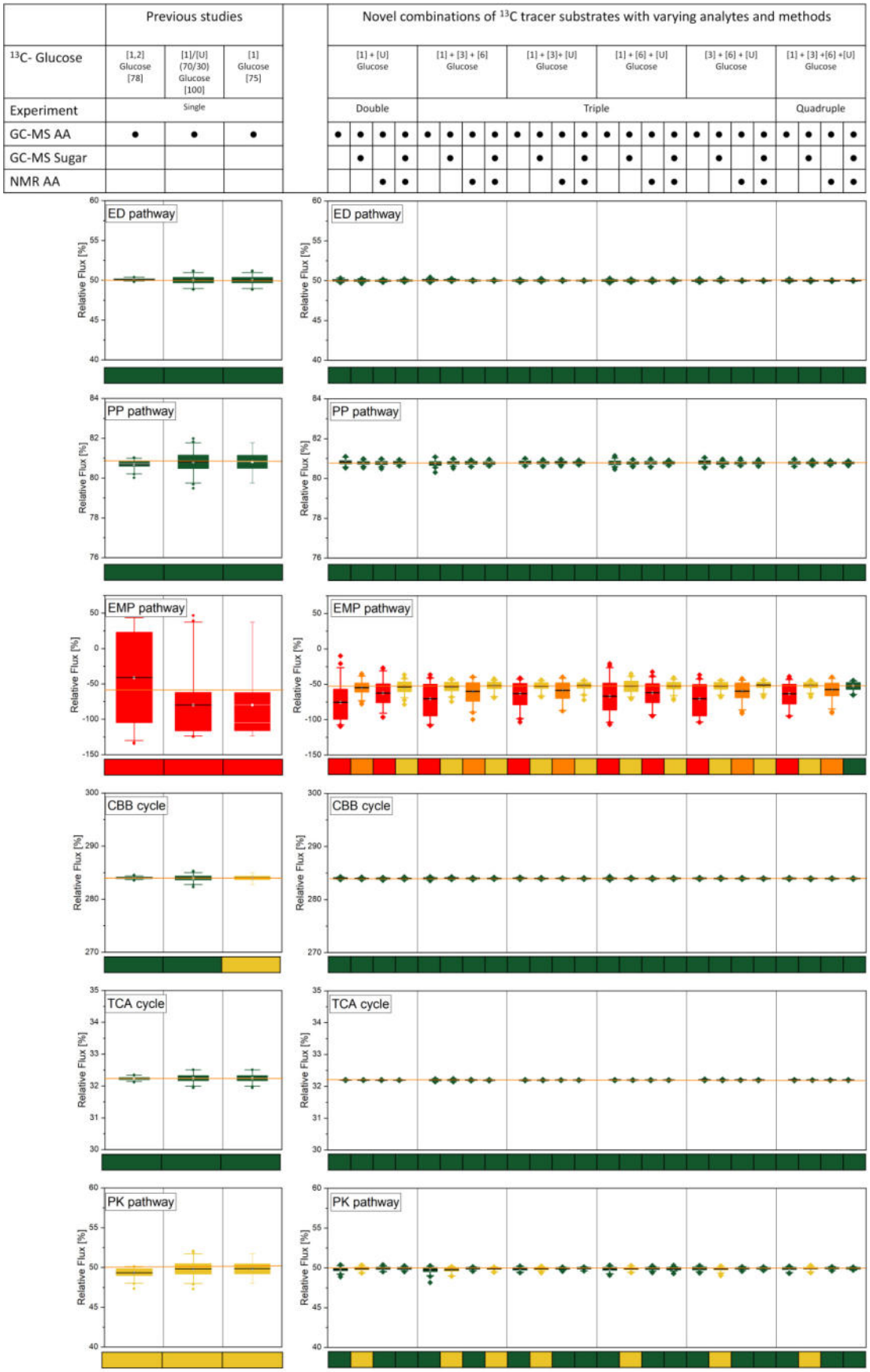

Figure 4.19: Comparison of fluxes for six different pathways of the central carbon metabolism of *Synechocystis* sp. PCC 6803 using different tracer substrate combinations and different analytes. Fluxes were obtained from 100 iterations of Monte-Carlo simulation based on isotopic distributions simulated with a hypothetical flux distribution that assumes ED and PK pathway fluxes of 50 %. Shown are box-whiskers plots for single tracer substrates with [1,2-^{13}C]- glucose, a mixture of [1-^{13}C$_6$] and [^{13}C$_6$] glucose in a ratio of 70:30, [1-^{13}C] glucose, a two substrate experiment with [1-13C] and [U-13C], all possible triplet permutations of [1-^{13}C], [3-^{13}C] , [6-^{13}C] and [^{13}C$_6$], and four parallel tracer experiments with [1-^{13}C], [3-^{13}C] , [6-^{13}C] and [^{13}C$_6$] glucose. Simulations were carried out with information for GC-MS based amino acid labelling (AA), GC-MS based data of amino acid and sugar labelling (AA + Carb), a combination of NMR and GC-MS analysis of amino acids (AA + NMR) and the combination of labelling data obtained with GC-MS data for amino acids and sugars and NMR data for amino acids (Full). Boxes represent the 25 % to 75 % quartiles; whiskers indicate the 1.5 interquartile range and line and circle indicate the mean value of the flux distribution obtained from 100 iteration of Monte-Carlo simulation. Outliners are represented as small rhombuses. Deviation of mean flux from original values are encoded in colours: red: >10 %, orange <10 %, yellow: <1.0%, green: <0.1%

First, a single tracer experiment with [1,2-^{13}C]-glucose as used by Ueda *et al.*[82] was simulated. This approach used labelling data from amino acids exclusively and was sufficient to resolve the ED pathway with low deviation. The reaction catalysed by phosphofructokinase and F16BP phosphates did not resolve. Under these conditions, the model was unfit to resolve accurately orientation and magnitude of fluxes connect to F6P and S7P. Activity of PK pathway was estimated with small deviations in all three cases. As were deviation for fluxes estimation of the CBB cycle and contribution of the PP pathway with differences below 1 %. Besides the approaches inability to resolve the EMP pathway, it was fit to determine contribution of CBB cycle and oxidative PP pathway accurately, as intended by the author of the mentioned study. Still, this single tracer setup was not chosen due to poor performance of resolution of the EMP pathway. The next tracer setup that was investigated was a mixture of [1-^{13}C]-glucose and [$^{13}C_6$]-glucose with a molar ratio of 70:30, as used by Nakajima *et al.*[102]. Resolution capabilities of this tracer compared to the one using [1,2-^{13}C]-glucose. Again, resolution of the EMP pathway was poor and in all three cases deviations for this pathway were high. A third single tracer setup was investigated using [1-^{13}C]-glucose. This tracer setup was chosen according to literature [79], although this setup was used to resolve heterotrophic metabolism. Still, this substrate appeared promising since the ED-pathway directly contributes to the labelling of alanine. Nevertheless, this tracer showed more shortcomings in comparison to the other single tracer setups. Most notably, in case of the 25 % activity scenario, the ED pathway was not estimated correctly and fluxes in general showed a wide dispersion. Furthermore, an inability to estimate the PK pathway activity correctly was observed.

As a next step, a two-tracer setup was chosen, since this means an increase in labelling information used for flux estimation. [1-^{13}C] and [$^{13}C_6$] were chosen since these were already used by Nakajima *et al.* [102]. Since recent literature demonstrated that using labelling for biomass sugars vastly improves the resolution power for complex metabolic networks including the ED pathway [51], they were included for this approach. Furthermore, position specific labelling obtained from NMR measurements was added to further increase resolution of this complex system [83]. The resolution power of a two-tracer setup was superior in comparison to single tracer experimental setup. Resolution power of the F6P/S7P reaction node was sufficient to resolve the orientation of the flux conducted by phosphofructokinase/ F16BP phosphatase. Still, deviations for these reactions were high and the flux through ED and PK pathway were not estimated correctly. Inclusion of labelling information from biomass sugars or NMR data did not resolve this issue.

Following the example of Kohlstedt and Wittmann [51] a three parallel tracer experiment setup was investigated. All possible permutations of [1-^{13}C]-glucose, [3-^{13}C]-glucose, [6-^{13}C]-glucose and [$^{13}C_6$]-glucose were thus tested. Again, contributions of different combinations of

measurements and analytes were considered. In general, for all three tested scenarios, resolution power for all pathways but EMP were good with deviation below 1 % from the defined flux distribution. In all four cases using labelling data from GC-MS measurements of amino acids alone was insufficient to correctly estimate the F6P/S7P node. Addition of labelling information for biomass sugars greatly reduced deviations, with the best solution coming from the combination of GC-MS measurement for amino acids and biomass sugars and NMR measurements for amino acids.

Finally, the three flux scenarios of Figures 24 to 26 were tested with all four mentioned glucose isoforms. Again, resolution for the mentioned pathways were excellent. Only when biomass sugar labelling was not considered, resolution of the EMP was poor. Most notably, accuracy for estimation of the F6P/S7P node was highest for all scenarios and tracer combinations. This approach yielded best precision and was thus used for estimation of fluxes for photomixotrophic growth. Still, it hast to be stated, that other tracer setups are well usable to investigate different metabolic pathway contributions. The best example is the work done by Ueda *et al.* [82]. The aim of their study was the investigation of metabolic response of the oxidative branch of the PP pathway to different conditions. For this aim, the chosen setup provides good precision. When evaluating previous tracer setups and models, it also has to be considered that ED and PK pathway were not know, when experiments were conducted [77, 101, 102, 106]. Still, the central carbon metabolism of *Synechocystis* sp. PCC 6803 as it is known to this point is only resolved, when four tracer substrates and labelling information from biomass sugars are combined.

The *in silico* studies presented here demonstrate the potential of aprioristic modelling as a potent tool that aids in experimental design. Any given metabolic model can be analysed for its complexity with low experimental and financial effort. Just recently, a software tool was released that analyses metabolic models and calculates the optimal tracer set up and the method of choice to allow for estimation of fluxes with high precision [107]. Regarding previous flux estimations found in the literature, the metabolic network of *Synechocystis* sp. PCC 6803 has not been known to its full extend, when labelling experiments have been conducted. Here, flux estimation was performed using four different tracer substrates that can provide a sufficient database for future estimations with the inclusion of novel metabolic pathways, not known at this time.

Anabolic activity contributes to the intracellular CO_2 pool

Apart from optimising tracer choice for highest resolution of the core metabolic network of *Synechocystis* sp. PCC 6803, its photomixotrophic lifestyle called for alternative approaches and workarounds for flux estimation. The major outstanding metabolic feature of *Synechocystis* sp. PCC 6803 is its ability to fix carbon dioxide with energy from photosynthesis. Under photomixotrophic conditions this organism incorporates more carbon into its biomass than taken up in form of glucose, as indicated by carbon yields listed in Table 4 that are exceeding 1.0 Cmol $Cmol^{-1}$. Since the metabolism does not merely contain reactions that include carbon fixation, the carbon yield is the sum of all carbon releasing and fixing reactions. During heterotrophic metabolism, this balance is on the side of CO_2 production and release, because the cell uses the energy contained in e.g., glucose to regenerate reducing equivalents by enzymatically catalysed oxidation. Carbon dioxide producing reaction are not exclusive to metabolic pathways involved in the cell's energy metabolism. Moreover, synthesis of some biomass constituents requires decarboxylation. During heterotrophic growth, carbon dioxide from anabolic and catabolic activity is leaving the cell due to a concentration gradient. It was demonstrated that the labelling information contained in the CO_2 leaving the cell can be used for ^{13}C metabolic flux analysis [108]. Fixing of CO_2 by heterotrophic bacteria is limited to TCA anaplerotic reactions and parts of the synthesis pathways for some biomass constituents and hence labelling incorporation by fixing of carbon dioxide from the cytosol can be neglected. In most metabolic models for ^{13}C flux analysis, biomass formation is implemented in form of direct precursor drain and CO_2 production is modelled as a mono directional flux out of the system. *Synechocystis* sp. PCC 6803 though inhibits the complete enzymatic make up to perform light and dark reaction of photosynthesis. Assuming that the intracellular CO_2 pool is well equilibrated, carbon dioxide released by anabolic reactions needs to be accounted for flux estimation during photomixotrophic growth. The carbon dioxide released during anabolic activity carries labelling information that is incorporated back into biomass constituents via carbon fixation reactions.

OpenFlux uses elementary metabolite units for estimation of fluxes [84]. To account for the fixation of carbon dioxide from anabolic activity, definition of biomass formation was amended from direct precursor drain to precise definition of all anabolic reactions that involved release of carbon dioxide, including their corresponding atom transitions. The consequence for the model's ability to fit measured and simulated data is shown in Figure 4.20. As an indicator for the goodness of fit the sum of squares for the linear regression is shown.

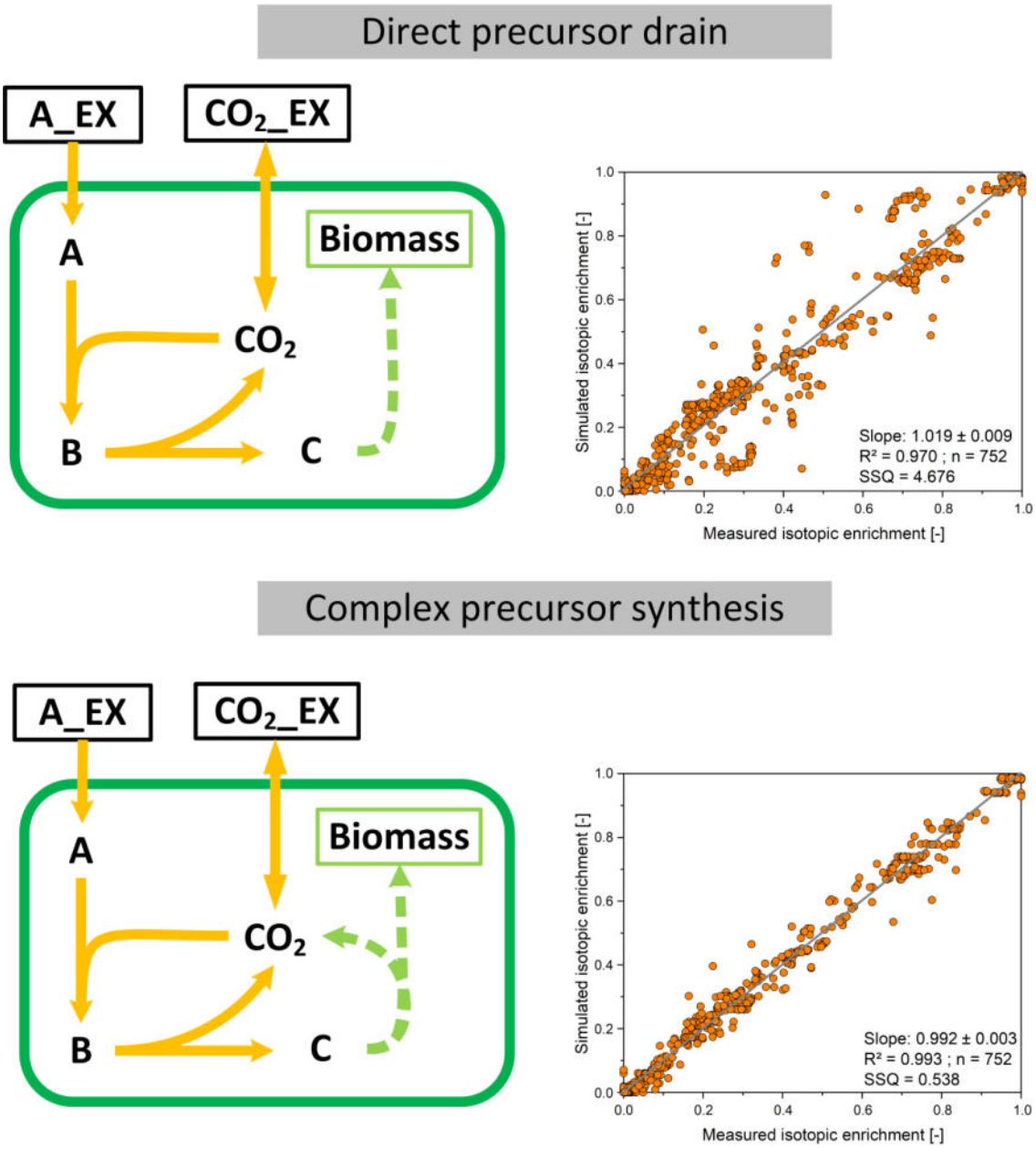

Figure 4.20: Goodness of fit between simulation with direct precursor drain and simulation using implementation of complex biomass formation to account for labelling contained in carbon dioxide originating from biomass synthesis. The left-hand side depicts a simplified network. Biomass synthesis is represented as green dashed arrows and squares. On the right-hand side simulated and measured isotopic enrichment are compared for the biomass synthesis implementations represented on the left side.

For flux estimation with *Synechocystis* sp. PCC 6803 the ability of the model to fit experimental and simulated isotopic data was evaluated using regression as shown in Figure 4.20. Applying other statistical methods like χ^2 tests that are commonly used for ^{13}C metabolic flux analysis [109, 110] are likely to fail for the complex network used here. Further complexity is added since four labelling experiments are combined in one dataset. Therefore, it is difficult to assess the χ^2-cutoff form measurement error and deviation between the individual data sets. Nevertheless, including labelling information from anabolic CO_2 decreased the dispersion between simulated and measured isotopic data and thus vastly increased the overall quality

of flux estimation. For future estimation of fluxes for organisms grown in photomixotrophic growth mode using the EMU framework it is necessary to implement complex biomass equations to include contribution of labelling information from carbon dioxide of anabolic origin.

In vivo fluxes in photomixotrophic growth mode under metabolic steady state

The optimisations discussed in the previous two chapters were used to estimate metabolic fluxes for *Synechocystis* sp. PCC 6803 in photomixotrophic growth mode. Labelling data from four parallel experiments one with [1-^{13}C]-glucose, one with [3-^{13}C]-glucose, one with [6-^{13}C]-glucose and one with [$^{13}C_6$]-glucose was combined into one large data set. It contained GC-MS and NMR measurements for amino acids and GC-MS measurements for biomass sugars, resulting in 556 individual labelling information pieces that are listed in Table A 4. The model with the underlying stoichiometry and biomass formation (listed in Table A 3) resulted in an excellent fit between simulated and measured data (SSR = 583, χ^2 cut-off = 615). Figure 4.21 depicts the correlation between simulated and measured data for the final flux estimation (Table A 4). In this figure data from different analytical origins are marked by different colour.

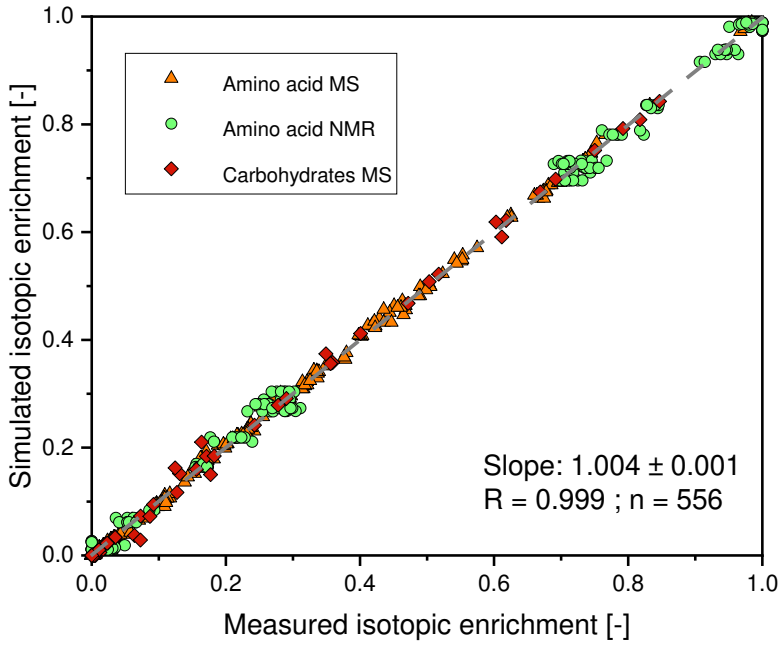

Figure 4.21: Correlation of simulated and measured labelling data for amino acids measured with GC-MS (orange triangles), sugars measured with GC-MS (red diamonds) and amino acids measured with NMR (green circles) for flux estimation with *Synechocystis* sp. PCC 6803 grown in photomixotrophic growth mode.

The goodness of fit for this large data set emphasizes the excellent nature of the underlying cultivation protocol and its usability for generation of labelled biomass. The ability of the model to fit data from four parallel experiments is a sign for a high degree of reproducibility for the

established experimental setup. Furthermore, the model was able to fit not only data for amino acids obtained from GC-MS measurements, but information from biomass sugars and NMR data for amino acids fitted well.

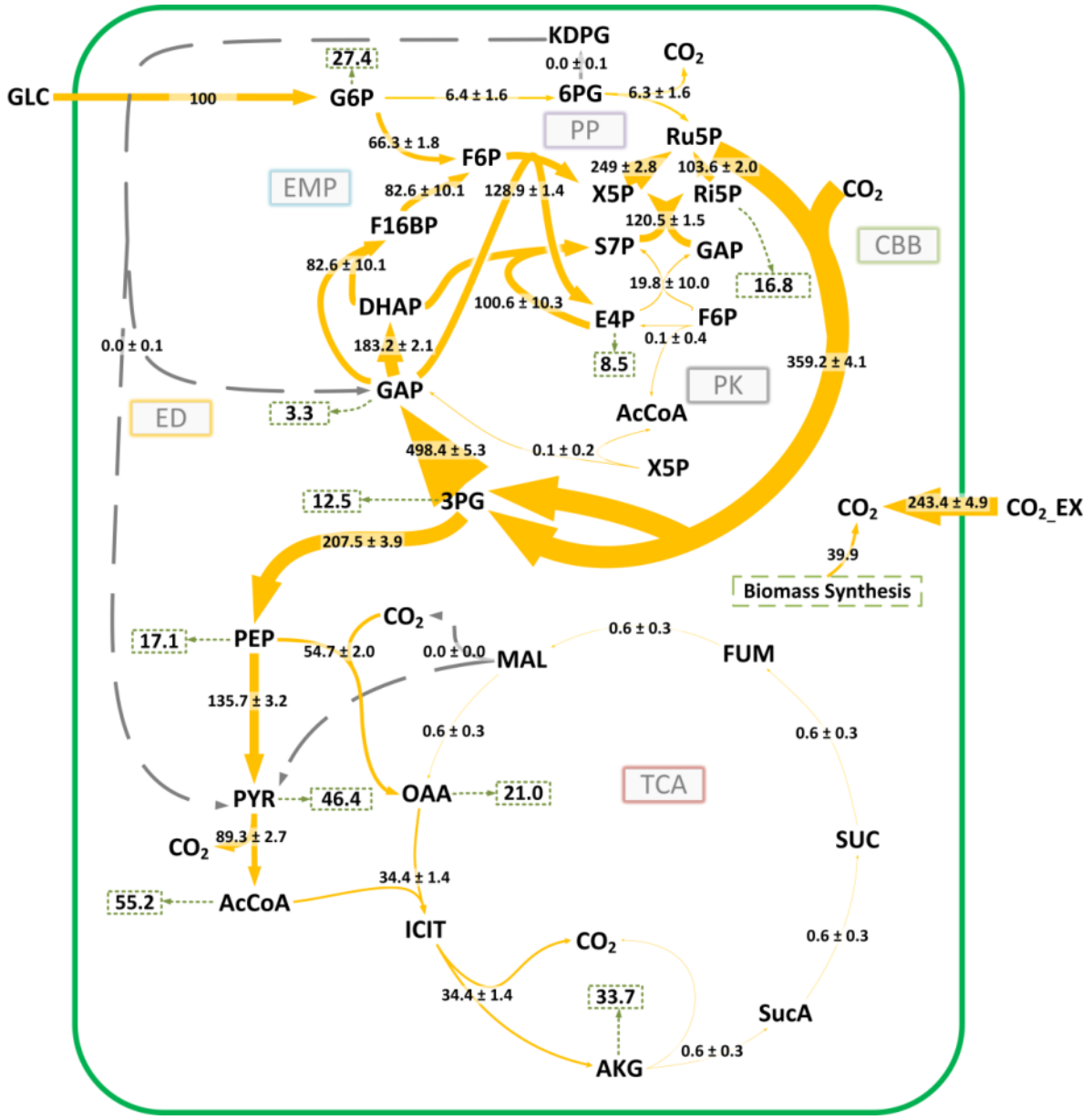

Figure 4.22: *In vivo* flux distribution for Synechocystis sp. PCC 6803 for photomixotrophic growth on glucose and CO_2. Fluxes are normalized to glucose uptake (100 %, q_s= 0.421 mmol g^{-1} h^{-1} ± 0.012 mmol g^{-1} h^{-1}). Biomass fluxes are represented as green dashed circles and arrows. Fluxes were obtained from amino acid and biomass sugar labelling measured with GC-MS and NMR data for amino acids originating from four parallel experiments ([1-^{13}C]-glucose, [3-^{13}C]-glucose, [6-^{13}C]-glucose, and [$^{13}C_6$]-glucose). Deviations result from 250 runs of Monte-Carlo simulation.

Estimation of fluxes and subsequent analysis for statistical feasibility with Monte-Carlo simulation yielded the *in vivo* flux distribution shown in Figure 4.22. Fluxes in this figure are normalized to glucose uptake rate (100 %, q_s= 0.421 mmol g^{-1} h^{-1} ± 0.012 mmol g^{-1} h^{-1}). The *in vivo* flux distribution of *Synechocystis* sp. PCC 6803 grown under photomixotrophic growth that is depicted in Figure 4.22 shows metabolic fluxes with low deviations. This can be seen

as a final confirmation of the high quality and inherent reproducibility of the underlying labelling and physiological data.

Glycolytic routes fuel carbon fixation.

Photomixotrophic growth is dominated by glucose as major substrate. It contributes 80 % of the carbon incorporated by the cell. Fixation of carbon dioxide is contribution 20 %. Still, carbon fixation via the CBB is the dominant pathway when looking at molar reaction rates. Glucose is directly channelled into the CBB cycle and is either entering via F6P (66%), where it is combined with C3 phosphates that originate from high rubisco activity (359 %), or it is following to a small extent the oxidative branch of the PP pathway (6 %). 3PG is the metabolite with the highest turnover, given its involvement in the CBB cycle and EMP pathway. About one third of 3PG molecules obtained from rubisco activity is following glycolytic routs toward the TCA cycle, whereas the rest is following the CBB cycle. The latter enters carbon rearrangement via transaldolase and transketolase with a fraction of 60 %. The remaining part is fused with E4P to form S7P. The most part of E4P for this reaction is directly originating from transketolase activity. The CBB cycle in *Synechocystis* sp. PCC 6803 is thus using glucose from the medium to boost its activity. The ability of *Synechocystis* sp. PCC 6803 to fix carbon dioxide with the help of glucose from medium under photomixotrophic growth was described by prior studies [77, 82, 102, 106]. Still, the flux estimation presented in this work for photomixotrophic growth resolved the accurate contributions of reactions connecting CBB cycle and EMP pathway for the first time. The resolution power achieved by incorporation of labelling data from four parallel experiments allowed to demonstrate, that the CBB cycle is operated to its full extend, and that EMP pathway is only operating downstream of 3PG that originates from high CBB cycle activity.

The TCA cycle operates as anabolic supplier.

As demonstrated by flux estimations found in literature [77, 82, 102, 106] the TCA cycle provides the cell with building blocks for biomass. Fluxes not directly yielding biomass precursors were estimated as marginally active. Due to this mere anabolic role of the TCA cycle, the part of 3PG that is flowing into the direction of the TCA cycle is directly depending on the cells demand for pyruvate, acetyl-CoA, oxaloacetate, and α-ketoglutarate. Still, the TCA cycle provides the cell with some reducing equivalents, but this could be considered a by-product of the reactions of biomass precursor generation.

Reducing equivalents are not regenerated from catabolic activity during photomixotrophic growth.

Under the experimental conditions presented here, *Synechocystis* sp. PCC 6803 is not depending on the generation of energy by direct oxidation of glucose. Reactions for regeneration of reducing equivalent were calculated with rates that are either directly

depending on precursor synthesis (isocitrate dehydrogenase, pyruvate dehydrogenase complex) or reactions are oriented in NADPH consuming direction (glyceraldehyde 3-phosphate dehydrogenase). The calculated flux distribution for mixotrophically growing *Synechocystis* sp. PCC 6803 suggests that the cells demand for NADPH is satisfied by photosynthesis under the conditions present during experiments. The small activity of 6.4 % of the oxidative branch of the PP pathway may not be directly connected to the energy demand of the cells but could act as a mechanism to maintain high fluxes of the CBB cycle. With changing lighting conditions, metabolic capacity of the PP pathway may fall below rubisco activity, calling for a rapid supply with C5 sugars from oxidation of glucose from medium. Alternatively, enzymes of the oxidative branch of the PP pathway could be expressed independent of the energy status of the cell, to allow for metabolic adoption to changes in environmental conditions. It was shown by Ueda *et al.* [82] that differences in light intensity cause a change in fluxes of the oxidative PP pathway. Most notably, under low light condition (10 µE m^2 s^{-1}) a flux of 73.1 % was calculated for glucose 6-phosphate oxidation, indicating, that this pathway is directly depending on the cells supply with light. Another example for a high activity of oxidative pentose phosphate pathway flux was reported by Nakajima *et al.* [102] (69.8 %). In this case, differences may arise from varying cultivation parameters and resulting growth rates. Temperature and light intensity (34° C, 40 µE m^2 s^{-1} [102]) have a large impact on growth rate (0.105 h^{-1} [102] and 0.076 h^{-1} this work) and may increase the demand for reducing equivalents for biomass precursor formation that is exceeding NADPH regeneration by photosynthesis. This difference may be compensated by activity of oxidative PP pathway. Nevertheless, these studies investigated fluxes in photomixotrophic growth mode. A strong connection between light intensity and energy charge was also demonstrated by Yu *et al.*[111] for autotrophic growth. This follows the observation that the alteration of fluxes of the CBB cycle leads to changes in decarboxylation rates of the oxidative pentose phosphate pathway [112], giving another example for the importance of the oxidative PP pathway´s role in regulation of the cells energy charge and its strong connection with the CBB cycle. Comparing the flux map, presented here (Figure 4.22) with results published by Abernathy *et al.* [113] for autotrophic growth with high light intensity and high carbon dioxide levels for *Synechococcus* sp. PCC 7002 yields the conclusion, that energy homeostasis of cyanobacteria is also depending on the atmospheric carbon dioxide level. For this microbe, little to no flux through the oxidative PP pathway was obtained under the mentioned conditions. The regulatory mechanisms of the cyanobacterial carbon fixation machinery are well known. To name just two examples: NADPH inhibits the activity of rubisco [114] and phosphoribosyl kinase is inhibited by PEP and ADP [115] . The inhibition of phosphoribosyl kinase by PEP is connected to the cells NADPH level, because 3-phosphoglycerate can only follow the CBB cycle if sufficient NAD(P)H is present in the cell. With the results presented here additional evidence for high

connectivity between metabolic fluxes, light supply, and the regulatory role of NDPH and ATP is shown.

Another novel insight is inactivity of the malic enzyme under photomixotrophic conditions. It was assumed inactive, because its activity was not detectable in an *ex vivo* enzyme assay (see Table 8). The hypothesis was made that the malic enzyme may play a role in NADPH homeostasis under changing conditions [101]. Assuring continuous light supply due to the optimised experimental setup presented in this work appears to have rendered this enzyme inactive. From comparison of the results presented here and those found in literature it become apparent that experimental setups vary greatly. Since a term like photomixotrophic growth is not defined by absolute values, evaluation of different results is difficult, and comparability may become limited.

Novel metabolic pathways are inactive under photomixotrophic conditions

Mirroring the physiological data for the deletion mutant, missing enzymes for either ED pathway of PK pathway, corresponding pathway were estimated as inactive. Neither the ED pathway nor the PK pathway was active. To verify this observation, metabolic fluxes were determined for all three deletion mutants. Therefore, labelling experiments were conducted with the same tracer combination of the wildtype. Flux estimation was carried out with GC-MS labelling data for amino acids and biomass sugars. The goodness of fit for all three flux estimations are shown in Figure 4.23. For flux estimation with Δ*eda* biomass formation was amended according to data on glycogen contents of this mutant in comparison to wildtype. Makowka *et al.* [13] showed, that the strain lacking KDPG aldolase has an about 30 % higher glycogen content. Hence, biomass formation was amended for this strain to account for this observation. The amendment was carried out by increasing the flux from G6P into the biomass by 30 %. This would have caused a drastic alteration in the carbon balance. Therefore, the increase in carbon flux into glycogen was compensated by lowering all other biomass fluxes according to their number of carbon atoms and original biomass fluxes.

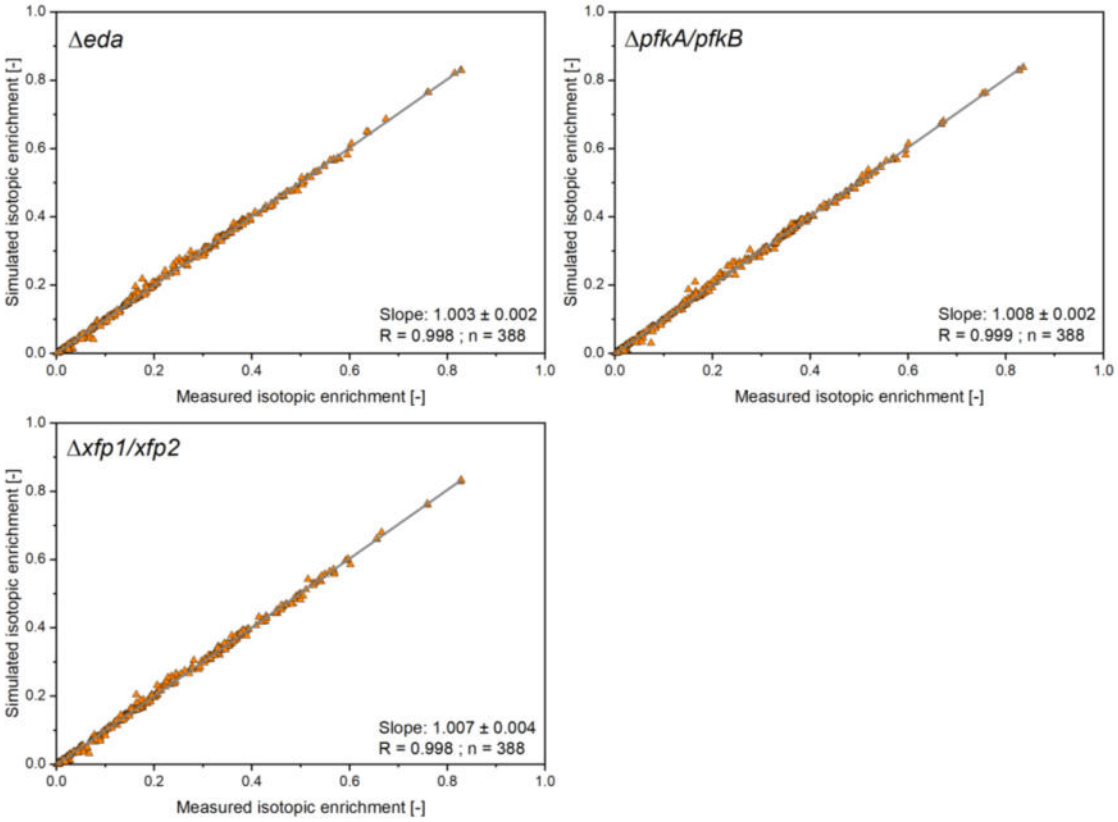

Figure 4.23: Correlations between simulated and measured isotopic distributions for amino acids and biomass sugars measured with GC-MS obtained from flux estimations for Δ*eda,* Δ*fpkA/pfkB* and Δ*xfp1/xfp2*. Statistical evaluation of the correlation is given for the shown linear regressions (grey lines). Isotopic data is found in Table A 5 (Δ*eda,* SSR= 394, χ^2 cut-off: 431), Table A 6 (Δ*pfkA/pfkB,* SSR= 401, χ^2 cut-off: 431), and Table A 7 (Δ*xfp1/xfp2,* SSR= 415, χ^2 cut-off: 430).

Correlations depicted in Figure 4.23 confirm once again the high quality and good reproducibility of the experimental data. In all three cases the model was able to fit experimental and simulated labelling exceptionally well. The individual *in vivo* fluxes are depicted in the following figure: Δ*eda* is shown in Figure 4.24, Δ*pfkA/pfkB* is shown in Figure 4.25 and Δ*xfp1/xfp2* is shown in Figure 4.26.

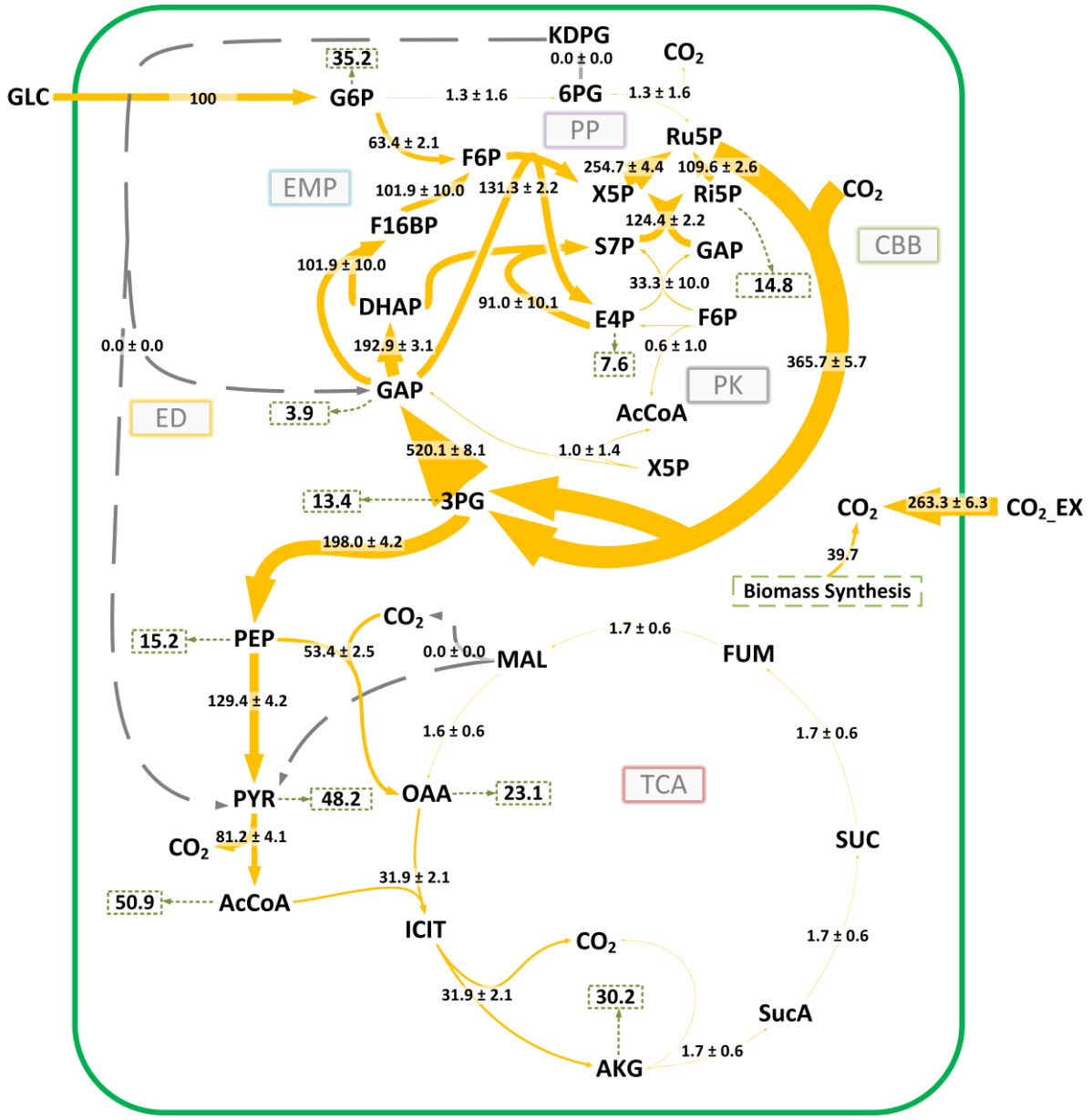

Figure 4.24: *In vivo* flux distribution for Δ*eda* in photomixotrophic growth mode. Fluxes are normalized to glucose uptake (100 %, q_s = 0.429 mmol g^{-1} h^{-1} ± 0.017 mmol g^{-1} h^{-1}). Biomass fluxes are represented as green dashed circles and arrows. Fluxes were obtained from amino acid and biomass sugar GC-MS data originating from four parallel experiments ([1-^{13}C]-glucose, [3-^{13}C]-glucose, [6-^{13}C]-glucose, and [$^{13}C_6$]-glucose). Deviations result from 250 runs of Monte-Carlo simulation.

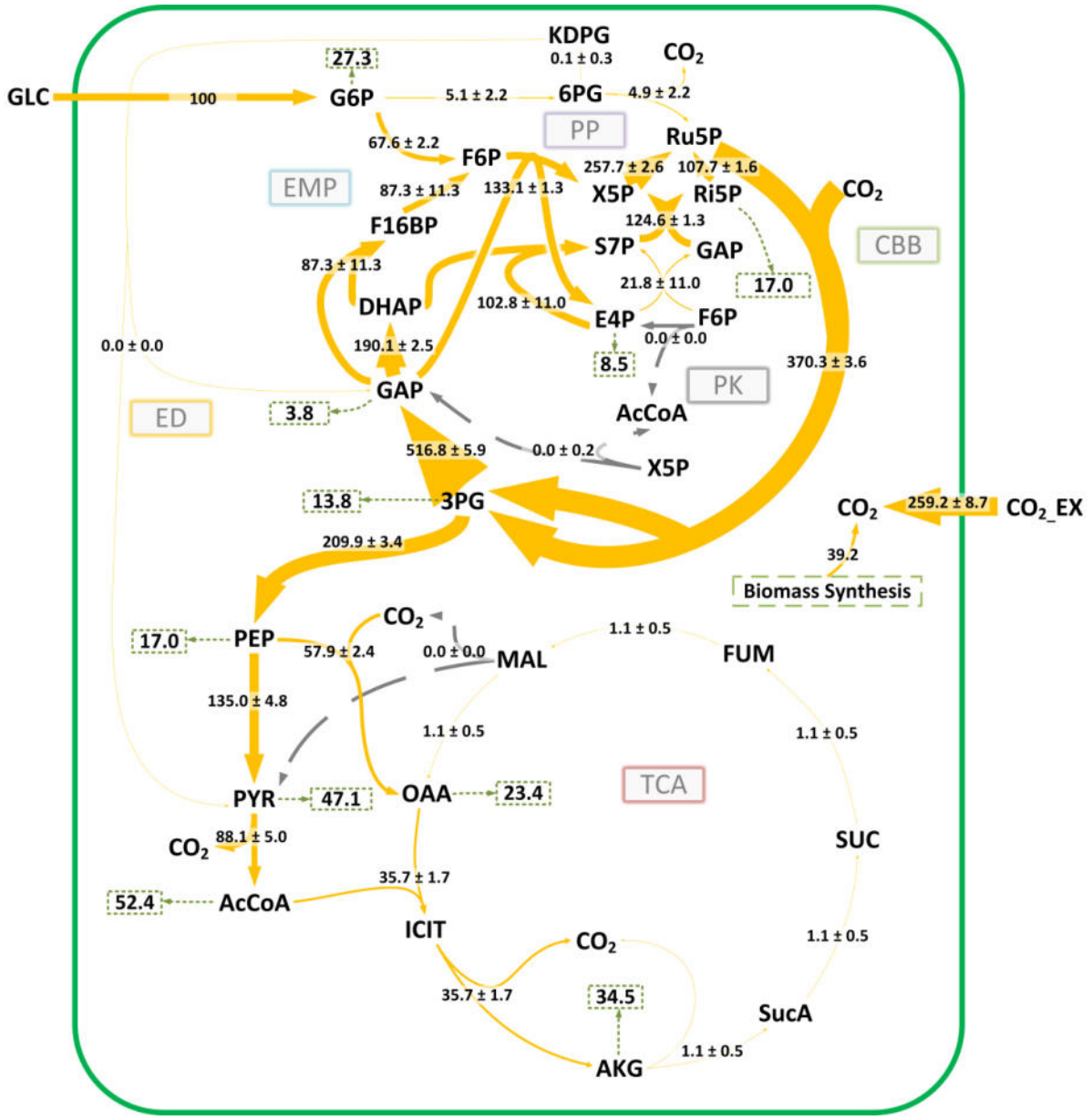

Figure 4.25: *In vivo* flux distribution for Δ*pfkA/pfkB* in photomixotrophic growth mode. Fluxes are normalized to glucose uptake (100 % q_s = 0.425 mmol g^{-1} h^{-1} ± 0.011 mmol g^{-1} h^{-1}). Biomass fluxes are represented as green dashed circles and arrows. Fluxes were obtained from amino acid and biomass sugar GC-MS data originating from four parallel experiments ([1-^{13}C]-glucose, [3-^{13}C]-glucose, [6-^{13}C]-glucose, and [$^{13}C_6$]-glucose). Deviations result from 250 runs of Monte-Carlo simulation.

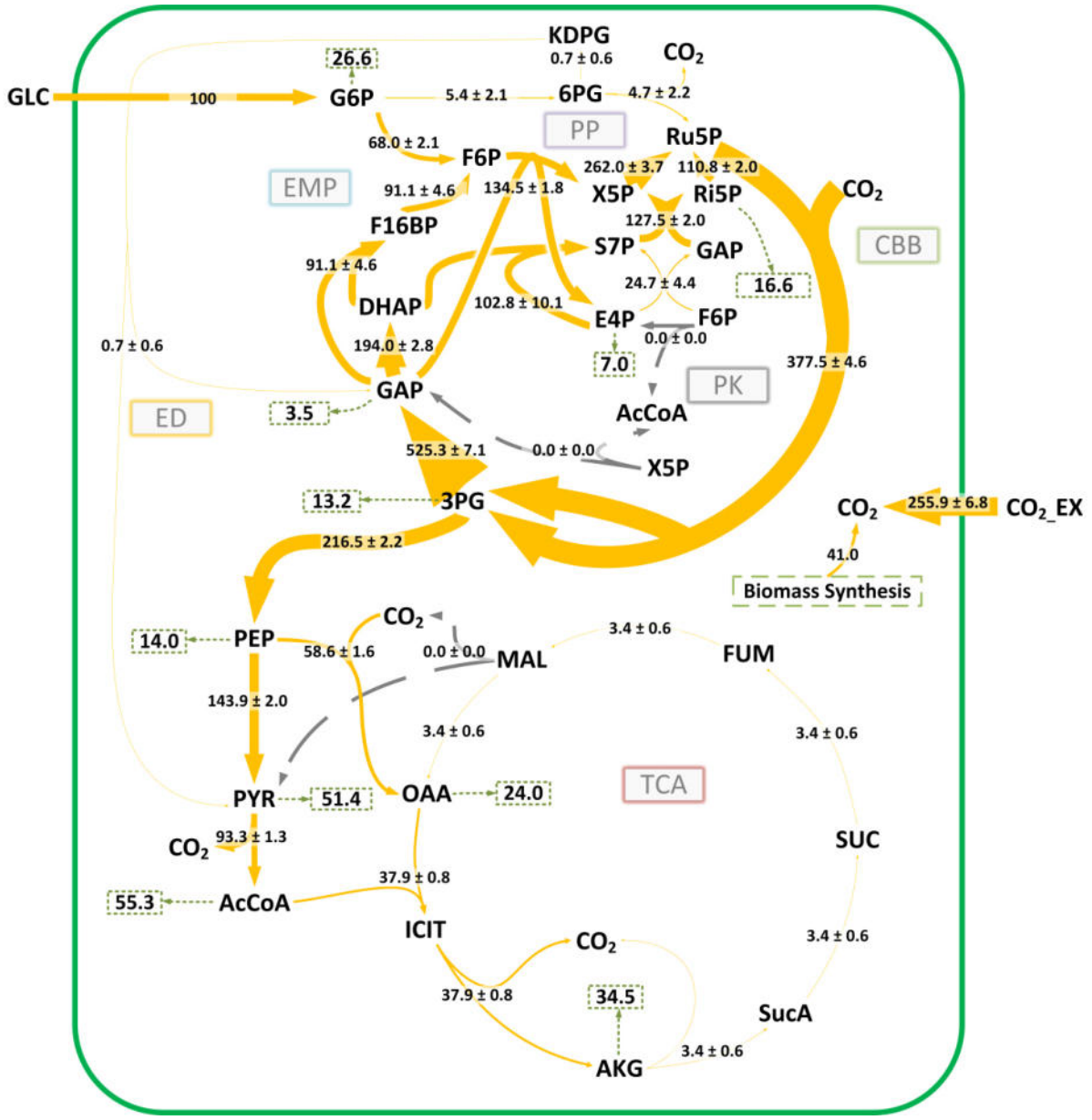

Figure 4.26: *In vivo* flux distribution for Δ*xfp1/xfp2* in photomixotrophic growth mode. Fluxes are normalized to glucose uptake (100 %, q_s = 0.468 mmol g^{-1} h^{-1} ± 0.012 mmol g^{-1} h^{-1}). Biomass fluxes are represented as green dashed circles and arrows. Fluxes were obtained from amino acid and biomass sugar GC-MS data originating from four parallel experiments ([1-^{13}C]-glucose, [3-^{13}C]-glucose, [6-^{13}C]-glucose, and [$^{13}C_6$]-glucose). Deviations result from 250 runs of Monte-Carlo simulation.

Estimation of fluxes for mutant strains yielded *in vivo* fluxes that are similar to those determined for wildtype. All three mutant strains facilitated glucose as the major substrate to fuel carbon fixation via the CBB cycle. None of the formerly inactive pathways were active with fluxes exceeding 1 % after genetic perturbations. Similarities between wildtype fluxes and those estimated for the mutants directly connect to physiological data (compare Table 4). The flux estimations for all three mutants demonstrate once more the ability of the experimental setup and approach to model building for high quality ^{13}C metabolic flux analysis with *Synechocystis* sp. PCC 6803. In all three cases the model was able to fit experimental data from four parallel

experiments with high precision and excellent fit between simulated and measured isotopic enrichments.

The alteration of the biomass formation equation for Δ*eda* to account for higher glycogen storage caused a reduction of the oxidative branch of the PP pathway. Although this pathway´s flux was determined with a low value, detection of KDPG aldolase almost rendered it inactive. This may be caused by the change in the fraction of carbon channelled directly into the glycogen pool and a decrease in all other biomass fluxes. Overall, estimation of fluxes for this deletion strain does not indicate any novel pathways under photomixotrophic conditions. It also shows that perturbations of novel pathways (Δ*eda* and Δ*xfp1*/*xfp*2) and the EMP (Δ*pfkA*/*pfkB*) are not causing major alterations of the central metabolism and physiology.

A flux analysis protocol for mixotrophic organisms

With the *in vivo* flux distribution presented for *Synechocystis* sp. PCC 6803 shown in Figure 4.22 a final resolution analysis was performed. Therefore, all tracer combinations as before were tested, combined with all four analyte-method combinations. The resulting simulation is shown in Figure 4.27.

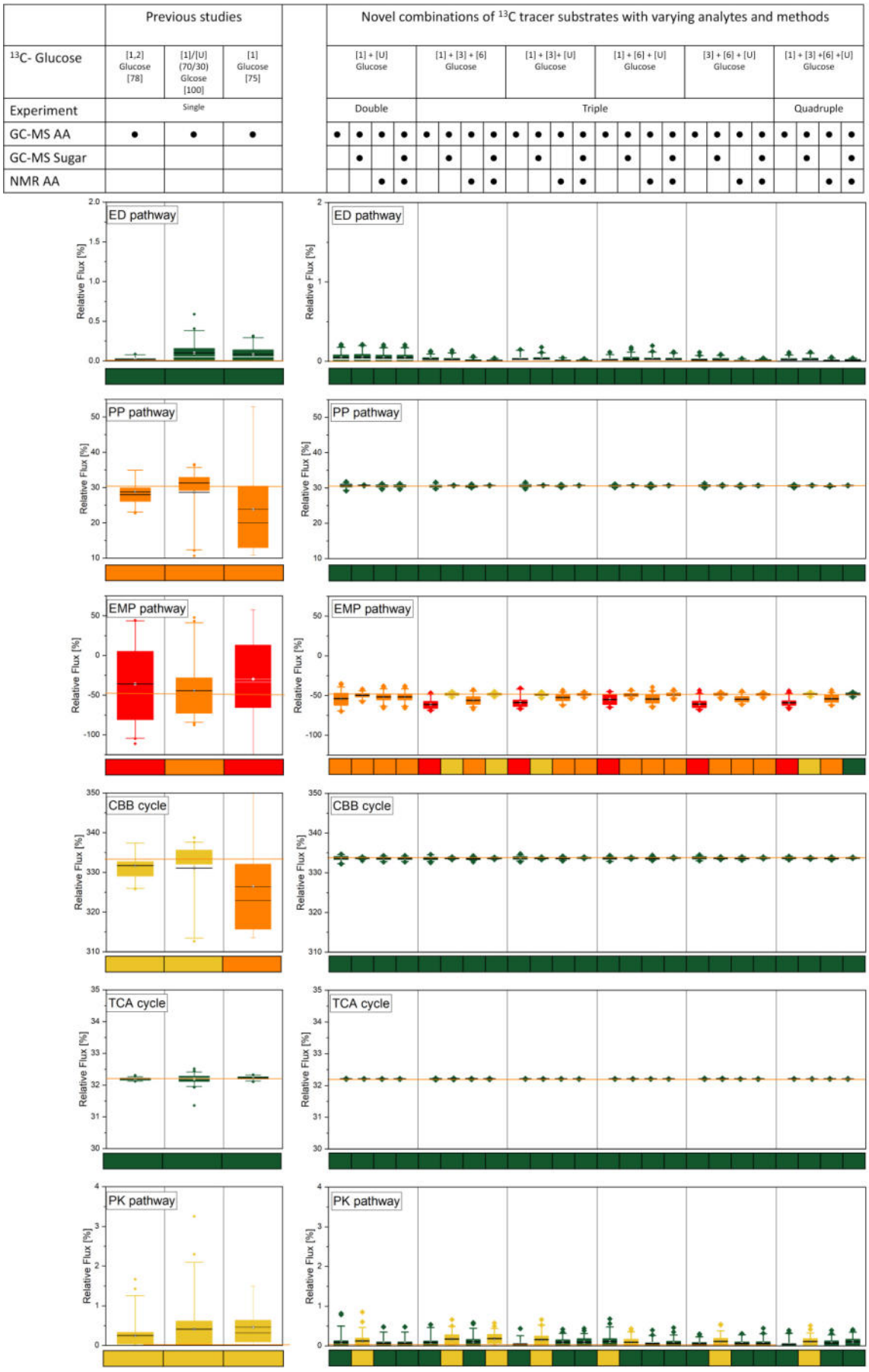

Figure 4.27: Comparison of fluxes for six different pathways of the central carbon metabolism of *Synechocystis* sp. PCC 6803 using different tracer substrate combinations and different analytes. Fluxes were obtained from 100 iterations of Monte-Carlo simulation based on isotopic distributions simulated with the flux distributions presented in Figure 4.22. Shown are box-whiskers plots for single tracer substrates with [1,2-^{13}C]- glucose, a mixture of [1-^{13}C$_6$] and [^{13}C$_6$] glucose in a ratio of 70:30, [1-^{13}C] glucose, a two substrate experiment with [1-13C] and [U-13C], all possible triplet permutations of [1-^{13}C], [3-^{13}C] and [^{13}C$_6$], and four parallel tracer experiments with [1-^{13}C], [3-^{13}C] , [6-^{13}C] and [^{13}C$_6$] glucose. Simulations were carried out with information for GC-MS based amino acid labelling (AA), GC-MS based data of amino acid and sugar labelling (AA + Carb), a combination of NMR and GC-MS analysis of amino acids (AA + NMR) and the combination of labelling data obtained with GC-MS data for amino acids and sugars and NMR data for amino acids (Full). Boxes represent the 25 % to 75 % quartiles; whiskers indicate the 1.5 interquartile range and line and circle indicate the mean value of the flux distribution obtained from 100 iteration of Monte-Carlo simulation. Outliners are represented as small rhombuses. Deviation of mean flux from original values are encoded in colours: red: >10 %, orange <10 %, yellow: <1.0%, green: <0.1%

Addition of biomass sugars can in case of a mixture of [1-$^{13}C_6$] and [$^{13}C_6$] glucose with a ratio of 70:30 help in increasing resolution power of the EMP pathway. The other two single tracer examples did not profit from addition of neither NMR data nor biomass sugar labelling. Still, observations made for hypothetical flux scenarios were found to be true for the final flux distributions obtained from real labelling data.

Efforts that led to the resolution of the core metabolism of *Synechocystis* sp. PCC 6803 under photomixotrophic conditions can easily be adopted for other cyanobacteria that are known to be able to grow in this growth mode. Examples are *Synechococcus* sp. [116], and *Spirulina* sp. [117] to name just two. Furthermore, microalgae could be promising subjects. The following species are also glucose tolerant and are promising candidates as future production hosts: *Nannochloropsis oculate* [118], *Euglena gracilis* [119], *Chlorella vulgaris* [118], and *Chlorella protothecoides* [120]. It must be emphasised, that aprioristic modelling is a must do to identify the best experimental setup according to subject and aim of a potential study.

In vivo fluxes in heterotrophic growth mode

Estimation of *in vivo* fluxes for *Synechocystis* sp. PCC 6803 grown in heterotrophic growth mode was carried in three parallel experiments instead of four differently labelled glucose isoforms. Because the enzymes ribosyl kinase and gap dehydrogenase (NADPH dependent) are controlled by light dependent redox systems [121-123], corresponding reactions were set to have zero flux. Fructose 1,6-bisphosphate aldolase in cyanobacteria also catalyses the formation of sedoheptulose 1,7-bisphosphate from DHAP and E4P and is not directly controlled. First flux estimation and subsequent Monte-Carlo simulation showed that a small fraction of flux estimations resulted in a flux through said reaction if considered active. Most solutions, as seen in Figure 4.28 estimated this reaction with zero flux. Yield space analysis for this reaction in heterotrophic growth mode returned a negative correlation between growth and S17BP forming activity of F16BP aldolase.

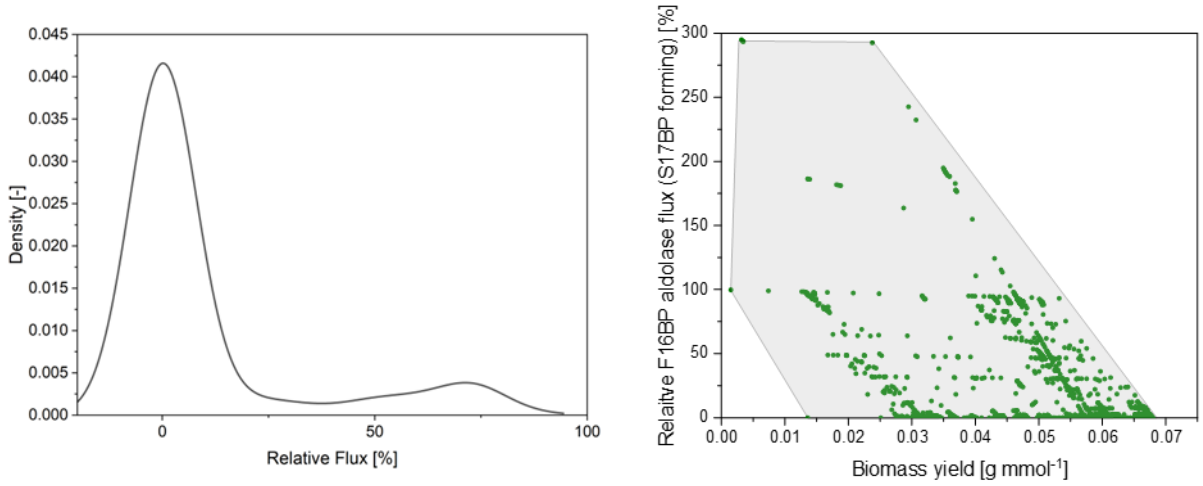

Figure 4.28: Left side: Density plot for fluxes estimated for S17BP forming activity of F16BP aldolase for 250 iterations of Monte-Carlo simulation for *Synechocystis* sp. PCC 6803 in heterotrophic growth mode. Right: Yield space analysis for biomass formation dependent on S17BP forming flux through F16BP aldolase.

Further investigating of obtained fluxes lead to the conclusion, that from an energetic and thermodynamical standpoint S17BP forming activity of F16BP aldolase can be considered absent under heterotrophic conditions. F16BP aldolase is probably saturated by GAP and DHAP originating from high PP pathway activity. Further consideration was that synthesis of S17BP would imply unnecessary loss of a phosphate group, meaning wasted energy. Combining these assumptions, the metabolic network closely resembles the core metabolism of *Pseudomonas putida*. According to *in silico* tracer studies by Kohlstedt and Wittmann [51] the following tracer setup was used in three parallel experiments: [1-^{13}C] glucose, [6-^{13}C] glucose and an equimolar mixture of naturally labelled glucose and [$^{13}C_6$]-glucose. Labelling was measured using GC-MS, including biomass sugars. To increase the overall precision of flux estimation, complex biomass formation equations were adopted, as described for photomixotrophic growth. Using direct biomass precursor drain for heterotrophic growth would have caused a difference in the carbon balance of 4 % (mol/mol) compared to complex biomass definition that accounts for amino acid synthesis. In Figure 4.29 the correlation for simulated and measured isotopic enrichment for flux estimation in heterotrophic growth is depicted (compare Table A 12).

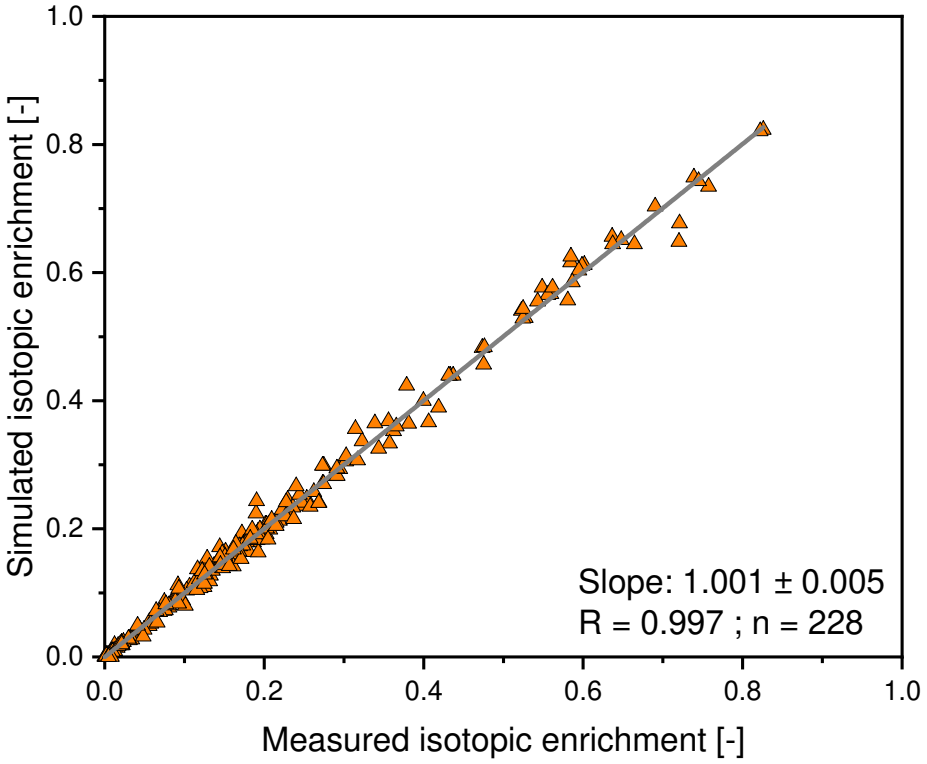

Figure 4.29: Correlation of simulated and measured labelling data for amino acids and sugars measured with GC-MS for the estimation of fluxes for heterotrophic growth of *Synechocystis* sp. PCC 6803 grown in three parallel experiments with [1-^{13}C] glucose, [6-^{13}C] glucose and 50 % [$^{13}C_6$] glucose and naturally labelled glucose.

From labelling data obtained from three parallel experiments, the model was able to estimate fluxes with high precision and a good match for simulated and measured isotopic enrichments, as shown in Figure 4.29 (SSR= 197, χ^2 cut-off = 221). Cultivation in heterotrophic growth mode were time demanding (see Figure 4.14) causing higher deviations for cultivation parameters in comparison to photomixotrophic growth. Additionally, measurement of amino acid labelling was encumbered by low stability of derivatised samples. The reason for this low stability is not known. This resulted in higher errors for the isotopic data because each measurement run had to be derivatised separately, increasing deviations. Therefore, an error of ±0.015 was adopted for both, amino acids and biomass sugars. Still, the model was able to derive a flux distribution with good accuracy and high statistical probability for the fluxes presented in Figure 4.30. The flux map presented for heterotrophic mode shows low deviations originating from 250 runs of Monte-Carlo simulation.

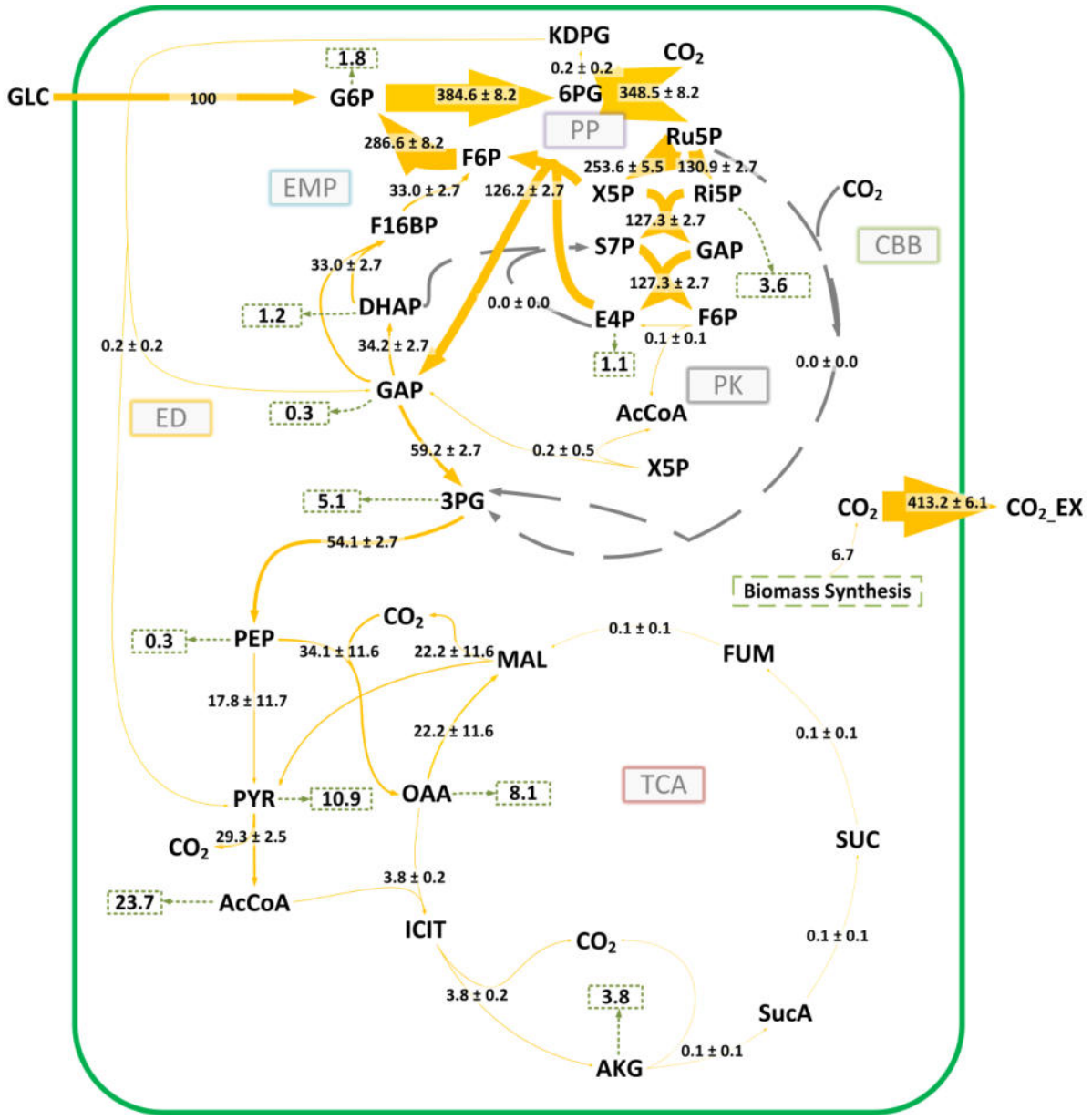

Figure 4.30: *In vivo* flux distribution for Synechocystis sp. PCC 6803 for heterotrophic growth on glucose. Fluxes are normalized to glucose uptake (100 %, q_s= 0.203 mmol g^{-1} h^{-1} ± 0.007 mmol g^{-1} h^{-1}). Fluxes were obtained from amino acid and biomass sugar GC-MS data originating from three parallel experiments ([1-^{13}C]-glucose, [3-^{13}C]-glucose and equimolar mixture of naturally labelled and [$^{13}C_6$] glucose). Deviations result from 250 runs of Monte-Carlo simulation.

Heterotrophic metabolism is dominated by the oxidative branch of the PP pathway.

The most dominant reaction under heterotrophic conditions of the central metabolism of *Synechocystis* sp. PCC 6803 is the oxidative branch of the PP pathway. Its activity exceeds the glucose uptake rate by a ratio of 1 to 3.8. Not only is glucose from the medium directly oxidized to regenerate NADPH but resulting pentose phosphates are channelled back into the G6P pool via the PP pathway. This way, glucose from the medium is cycled through the oxidative PP pathway to obtain NADPH. Carbon that is needed for generation of biomass is drawn from this metabolic circle in form of GAP that originates from high transaldolase activity. This observation also provides the answer to the question for the reason of a lack of

phenotypical change of Δ*pfkA/pfkB*. Those enzymes are not needed, since F16BP is synthesised from GAP and DHAP and not from F6P. The role of NADPH for the energy household of this microbe was already discussed for photomixotrophic growth. The extent to which *Synechocystis* sp. PCC 6803 is using glucose in the absence of photosynthesis to regenerate NADPH is extraordinary and sets it apart from other organisms with a chemoheterotrophic lifestyle. One of the reasons this organism can heavily rely on NADPH as its main energy currency is the presence of NAD(P)H plastoquinone oxidoreductase. This enzyme allows the use of NADPH to channel electrons into the respiratory chain and to subsequently regenerate ATP. Another reason why so much NADPH is regenerated by the cell is found in the composition of the medium used for cultivation. In BG11 medium in the form it was used here, nitrate is the sole source of nitrogen. Conversion of one molecule nitrate results in the loss of six molar equivalents of reduced ferredoxin, which in turn demands six NADPH molecules to recover. Under photo- or mixo-/trophic conditions this nitrogen source acts as an electron sink for *Synechocystis* sp. PCC 6803 to cope with an overflow of exited electrons from its photosystems. It is well known, that *Synechocystis* sp. PCC 6803 needs an ATP to NADPH ratio of 1.50 for optimum growth, but photosynthesis provides a ratio of 1.28 [78]. Using nitrate oxidation as a sink for NADPH allows for a more beneficial ATP/NADPH ratio. Of course, in heterotrophic growth, no oversupply with reducing potential is present and NADPH is regenerated via oxidative PP pathway.

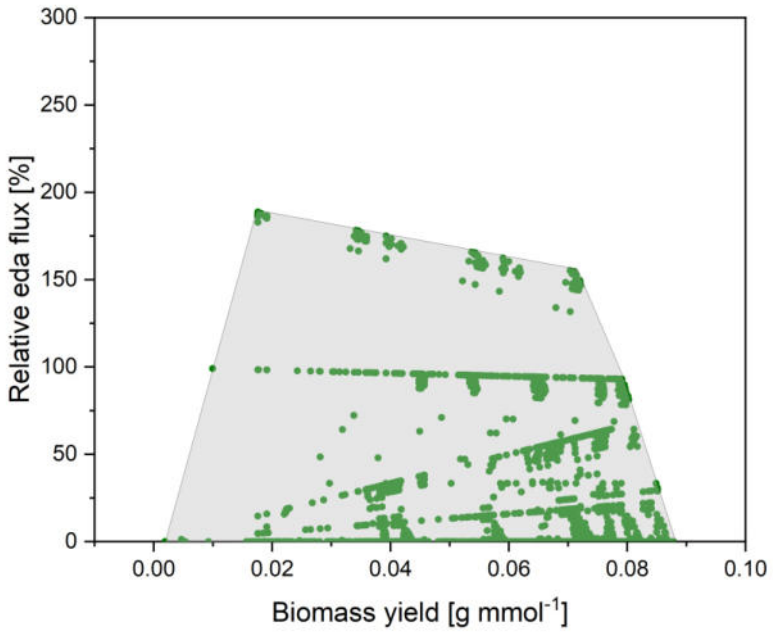

Figure 4.31: Hypothetical yield space for biomass formation depending on the relative flux through the ED pathway for *Synechocystis* sp. PCC 6803 in heterotrophic growth with NH_4 as nitrogen source.

Calculation of elementary flux modes with ammonium salts as sole nitrogen source, as shown in Figure 4.31 demonstrates that a vast portion of the energy generated by the cell is needed for nitrogen uptake. Eliminating this factor increased the theoretical maximum biomass yield by about 25 %.

TCA and EMP provide biomass building blocks under heterotrophic conditions.

As a recurring theme, TCA cycle activity and the part of the EMP pathway not sharing enzymes with the CBB cycle are merely providing the cell with biomass building blocks. Reaction of the TCA cycle that are not connected to biomass precursor synthesis are below 1.0 %. As discussed above, the cell heavily relies on NADPH as its major energy currency. Reactions that generate NADH and were calculated to have larger fluxes are directly depending on biomass fluxes. This behaviour of central carbon metabolism of *Synechocystis* sp. PCC 6803 under heterotrophic conditions was also observed by Wan *et al.*[79]. In contrast to photomixotrophic growth, the malic enzyme was found active during heterotrophic growth. In this case, it may act as a mechanism for a conversion of NADH into NADPH, since OAA is reduced to form MAL that is subsequently oxidised by the malic enzyme to regenerate NADPH.

Novel pathways are inactive under heterotrophic growth

As seen for photomixotrophic growth, ED and PK pathway are inactive under heterotrophic conditions as well. Inactivity of the latter was expected due to physiological parameters that changed within the errors of the cultivation system. In case of the ED pathway inactivity is surprising, since a change in phenotype was observed. For this reason, ^{13}C flux analysis of this mutant under heterotrophic conditions may yield additional insight.

Flux analysis of Δ*eda* in heterotrophic growth mode.

Since the deletion strain missing KDPG aldolase showed the largest divergence of growth characteristics from wildtype under heterotrophic conditions, ^{13}C metabolic flux analysis of this strain promised the most knowledge gain on the role of the ED pathway. Estimation of this pathways flux resulted in no activity. Together with absence of KDPG aldolase activity in a cell extract of wildtype *in vivo* fluxes could directly show the influences of the *eda* gene on the fluxome. Therefore, the same tracer setup and model were used as for the wildtype to determine *in vivo* fluxes for heterotrophic metabolism.

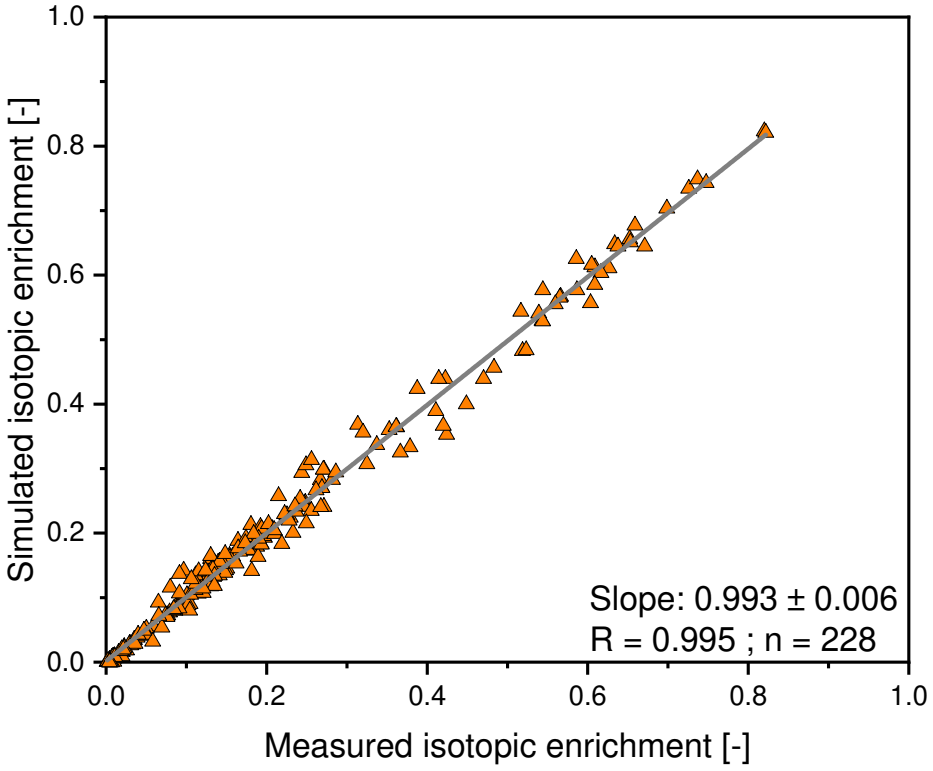

Figure 4.32: Correlation of simulated and measured labelling data for amino acids and sugars measured with GC-MS for the estimation of fluxes for heterotrophic growth of Δ*eda* grown in three parallel experiments with [1-^{13}C] glucose, [6-^{13}C] glucose and 50 % [$^{13}C_6$] glucose and naturally labelled glucose.

As for estimation of metabolic fluxes for Δ*eda* in heterotrophic growth mode, labelling data was obtained for three parallel experiments (compare Table A 13). Fluxes were estimated from GC-MS measurement of amino acids and biomass sugars. Measurement of isotopic enrichments for amino acids for this strain were encumbered by low stability of measured samples after derivatisation as well. Still, resolution power was high, and the model was able to generate a good fit between simulated and measured isotopic enrichment, as seen in Figure 4.32 (SSR= 148, χ^2 cut-off = 220).

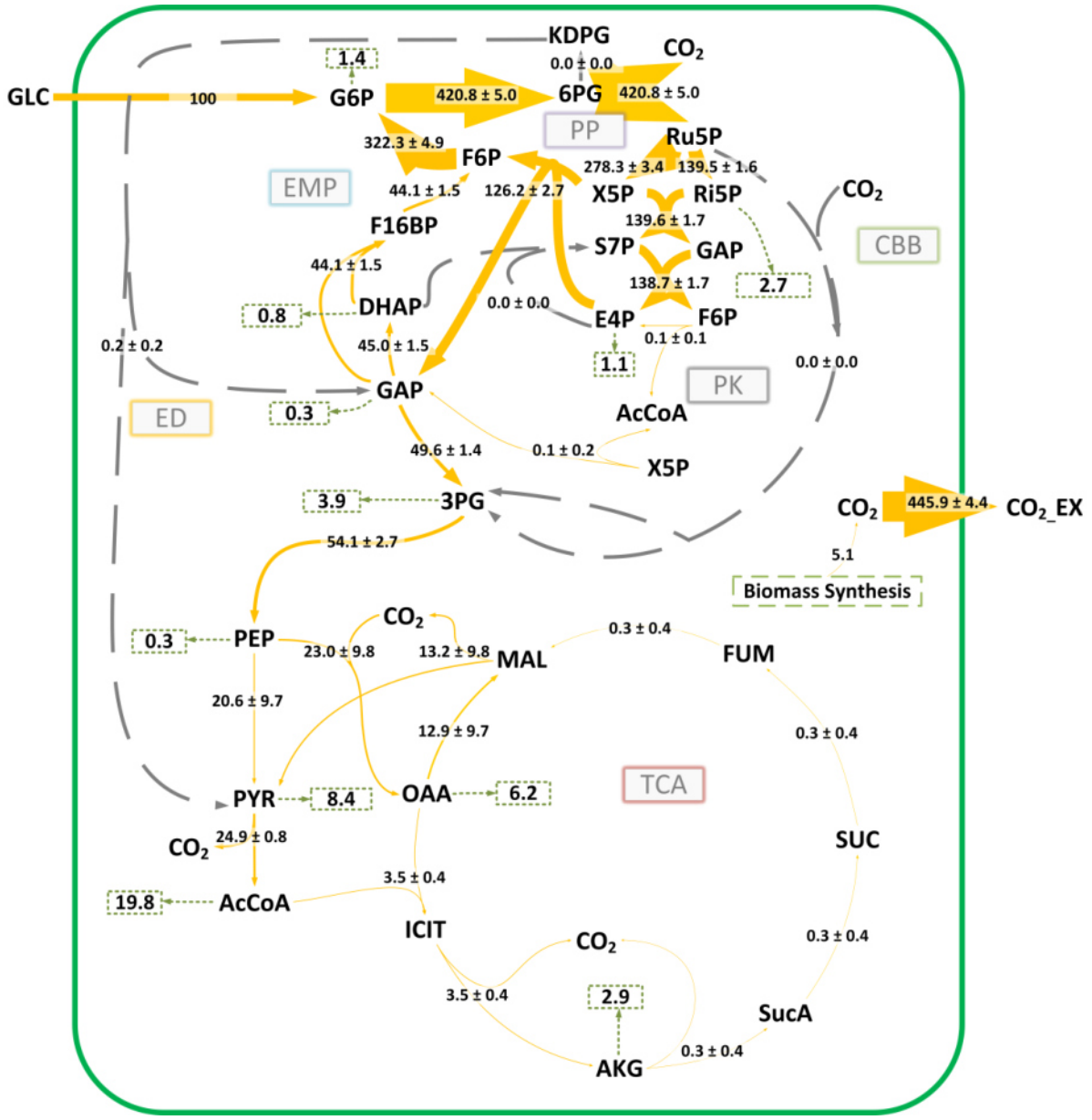

Figure 4.33: *In vivo* flux distribution for Δ*eda* for heterotrophic growth on glucose. Fluxes are normalized to glucose uptake (100 %, q_s= 0.345 mmol g^{-1} h^{-1} ± 0.010 mmol g^{-1} h^{-1}). Fluxes were obtained from amino acid and biomass sugar GC-MS data originating from three parallel experiments ([1-^{13}C]-glucose, [3-^{13}C]-glucose and equimolar mixture of naturally labelled and [$^{13}C_6$] glucose). Deviations result from 250 runs of Monte-Carlo simulation.

Fluxes obtained for Δ*eda* grown in heterotrophic growth mode as shown in Figure 4.33 demonstrate the stunning plasticity of the central metabolism of *Synechocystis* sp. PCC 6803. Observed decrease in biomass yield was routed in a higher flux through the oxidative PP pathway. Other pathways remained almost equal to those of the wildtype. Fluxes not connected to regeneration of NADPH remained directly depending on biomass fluxes. Surely, specific reaction rates increased, but fluxes normalized to glucose uptake remained in the same magnitude as wildtype. Furthermore, deletion of KDPG aldolase did not cause activation or reorientation of metabolic pathways. The general mode of operation remained the same: regeneration of NADPH via the oxidative branch of the PP pathway and anabolic supply of

precursors for all other pathways. Estimation of fluxes for Δ*eda* demonstrates that although more energy is regenerated by the cell, metabolic fluxes under heterotrophic growth are operated in the same manner as in wildtype *Synechocystis* sp. PCC 6803. This metabolic plasticity is probably originating from the fact that this organism is operating under high metabolic pressure when no light is present for regeneration of energy metabolites. The mode of action in this case appears to be generation of high quantities of NADPH and supply of biomass precursors that are generated as a side stream in form of C3 phosphates drawn away from a cyclically operating oxidative PP pathway.

Novel insights into the energy metabolism of *Synechocystis* sp. PCC 6803.

Flux estimation presented in this work allows in-depth analysis of all reactions of the central metabolism of *Synechocystis* sp. PCC 6803. The ability of this microbe to perform oxygenic photosynthesis makes its energy household different from other bacteria. Cyanobacteria do not discriminate between anabolic and catabolic reducing equivalents, because they are able to convert NADPH into ATP via NAD(P)H quinone oxidoreductase [124]. The exact P/O ratio for cyanobacteria remains disputed [125, 126]; for this work and the following calculations a ratio of 1.5 is assumed. During photosynthesis NADPH is obtained by harnessing light energy. As discussed before, BG11 medium contains nitrate that may provide *Synechocystis* sp. PCC 6803 with an electron sink and thus reducing redux stress under high light conditions. Flux estimations performed under photomixotrophic growth mode show that regeneration of NADPH from oxidation of metabolites only occurs to a minor extent. It is mostly connected to biomass precursor supply. Additionally, a big part of NADPH is used to transform 3PG from rubisco activity into DHAP. Flux estimation by Ueda *et al.* [82] demonstrated that activity of the oxidative branch of the PP pathway is directly depending on light intensity, which is in agreement with the data presented here. Assuring light supply throughout cultivation is mirrored in the low flux through said pathway obtained for photomixotrophic growth mode during this work. On the other side of the scale regarding energy supply is growth in heterotrophic growth mode. In this case, the oxidative PP pathway dominates all other pathways. In wildtype molar NAPDH regeneration rates cumulate in almost 800 % relative to glucose uptake. NADH is regenerated at a rate of 70 % relative to glucose uptake. This difference is staggering and raises the question for the reason of this large difference. In comparison to a heterotroph, e.g., *Pseudomonas putida* KT2440 the biomass yield on glucose of *Synechocystis* sp. PCC 6803 is much smaller (*P. putida* $Y_{X/S}$ =81.6 g mol^{-1}, μ = 0.55 h^{-1}[51], *Synechocystis* sp. PCC 6803 $Y_{X/S}$ = 64.1 g mol^{-1} μ= 0.013). Following the example of Bolten *et al.* [127], ATP production and consumption were estimated from *in vivo* fluxes for the wildtype and Δ*eda* in heterotrophic growth mode using data from literature [77]. Anabolic NADPH demand and consumption for assimilation of nitrogen were subtracted and were thus not included in the ATP regeneration balance. Resulting specific rates are listed in Table 7.

Table 7: Specific rates for ATP regeneration and consumption calculated from flux estimations for wildtype *Synechocystis* sp. PCC 6803 and ∆*eda* in heterotrophic growth mode.

Specific rate	Wildtype	∆eda
$ATP_{generation}$	1.034 mmol g^{-1} h^{-1}	2.667 mmol g^{-1} h^{-1}
$ATP_{anabolism}$	0.510 mmol g^{-1} h^{-1}	0.667 mmol g^{-1} h^{-1}
$ATP_{maintenance}$	0.524 mmol g^{-1} h^{-1}	2.000 mmol g^{-1} h^{-1}

Observation made for *Sorangium cellulosum* regarding maintenance requirements of slow growing bacteria [127] were also confirmed for *Synechocystis* sp. PCC 6803 for heterotrophic growth mode. The wildtype uses 50 % of ATP regenerated to satisfy cellular maintenance requirements. Regarding these numbers and including results for cultivation experiments, the conclusion can be drawn that this microbe has not evolved to grow quickly in the absence of light. With doubling times vastly exceeding average night cycles (t_2 = 53.3 h) it appears that these organisms switch into cellular preservation mode to survive, until photosynthesis is activated again. Cyanobacteria are a group of highly diverse organisms with varying ability to consume a variety of organic substrates [40, 41]. The heterotrophic growth mode present during the experiments conducted here is highly artificial and it can be assumed that under natural conditions growth is even further limited. Furthermore, glucose as a substrate is almost non-existing in the habitat of *Synechocystis* sp. PCC 6803. Cells may only consume their energy storage at rates that merely justify their maintenance requirements. Considering that cyanobacteria must compete with other organisms for scarce carbon sources during night-time makes this hypothesis appear even more likely. Specific uptake rates obtained for experiments in heterotrophic growth modes that are presented in this work are dwarfed by values found for other microbes [51, 67]. As discussed above, deletion of KDPG aldolase (∆*eda*) caused an increase in growth rate and a decrease in biomass yield. This translated into higher activity of the oxidative part of the PP pathway. Comparing specific rates for ATP consumption and regeneration for this strain with values obtained for wildtype reveals that this genetic perturbation caused a massive increase in overall ATP regeneration and cellular maintenance. This effect is stunning since flux estimations and enzyme assays demonstrated that this pathway is inactive under the tested conditions. The observation of alteration of glycogen contents under photomixotrophic conditions also hints towards the connection of energy metabolism and the ED pathway. It is stated in literature [111] that *Synechocystis* sp. PCC 6803 is using glycogen to adjust its ATP/NADPH ratio. These results point towards a yet unknown function of ED pathway enzymes in the regulation of growth and energy metabolism. This hypothesis is only reinforced by the lack of growth alteration by the same deletion mutant under photomixotrophic conditions when sufficient NADPH and thus ATP is present. Growth alteration under photomixotrophic growth as stated in literature [12] may be caused by this effect on energy metabolism, since cells encounter varying lighting conditions throughout

cultivation in tubular bubble columns (compare Figure 4.1 and Figure 4.5). Furthermore, the data presented here yields the conclusion that the slow growth rate observed for heterotrophic growth is not limited by kinetics for glucose uptake or energy regeneration. Overall, flux analysis in heterotrophic growth revealed an additional subject for future research into the role of the ED pathway for *Synechocystis* sp. PCC 6803.

Metabolism in darkness is an important topic for establishing large scale production with cyanobacteria as production hosts. Designing strains of cyanobacteria for e.g., biofuel production that allows sequestering of carbon from the atmosphere must be able to compete with fossil fuel extraction and refinement [128, 129]. The assumption that *Synechocystis* sp. PCC 6803 is mostly operating in cell maintenance mode when photosynthesis is inactive implies that during night-time (e.g., in open pond systems) carbon fixed during the day is lost due to cell maintenance, which may also mean consumption of product. This reduces the overall efficiency of the process. Counter measure is illumination during night-time, which is energy and cost intensive, somewhat contradicting the whole purpose of using phototrophs for production [130]. Deletion of the ED pathway as part of strain design harbours the risk of creating a strain that loses a lot of carbon during night times. Furthermore, the data presented in this work emphasizes that production with cyanobacteria as production host is limited by light supply. Measurements for light intensities and subsequent calculation for radial profiles demonstrate that design of cultivation equipment for maximum light supply is key to avoid loss of carbon and product by cells switching into preservation mode. With flux estimation protocols presented in this work, a potent tool for investigation of future production host was established that can be implemented for other photomixotrophs as well. Further focus should also be on investigation of other substrates. Bioprocessing that uses complex substrate mixtures in form of waste streams is a promising field of research to establish economically viable applications of cyanobacteria.

The role of ED pathway for *Synechocystis* sp. PCC 6803.

Summing up the results obtained for ^{13}C metabolic flux analysis and cultivation results of *Synechocystis* sp. PCC 6803 in heterotrophic and photomixotrophic growth mode, it remains unclear, which role the ED pathway plays in this microbe. Certainly, it does not take part in conducting metabolic fluxes under the conditions tested here. To investigate the role of the ED pathway, enzyme activity of KDPG aldolase was assayed in cell extracts obtained for both growth modes. In both cases, activity was below detection limit. Furthermore, quantification of KDPG, the unique intermediate of the ED pathway, was performed by using ultrasensitive LC-MS measurements. For both growth modes no quantifiable amounts (limit of quantification: 0.02 nmol g^{-1}) of this compound were detected. As a reference, *Pseudomonas putida* was subjected to the same analysis since it is known to heavily rely on the ED pathway. For this

microbe a KDPG content of 1.4 ± 0.2 µmol g^{-1} was determined and it was positive for KDPG aldolase activity. This comparison emphasises that the role of the ED pathway may not be conducting metabolic fluxes. Genes of this pathway appear to play an important role in the regulation of growth behaviour and energy metabolism. Apart from the data presented here, differences in growth behaviour were observed when Δ*eda* was cultivated in tubular bioreactors [12] and the combination of different gene deletions showed similar effects on growth characteristics, independent of cultivation equipment [13].

The difference of *in vivo* fluxes determined for heterotrophic and photomixotrophic growth obtained during this work cannot be more different. The two growth modes represent two extrema, one being a metabolism that operates with a net consumption of reducing equivalents by carbon fixation, and the other being a metabolism that runs glucose taken from medium in a circle to obtain as much NADPH as possible. Having to switch from one extremum to the other is part of the cyanobacterial life cycle. Cyanobacteria living in biofilms probably encounter slow changes in metabolic states during dusk and dawn. For species living as single cells a more drastic change in lighting conditions is possible by, e.g., shade cast by objects in the surrounding environment. Cells may also be swept away by water motion to a place with low light intensities. In an attempt to mimic a quick transfer between light and dark growth mode, cultivation was carried out with light dark cycles with a frequency of 1 min^{-1}, yielding the semi-logarithmic profiles shown in Figure 4.34. The resulting growth rates of this experiment with varying lighting conditions recreated the results that were stated in literature [12]: deletion of KDPG aldolase (Δ*eda*) decreases the growth rate. Again, a connection between the cell's energy state and the role of the ED pathway seems to be present.

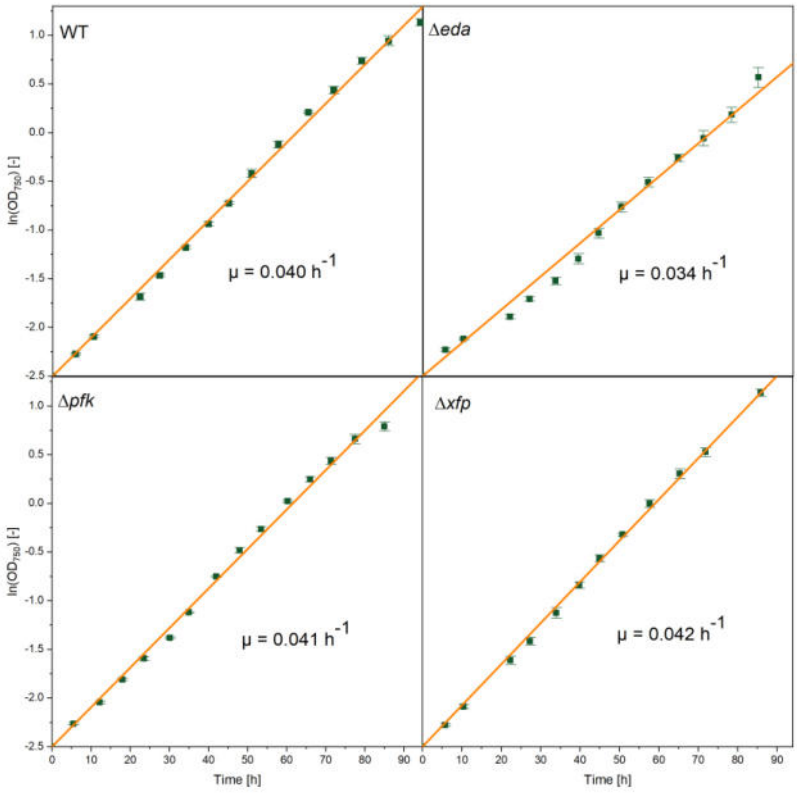

Figure 4.34: Semi logarithmic profiles of Synechocystis sp. PCC 6803 cultivated with altering light and dark cycles with a frequency of 1 min^{-1}.

Photomixotrophic and heterotrophic growth are just two possible options for *Synechocystis* sp. PCC 6803 to grow. Within these growth modes even small variations of cultivation parameters are proven to effect flux distributions [79, 82]. The results presented here demonstrate, how differently just one genetic alteration can play out when looking at physiological parameters alone. ED pathway and PK pathway contribute bypass reactions and connections with other core metabolic pathways of *Synechocystis* sp. PCC 6803.

As discussed for the energy metabolism of this microbe, metabolic control is complex and highly interconnected. For instance, the ED pathway has the unique intermediate 2-keto-3-desoxy-6-phosphogluconate. It was shown by Chen *et al.* [12] that in some instances, measurable concentrations of this intermediate are present in *Synechocystis* sp. PCC 6803. The importance of the oxidative PP pathway for energy homeostasis may call for an overflow valve that is present in form of the EDP or the PK. These pathways can become active when the pentose-5-phosphate pool is exceeding levels that cause inhibition of other pathways. Different scenarios can be created where the activity of one or both novel pathways play a role in response to environmental stress. The observation that pathways are not used fits the observation that enzymes are operating below full capacity. Table 8 shows activities determined for different key enzymes of the core metabolism of *Synechocystis* sp. PCC 6803

grown in photomixotrophic growth mode. *In vivo* fluxes obtained for said enzymes are smaller than those determined for cell extracts. Especially high activity of phosphofructokinase is a good example, since this enzyme is not catalysing a major flux during photomixotrophic growth.

Table 8: Activities of enzymes measured in cell extract for *Synechocystis* sp. PCC 6803 grown in photomixotrophic growth mode. Additionally, measured enzyme capacities were normalized to q_S for wildtype gown in shake flaks.

Enzyme	Activity [unit g^{-1}]	Normalised to q_s [%]	Specific rate [mmol g^{-1} h^{-1}]
Phosphofructokinase	5.2 ± 0.8	78.5 ± 12.6	33.0 ± 5.3
Fructose 1,6-bisphosphatase	3.2 ± 0.2	48.7 ± 2.6	20.5 ± 1.1
Isocitrate dehydrogenase	30.7 ± 2.7	464.5 ± 40.9	195.6 ± 17.4
Malic enzyme	0.0 ± 0.0	0.0 ± 0.0	0.0 ± 0.0
Phosphoketolase	0.0 ± 0.0	0.0 ± 0.0	0.0 ± 0.0
KDPG aldolase	0.0 ± 0.0	0.0 ± 0.0	0.0 ± 0.0

Under laboratory conditions cells are kept under constant conditions. For stationary ^{13}C metabolic flux analysis this is the major criterium to enable the calculation of fluxes. In their natural habitat, *Synechocystis* sp. PCC 6803 cells rarely encounter photomixotrophic conditions with metabolic steady state. It is crucial for the cell to be able to react to changing environmental conditions. With the flux distribution and measured enzyme activities obtained here, a brief impression the cells strategies of stress response are given. For example, estimated fluxes of phosphofructokinase and fructose 1,6-bisphophatase are agreeing with *ex vivo* enzyme assays. Although, no flux through phosphofructokinase was estimated, activity of this enzyme was measured, indicating constitutive expression of *pfk* for quick metabolic response to environmental changes. A rapid shift into darkness demands shifting the metabolism to heterotrophy. Estimated flux for fructose bisphosphatase was below the determined *ex vivo* activity, indicating, that this enzyme is not used with maximum capacity. This metabolic reserve may be needed when cells are shifting to autotrophic growth. Again, enzymes are probably expressed constitutively to allow for quick metabolic adaptation to changing environmental conditions. Another example for high metabolic flexibility is the determined capacity of isocitrate dehydrogenase. This enzyme´s capacity exceeds its determined flux by a high magnitude, indicating that the TCA cycle capacity is kept at high levels to be able to switch to regeneration of reducing equivalents when photosynthesis is stopped by environmental changes. Still, all these scenarios are in the realm of speculation. Including all the information obtained during this work and literature it is possible to state that the ED pathway must play a role on some level other than the fluxome of *Synechocystis* sp. PCC 6803. Effects on growth behaviour are most likely *moonlighting* effects [131-134] that are rooted somewhere in the cellular organisation, but not the fluxome.

5. Conclusion

Resolving the highly interconnected metabolic fluxes was the main task in this work to investigate the hypothesis, that fluxes through the ED pathway are essential for the growth of *Synechocystis* sp. PCC 6803. The data presented here disproves it and another hypothesis needs to be found to explain changes in physiology by disruption of the ED pathway. This statement is backed by experimental data that stands on the ground of detailed analysis of cultivation parameters and modelling. Living cells are organized on different levels. Each level of organisation has its own regulatory system and interacts with other structures. The fluxome as determined in this work is the result of genome, proteome, and metabolome. It describes the metabolites into each other. As demonstrated by this work, the fluxome of *Synechocystis* sp. PCC 6803 shows high plasticity. Observed alteration of physiological parameters must be investigated on other levels of organisation apart from the fluxome. Rough estimation of ATP metabolism already provides an orientation in which direction future analysis may lead. This work can only emphasise that a more general analysis of *Synechocystis* sp. PCC 6803 is necessary to resolve the role of the ED pathway. Systems biology approaches are widely accessible and are well documented for multiple organisms and application for production host optimisation in the context of biotechnology [55, 135-138]. For *Synechocystis* sp. PCC6803 first examples exist that attempted to combine metabolome and fluxome [102]. Cultivation methods described in this work can builds a foundation to generate high quality data sets with excellent consistency to conduct future holistic analysis of this microbe. Furthermore, fluxes determined for deletion mutants show that drawing information on pathway role from gene deletion experiments is limited due to the high metabolic plasticity of this organism. Nevertheless, it is one key element in the toolbox to investigate this group of microbes with rich metabolic potential. Exploiting this potential could also include analysis of the metabolism as presented here with other substrates than glucose. Promising alternatives may be compounds that originate from decay of plant material, since these are more likely to be present in the natural habitat of *Synechocystis* sp. PCC 6803 than glucose.

6. Outlook

Considering the looming climate catastrophe caused by anthropogenic activity, establishing of sustainable bioprocessing is one of the most promising ways to reduction of emissions on a large scale. According to the Paris climate accord (Paris Agreement, Dec. 12, 2015, T.I.A.S. No. 16-1104) a maximum global carbon dioxide emission budget of 420 Gt_C was estimated to avoid an increase in mean global temperature of less than 1.5 °C. Currently, an annual emission of approximately 7.0 Gt_C is caused by burning of fossil fuels for energy generation, transport, and production of goods [139]. Generation of heat and energy from sustainable sources like wind power, sunlight and biomass has a vast potential of greenhouse gas emission reduction since about a quarter of annual emissions originate from electricity generation [140]. The magnitude in which bioenergy can contribute to reduction of greenhouse gas emissions is disputed and various models exist that try to answer this question [141-143]. Most bioenergy sources rely on using agricultural products or waste streams, coming with the disadvantage of food vs. fuel controversies [144, 145]. Avoiding competition for arable land to grow crops for production of fuel is the use of micro algae [32, 34, 146, 147]. Flux estimations that are presented in this work enable knowledge driven strain design using *Synechocystis* sp. PCC 6803 as host for biofuel production. Resolving the metabolic network of this microbe allows for identification of targets for metabolic engineering. Most notably, the observation that *Synechocystis* sp. PCC 6803 is switching into a cell maintenance-oriented metabolism brings implications for future optimization strategies. Life-cycle assessments of bioprocesses with cyanobacteria must consider carbon loss during night-time.

7. Sources

1. Solomon S, Plattner GK, Knutti R, Friedlingstein P: **Irreversible climate change due to carbon dioxide emissions.** *Proceedings of the National Academy of Sciences of the United States of America* 2009, **106:**1704-1709.
2. Masson-Delmotte V, Zhai P, Pirani A, Connors SL, Péan C, Berger S, Caud N, Chen Y, Goldfarb L, Gomis MI, et al: **Climate Change 2021: The Physical Science Basis. Contribution of Working Group I to the Sixth Assessment Report of the Intergovernmental Panel on Climate Change** *Cambridge University Press* 2021.
3. Hidalgo D, Sanchez R, Lalaleo L, Bonfill M, Corchete P, Palazon J: **Biotechnological Production of Pharmaceuticals and Biopharmaceuticals in Plant Cell and Organ Cultures.** *Current medicinal chemistry* 2018, **25:**3577-3596.
4. Bhatia S, Dahiya R: **Chapter 8 - Plant-Based Biotechnological Products With Their Production Host, Modes of Delivery Systems, and Stability Testing.** In *Modern Applications of Plant Biotechnology in Pharmaceutical Sciences.* Edited by Bhatia S, Sharma K, Dahiya R, Bera T. Boston: Academic Press; 2015: 293-331
5. Voloshin RA, Rodionova MV, Zharmukhamedov SK, Nejat Veziroglu T, Allakhverdiev SI: **Review: Biofuel production from plant and algal biomass.** *International Journal of Hydrogen Energy* 2016, **41:**17257-17273.
6. Witcover J, Yeh S, Sperling D: **Policy options to address global land use change from biofuels.** *Energy Policy* 2013, **56:**63-74.
7. Singh S, Pereira APA, Verma JP: **Research and Production of Third-Generation Biofuels.** *Bioprocessing for Biomolecules Production* 2019**:**401-416.
8. Borrero-de Acuña JM, Gutierrez-Urrutia I, Hidalgo-Dumont C, Aravena-Carrasco C, Orellana-Saez M, Palominos-Gonzalez N, van Duuren JBJH, Wagner V, Gläser L, Becker J, et al: **Channelling carbon flux through the meta-cleavage route for improved poly(3-hydroxyalkanoate) production from benzoate and lignin-based aromatics in *Pseudomonas putida* H.** *Microbial Biotechnology* 2020, **n/a**.
9. Poblete-Castro I, Hoffmann S-L, Becker J, Wittmann C: **Cascaded valorization of seaweed using microbial cell factories.** *Current opinion in biotechnology* 2020, **65:**102-113.
10. Liguori R, Amore A, Faraco V: **Waste valorization by biotechnological conversion into added value products.** *Applied microbiology and biotechnology* 2013, **97:**6129-6147.
11. Savakis P, Hellingwerf KJ: **Engineering cyanobacteria for direct biofuel production from CO_2.** *Current opinion in biotechnology* 2015, **33:**8-14.
12. Chen X, Schreiber K, Appel J, Makowka A, Fähnrich B, Roettger M, Hajirezaei MR, Sönnichsen FD, Schönheit P, Martin WF, Gutekunst K: **The Entner-Doudoroff pathway is an overlooked glycolytic route in cyanobacteria and plants.** *Proceedings of the National Academy of Sciences of the United States of America* 2016, **113:**5441-5446.
13. Makowka A, Nichelmann L, Schulze D, Spengler K, Wittmann C, Forchhammer K, Gutekunst K: **Glycolytic Shunts Replenish the Calvin-Benson-Bassham Cycle as Anaplerotic Reactions in Cyanobacteria.** *Molecular plant* 2020, **13:**471-482.
14. Xiong W, Lee T-C, Rommelfanger S, Gjersing E, Cano M, Maness P-C, Ghirardi M, Yu J: **Phosphoketolase pathway contributes to carbon metabolism in cyanobacteria.** *Nature plants* 2015, **2:**15187.
15. Lem NW, Glick BR: **Biotechnological uses of cyanobacteria.** *Biotechnology advances* 1985, **3:**195-208.
16. Schopf JW: **Microfossils of the Early Archean Apex Chert - New Evidence of the Antiquity of Life.** *Science* 1993, **260:**640-646.
17. Demoulin CF, Lara YJ, Cornet L, Francois C, Baurain D, Wilmotte A, Javaux EJ: **Cyanobacteria evolution: Insight from the fossil record.** *Free radical biology & medicine* 2019, **140:**206-223.

18. Kaneko T, Sato S, Kotani H, Tanaka A, Asamizu E, Nakamura Y, Miyajima N, Hirosawa M, Sugiura M, Sasamoto S, et al: **Sequence analysis of the genome of the unicellular cyanobacterium *Synechocystis* sp. strain PCC6803. II. Sequence determination of the entire genome and assignment of potential protein-coding regions.** *DNA research : an international journal for rapid publication of reports on genes and genomes* 1996, **3:**109-136.
19. Smith AJ, London J, Stanier RY: **Biochemical basis of obligate autotrophy in blue-green algae and thiobacilli.** *Journal of bacteriology* 1967, **94:**972-983.
20. Zhang S, Bryant DA: **The tricarboxylic acid cycle in cyanobacteria.** *Science* 2011, **334:**1551-1553.
21. Lea-Smith DJ, Bombelli P, Vasudevan R, Howe CJ: **Photosynthetic, respiratory and extracellular electron transport pathways in cyanobacteria.** *Biochimica et biophysica acta* 2016, **1857:**247-255.
22. Colyer CL, Kinkade CS, Viskari PJ, Landers JP: **Analysis of cyanobacterial pigments and proteins by electrophoretic and chromatographic methods.** *Analytical and bioanalytical chemistry* 2005, **382:**559-569.
23. Shen G, Boussiba S, Vermaas WF: **Synechocystis sp PCC 6803 strains lacking photosystem I and phycobilisome function.** *The Plant cell* 1993, **5:**1853-1863.
24. Fan DY, Hope AB, Smith PJ, Jia H, Pace RJ, Anderson JM, Chow WS: **The stoichiometry of the two photosystems in higher plants revisited.** *Biochimica et biophysica acta* 2007, **1767:**1064-1072.
25. Vermaas WFJ: **Photosynthesis and Respiration in Cyanobacteria.** In *eLS.* John Wiley & Sons, Ltd; 2001
26. Vinyard DJ, Ananyev GM, Dismukes GC: **Photosystem II: the reaction center of oxygenic photosynthesis.** *Annual review of biochemistry* 2013, **82:**577-606.
27. Kurisu G, Zhang H, Smith JL, Cramer WA: **Structure of the Cytochrome b_6f Complex of Oxygenic Photosynthesis: Tuning the Cavity.** *Science* 2003, **302:**1009-1014.
28. Hepburn C: **Carbon Trading: A Review of the Kyoto Mechanisms.** *Annual Review of Environment and Resources* 2007, **32:**375-393.
29. Gudmundsson S, Nogales J: **Cyanobacteria as photosynthetic biocatalysts: a systems biology perspective.** *Molecular bioSystems* 2015, **11:**60-70.
30. Nozzi NE, Oliver JW, Atsumi S: **Cyanobacteria as a Platform for Biofuel Production.** *Frontiers in bioengineering and biotechnology* 2013, **1:**7.
31. Deng MD, Coleman JR: **Ethanol synthesis by genetic engineering in cyanobacteria.** *Applied and Environmental Microbiology* 1999, **65:**523-528.
32. Atsumi S, Higashide W, Liao JC: **Direct photosynthetic recycling of carbon dioxide to isobutyraldehyde.** *Nature biotechnology* 2009, **27:**1177-1180.
33. Hu Q, Sommerfeld M, Jarvis E, Ghirardi M, Posewitz M, Seibert M, Darzins A: **Microalgal triacylglycerols as feedstocks for biofuel production: perspectives and advances.** *The Plant journal : for cell and molecular biology* 2008, **54:**621-639.
34. Liu X, Sheng J, Curtiss R, 3rd: **Fatty acid production in genetically modified cyanobacteria.** *Proceedings of the National Academy of Sciences of the United States of America* 2011, **108:**6899-6904.
35. Wang W, Liu X, Lu X: **Engineering cyanobacteria to improve photosynthetic production of alka(e)nes.** *Biotechnology for biofuels* 2013, **6:**69.
36. Roles J, Yarnold J, Wolf J, Stephens E, Hussey K, Hankamer B: **Charting a development path to deliver cost competitive microalgae-based fuels.** *Algal Research* 2020, **45:**101721.
37. Scheelhaase J, Maertens S, Grimme W: **Synthetic fuels in aviation – Current barriers and potential political measures.** *Transportation Research Procedia* 2019, **43:**21-30.
38. Asada Y, Miyake M, Miyake J, Kurane R, Tokiwa Y: **Photosynthetic accumulation of poly-(hydroxybutyrate) by cyanobacteria--the metabolism and potential for CO_2 recycling.** *International journal of biological macromolecules* 1999, **25:**37-42.
39. Osanai T, Numata K, Oikawa A, Kuwahara A, Iijima H, Doi Y, Tanaka K, Saito K, Hirai MY: **Increased bioplastic production with an RNA polymerase sigma factor SigE**

during nitrogen starvation in *Synechocystis* sp. PCC 6803. *DNA research : an international journal for rapid publication of reports on genes and genomes* 2013, **20:**525-535.
40. Rippka R, Deruelles J, Waterbury JB, Herdman M, Stanier RY: **Generic Assignments, Strain Histories and Properties of Pure Cultures of Cyanobacteria.** *Microbiology* 1979, **111:**1-61.
41. Stal LJ, Moezelaar R: **Fermentation in cyanobacteria.** *FEMS Microbiology Reviews* 1997, **21:**179-211.
42. El-Sheekh M, El-Dalatony MM, Thakur N, Zheng Y, Salama E-S: **Role of microalgae and cyanobacteria in wastewater treatment: genetic engineering and omics approaches.** *International Journal of Environmental Science and Technology* 2021.
43. Papadopoulos KP, Economou CN, Tekerlekopoulou AG, Vayenas DV: **A Cyanobacteria-Based Biofilm System for Advanced Brewery Wastewater Treatment.** *Applied Sciences* 2021, **11**.
44. Hagiwara Y, Sugishima M, Khawn H, Kinoshita H, Inomata K, Shang L, Lagarias JC, Takahashi Y, Fukuyama K: **Structural insights into vinyl reduction regiospecificity of phycocyanobilin:ferredoxin oxidoreductase (PcyA).** *The Journal of biological chemistry* 2010, **285:**1000-1007.
45. Chen C-Y, Yeh K-L, Aisyah R, Lee D-J, Chang J-S: **Cultivation, photobioreactor design and harvesting of microalgae for biodiesel production: A critical review.** *Bioresource Technology* 2011, **102:**71-81.
46. Park JBK, Craggs RJ, Shilton AN: **Wastewater treatment high rate algal ponds for biofuel production.** *Bioresource Technology* 2011, **102:**35-42.
47. Kanehisa M, Goto S: **KEGG: kyoto encyclopedia of genes and genomes.** *Nucleic acids research* 2000, **28:**27-30.
48. Kanehisa M: **Toward understanding the origin and evolution of cellular organisms.** *Protein Science* 2019, **28:**1947-1951.
49. Kanehisa M, Furumichi M, Sato Y, Ishiguro-Watanabe M, Tanabe M: **KEGG: integrating viruses and cellular organisms.** *Nucleic acids research* 2021, **49:**D545-D551.
50. Mills LA, McCormick AJ, Lea-Smith DJ: **Current knowledge and recent advances in understanding metabolism of the model cyanobacterium *Synechocystis* sp. PCC 6803.** *Bioscience reports* 2020, **40**.
51. Kohlstedt M, Wittmann C: **GC-MS-based ^{13}C metabolic flux analysis resolves the parallel and cyclic glucose metabolism of *Pseudomonas putida* KT2440 and *Pseudomonas aeruginosa* PAO1.** *Metabolic engineering* 2019, **54:**35-53.
52. Flamholz A, Noor E, Bar-Even A, Liebermeister W, Milo R: **Glycolytic strategy as a tradeoff between energy yield and protein cost.** *Proceedings of the National Academy of Sciences* 2013, **110:**10039.
53. Klingner A, Bartsch A, Dogs M, Wagner-Döbler I, Jahn D, Simon M, Brinkhoff T, Becker J, Wittmann C, Nojiri H: **Large-Scale ^{13}C Flux Profiling Reveals Conservation of the Entner-Doudoroff Pathway as a Glycolytic Strategy among Marine Bacteria That Use Glucose.** *Applied and environmental microbiology* 2015, **81:**2408-2422.
54. Gu C, Kim GB, Kim WJ, Kim HU, Lee SY: **Current status and applications of genome-scale metabolic models.** *Genome Biology* 2019, **20:**121.
55. Kohlstedt M, Becker J, Wittmann C: **Metabolic fluxes and beyond—systems biology understanding and engineering of microbial metabolism.** *Applied microbiology and biotechnology* 2010, **88:**1065-1075.
56. Becker J, Zelder O, Häfner S, Schröder H, Wittmann C: **From zero to hero—Design-based systems metabolic engineering of *Corynebacterium glutamicum* for L-lysine production.** *Metabolic engineering* 2011, **13:**159-168.
57. Cooney CL, Acevedo F: **Theoretical conversion yields for penicillin synthesis.** *Biotechnology and bioengineering* 1977, **19:**1449-1462.
58. Antoniewicz MR: **Methods and advances in metabolic flux analysis: a mini-review.** *Journal of industrial microbiology & biotechnology* 2015, **42:**317-325.

59. Volkova S, Matos MRA, Mattanovich M, Marin de Mas I: **Metabolic Modelling as a Framework for Metabolomics Data Integration and Analysis.** *Metabolites* 2020, **10**.
60. Klamt S, Hädicke O, von Kamp A: **Stoichiometric and Constraint-Based Analysis of Biochemical Reaction Networks.** In *Large-Scale Networks in Engineering and Life Sciences.* Edited by Benner P, Findeisen R, Flockerzi D, Reichl U, Sundmacher K. Cham: Springer International Publishing; 2014: 263-316
61. Millard P, Smallbone K, Mendes P: **Metabolic regulation is sufficient for global and robust coordination of glucose uptake, catabolism, energy production and growth in *Escherichia coli*.** *PLoS computational biology* 2017, **13:**e1005396.
62. Wiechert W: **^{13}C Metabolic Flux Analysis.** *Metabolic engineering* 2001, **3:**195-206.
63. Park SM, Klapa MI, Sinskey AJ, Stephanopoulos G: **Metabolite and isotopomer balancing in the analysis of metabolic cycles: II. Applications.** *Biotechnology and bioengineering* 1999, **62:**392-401.
64. Antoniewicz MR, Kelleher JK, Stephanopoulos G: **Elementary metabolite units (EMU): a novel framework for modeling isotopic distributions.** *Metabolic engineering* 2007, **9:**68-86.
65. Fischer E, Sauer U: **Metabolic flux profiling of *Escherichia coli* mutants in central carbon metabolism using GC-MS.** *European journal of biochemistry* 2003, **270:**880-891.
66. Lange A, Becker J, Schulze D, Cahoreau E, Portais J-C, Haefner S, Schröder H, Krawczyk J, Zelder O, Wittmann C: **Bio-based succinate from sucrose: High-resolution ^{13}C metabolic flux analysis and metabolic engineering of the rumen bacterium *Basfia succiniciproducens*.** *Metabolic engineering* 2017, **44:**198-212.
67. Kohlstedt M, Sappa PK, Meyer H, Maaß S, Zaprasis A, Hoffmann T, Becker J, Steil L, Hecker M, van Dijl JM, et al: **Adaptation of *Bacillus subtilis* carbon core metabolism to simultaneous nutrient limitation and osmotic challenge: a multi-omics perspective.** *Environmental Microbiology* 2014, **16:**1898-1917.
68. Wittmann C, Heinzle E: **Mass spectrometry for metabolic flux analysis.** *Biotechnology and bioengineering* 1999, **62:**739-750.
69. Szyperski T: **Biosynthetically directed fractional ^{13}C-labeling of proteinogenic amino acids. An efficient analytical tool to investigate intermediary metabolism.** *European journal of biochemistry* 1995, **232:**433-448.
70. Becker J, Klopprogge C, Wittmann C: **Metabolic responses to pyruvate kinase deletion in lysine producing *Corynebacterium glutamicum*.** *Microbial Cell Factories* 2008, **7:**8.
71. Wittmann C, Heinzle E: **Application of MALDI-TOF MS to lysine-producing *Corynebacterium glutamicum*: a novel approach for metabolic flux analysis.** *European journal of biochemistry* 2001, **268:**2441-2455.
72. Wittmann C, Weber J, Betiku E, Krömer J, Böhm D, Rinas U: **Response of fluxome and metabolome to temperature-induced recombinant protein synthesis in *Escherichia coli*.** *Journal of biotechnology* 2007, **132:**375-384.
73. Feist AM, Palsson BO: **The biomass objective function.** *Current Opinion in Microbiology* 2010, **13:**344-349.
74. Hanegraaf PP, Muller EB: **The dynamics of the macromolecular composition of biomass.** *Journal of theoretical biology* 2001, **212:**237-251.
75. Zanghellini J, Ruckerbauer DE, Hanscho M, Jungreuthmayer C: **Elementary flux modes in a nutshell: properties, calculation and applications.** *Biotechnology journal* 2013, **8:**1009-1016.
76. Hildebrandt S: **Revision of the central carbon metabolism in a photoautotrophic organism.** 2020.
77. Shastri AA, Morgan JA: **Flux balance analysis of photoautotrophic metabolism.** *Biotechnology progress* 2005, **21:**1617-1626.
78. Nogales J, Gudmundsson S, Knight EM, Palsson BO, Thiele I: **Detailing the optimality of photosynthesis in cyanobacteria through systems biology analysis.** *Proceedings of the National Academy of Sciences of the United States of America* 2012, **109:**2678-2683.

79. Wan N, DeLorenzo DM, He L, You L, Immethun CM, Wang G, Baidoo EEK, Hollinshead W, Keasling JD, Moon TS, Tang YJ: **Cyanobacterial carbon metabolism: Fluxome plasticity and oxygen dependence.** *Biotechnology and bioengineering* 2017, **114:**1593-1602.
80. Terzer M, Stelling J: **Parallel Extreme Ray and Pathway Computation.** In*; Berlin, Heidelberg*. Springer Berlin Heidelberg; 2010: 300-309.
81. Wittmann C: **Fluxome analysis using GC-MS.** *Microbial Cell Factories* 2007, **6:**6.
82. Ueda K, Nakajima T, Yoshikawa K, Toya Y, Matsuda F, Shimizu H: **Metabolic flux of the oxidative pentose phosphate pathway under low light conditions in *Synechocystis* sp. PCC 6803.** *Journal of bioscience and bioengineering* 2018, **126:**38-43.
83. Schwechheimer SK, Becker J, Peyriga L, Portais J-C, Sauer D, Müller R, Hoff B, Haefner S, Schröder H, Zelder O, Wittmann C: **Improved riboflavin production with *Ashbya gossypii* from vegetable oil based on ^{13}C metabolic network analysis with combined labeling analysis by GC/MS, LC/MS, 1D, and 2D NMR.** *Metabolic engineering* 2018, **47:**357-373.
84. Quek L-E, Wittmann C, Nielsen LK, Krömer JO: **OpenFLUX: efficient modelling software for ^{13}C-based metabolic flux analysis.** *Microbial Cell Factories* 2009, **8:**25.
85. Wittmann C, Kim HM, Heinzle E: **Metabolic network analysis of lysine producing *Corynebacterium glutamicum* at a miniaturized scale.** *Biotechnology and bioengineering* 2004, **87:**1-6.
86. Wittmann C, Heinzle E: **Genealogy profiling through strain improvement by using metabolic network analysis: metabolic flux genealogy of several generations of lysine-producing corynebacteria.** *Applied and environmental microbiology* 2002, **68:**5843-5859.
87. Krömer JO, Bolten CJ, Heinzle E, Schroder H, Wittmann C: **Physiological response of *Corynebacterium glutamicum* to oxidative stress induced by deletion of the transcriptional repressor *McbR*.** *Microbiology* 2008, **154:**3917-3930.
88. Ling KH, Marcus F, Lardy HA: **Purification and Some Properties of Rabbit Skeletal Muscle Phosphofructokinase.** *The Journal of biological chemistry* 1965, **240:**1893-1899.
89. Pongratz RL, Kibbey RG, Cline GW: **Investigating the roles of mitochondrial and cytosolic malic enzyme in insulin secretion.** *Methods in enzymology* 2009, **457:**425-450.
90. Shiio I, Ozaki H: **Concerted Inhibition of Isocitrate Dehydrogenase by Glyoxylate Plus Oxalacetate.** *The Journal of Biochemistry* 1968, **64:**45-53.
91. Glenn K, Ingram-Smith C, Smith KS: **Biochemical and Kinetic Characterization of Xylulose 5-Phosphate/Fructose 6-Phosphate Phosphoketolase 2 (*Xfp2*) from *Cryptococcus neoformans*.** *Eukaryotic Cell* 2014, **13:**657.
92. Gläser L, Kuhl M, Jovanovic S, Fritz M, Vögeli B, Erb TJ, Becker J, Wittmann C: **A common approach for absolute quantification of short chain CoA thioesters in prokaryotic and eukaryotic microbes.** *Microbial Cell Factories* 2020, **19:**160.
93. Pulz O: **Photobioreactors: production systems for phototrophic microorganisms.** *Applied microbiology and biotechnology* 2001, **57:**287-293.
94. Ogbonna JC, Tanaka H: **Light requirement and photosynthetic cell cultivation – Development of processes for efficient light utilization in photobioreactors.** *Journal of Applied Phycology* 2000, **12:**207-218.
95. Molina Grima E, Fernández FGA, García Camacho F, Chisti Y: **Photobioreactors: light regime, mass transfer, and scaleup.** *Journal of biotechnology* 1999, **70:**231-247.
96. Acién FG, Molina E, Reis A, Torzillo G, Zittelli GC, Sepúlveda C, Masojídek J: **1 - Photobioreactors for the production of microalgae.** In *Microalgae-Based Biofuels and Bioproducts.* Edited by Gonzalez-Fernandez C, Muñoz R: Woodhead Publishing; 2017: 1-44
97. Schiefelbein S, Fröhlich A, John GT, Beutler F, Wittmann C, Becker J: **Oxygen supply in disposable shake-flasks: prediction of oxygen transfer rate, oxygen saturation**

and maximum cell concentration during aerobic growth. *Biotechnology letters* 2013, **35:**1223-1230.
98. Anderson SL, McIntosh L: **Light-activated heterotrophic growth of the cyanobacterium *Synechocystis* sp. strain PCC 6803: a blue-light-requiring process.** *Journal of bacteriology* 1991, **173:**2761-2767.
99. Zhang A, Carroll AL, Atsumi S: **Carbon recycling by cyanobacteria: improving CO_2 fixation through chemical production.** *Fems Microbiology Letters* 2017, **364**.
100. Zhou J, Zhu T, Cai Z, Li Y: **From cyanochemicals to cyanofactories: areview and perspective.** *Microbial cell factories* 2016, **15:**2.
101. Yang C, Hua Q, Shimizu K: **Metabolic flux analysis in *Synechocystis* using isotope distribution from ^{13}C-labeled glucose.** *Metabolic engineering* 2002, **4:**202-216.
102. Nakajima T, Kajihata S, Yoshikawa K, Matsuda F, Furusawa C, Hirasawa T, Shimizu H: **Integrated Metabolic Flux and Omics Analysis of *Synechocystis* sp. PCC 6803 under Mixotrophic and Photoheterotrophic Conditions.** *Plant and Cell Physiology* 2014, **55:**1605-1612.
103. Long CP, Au J, Gonzalez JE, Antoniewicz MR: **^{13}C metabolic flux analysis of microbial and mammalian systems is enhanced with GC-MS measurements of glycogen and RNA labeling.** *Metabolic engineering* 2016, **38:**65-72.
104. Massou S, Nicolas C, Letisse F, Portais J-C: **NMR-based fluxomics: Quantitative 2D NMR methods for isotopomers analysis.** *Phytochemistry* 2007, **68:**2330-2340.
105. Giraudeau P: **NMR-based metabolomics and fluxomics: developments and future prospects.** *Analyst* 2020, **145:**2457-2472.
106. You L, Berla B, He L, Pakrasi HB, Tang YJ: **^{13}C-MFA delineates the photomixotrophic metabolism of *Synechocystis* sp. PCC 6803 under light- and carbon-sufficient conditions.** *Biotechnology journal* 2014, **9:**684-692.
107. Millard P, Sokol S, Kohlstedt M, Wittmann C, Létisse F, Lippens G, Portais J-C: **IsoSolve: an integrative framework to improve isotopic coverage and consolidate isotopic measurements by MS and/or NMR.** *bioRxiv* 2021**:**2021.2003.2008.430771.
108. Yang TH, Heinzle E, Wittmann C: **Theoretical aspects of ^{13}C metabolic flux analysis with sole quantification of carbon dioxide labeling.** *Computational biology and chemistry* 2005, **29:**121-133.
109. Antoniewicz MR: **A guide to ^{13}C metabolic flux analysis for the cancer biologist.** *Experimental & Molecular Medicine* 2018, **50:**1-13.
110. Antoniewicz MR, Kelleher JK, Stephanopoulos G: **Determination of confidence intervals of metabolic fluxes estimated from stable isotope measurements.** *Metabolic engineering* 2006, **8:**324-337.
111. Cano M, Holland SC, Artier J, Burnap RL, Ghirardi M, Morgan JA, Yu J: **Glycogen Synthesis and Metabolite Overflow Contribute to Energy Balancing in Cyanobacteria.** *Cell Reports* 2018, **23:**667-672.
112. Yu King Hing N, Liang F, Lindblad P, Morgan JA: **Combining isotopically non-stationary metabolic flux analysis with proteomics to unravel the regulation of the Calvin-Benson-Bassham cycle in *Synechocystis* sp. PCC 6803.** *Metabolic engineering* 2019, **56:**77-84.
113. Abernathy MH, Czajka JJ, Allen DK, Hill NC, Cameron JC, Tang YJ: **Cyanobacterial carboxysome mutant analysis reveals the influence of enzyme compartmentalization on cellular metabolism and metabolic network rigidity.** *Metabolic engineering* 2019, **54:**222-231.
114. Tabita FR, Colletti C: **Carbon dioxide assimilation in cyanobacteria: regulation of ribulose, 1,5-bisphosphate carboxylase.** *Journal of bacteriology* 1979, **140:**452-458.
115. Marsden WJN, Codd GA: **Purification and Molecular and Catalytic Properties of Phosphoribulokinase from the Cyanobacterium *Chlorogloeopsis fritschii*.** *Microbiology* 1984, **130:**999-1006.
116. Kang R, Wang J, Shi D, Cong W, Cai Z, Ouyang F: **Interactions between organic and inorganic carbon sources during mixotrophic cultivation of *Synechococcus* sp.** *Biotechnology letters* 2004, **26:**1429-1432.

117. Chojnacka K, Noworyta A: **Evaluation of *Spirulina* sp. growth in photoautotrophic, heterotrophic and mixotrophic cultures.** *Enzyme and Microbial Technology - ENZYME MICROB TECHNOL* 2004, **34:**461-465.
118. Pagnanelli F, Altimari P, Trabucco F, Toro L: **Mixotrophic growth of *Chlorella vulgaris* and *Nannochloropsis oculata*: interaction between glucose and nitrate.** *Journal of Chemical Technology & Biotechnology* 2014, **89:**652-661.
119. Yamane Y-i, Utsunomiya T, Watanabe M, Sasaki K: **Biomass production in mixotrophic culture of *Euglena gracilis* under acidic condition and its growth energetics.** *Biotechnology letters* 2001, **23:**1223-1228.
120. Heredia-Arroyo T, Wei W, Hu B: **Oil Accumulation via Heterotrophic/Mixotrophic *Chlorella protothecoides*.** *Applied Biochemistry and Biotechnology* 2010, **162:**1978-1995.
121. Michelet L, Zaffagnini M, Morisse S, Sparla F, Pérez-Pérez ME, Francia F, Danon A, Marchand C, Fermani S, Trost P, Lemaire S: **Redox regulation of the Calvin–Benson cycle: something old, something new.** *Frontiers in Plant Science* 2013, **4:**470.
122. McFarlane CR, Shah NR, Kabasakal BV, Echeverria B, Cotton CAR, Bubeck D, Murray JW: **Structural basis of light-induced redox regulation in the Calvin–Benson cycle in cyanobacteria.** *Proceedings of the National Academy of Sciences* 2019, **116:**20984.
123. Tamoi M, Miyazaki T, Fukamizo T, Shigeoka S: **The Calvin cycle in cyanobacteria is regulated by CP12 via the NAD(H)/NADP(H) ratio under light/dark conditions.** *The Plant Journal* 2005, **42:**504-513.
124. Matsuo M, Endo T, Asada K: **Isolation of a Novel NAD(P)H-Quinone Oxidoreductase from the Cyanobacterium *Synechocystis* PCC6803.** *Plant and Cell Physiology* 1998, **39:**751-755.
125. Lea-Smith DJ, Bombelli P, Vasudevan R, Howe CJ: **Photosynthetic, respiratory and extracellular electron transport pathways in cyanobacteria.** *Biochimica et Biophysica Acta (BBA) - Bioenergetics* 2016, **1857:**247-255.
126. Pogoryelov D, Reichen C, Klyszejko Adriana L, Brunisholz R, Muller Daniel J, Dimroth P, Meier T: **The Oligomeric State of c Rings from Cyanobacterial F-ATP Synthases Varies from 13 to 15.** *Journal of bacteriology* 2007, **189:**5895-5902.
127. Bolten CJ, Heinzle E, Müller R, Wittmann C: **Investigation of the central carbon metabolism of *Sorangium cellulosum*: metabolic network reconstruction and quantification of pathway fluxes.** *Journal of microbiology and biotechnology* 2009, **19:**23-36.
128. Chen H, Li T, Wang Q: **Ten years of algal biofuel and bioproducts: gains and pains.** *Planta* 2019.
129. Gnansounou E, Kenthorai Raman J: **Life cycle assessment of algae biodiesel and its co-products.** *Applied Energy* 2016, **161:**300-308.
130. Branco-Vieira M, Mata TM, Martins AA, Freitas MAV, Caetano NS: **Economic analysis of microalgae biodiesel production in a small-scale facility.** *Energy Reports* 2020, **6:**325-332.
131. Gancedo C, Flores C-L: **Moonlighting Proteins in Yeasts.** *Microbiology and Molecular Biology Reviews* 2008, **72:**197-210.
132. Jeffery CJ: **Moonlighting proteins.** *Trends in Biochemical Sciences* 1999, **24:**8-11.
133. Mani M, Chen C, Amblee V, Liu H, Mathur T, Zwicke G, Zabad S, Patel B, Thakkar J, Jeffery CJ: **MoonProt: a database for proteins that are known to moonlight.** *Nucleic acids research* 2015, **43:**D277-D282.
134. Sauer UH, Mishra Y, Hall M, Nam K, Jansson S, Schroder WP: **Dimeric cyanobacterial 1-Cys Prx6 is a moonlighting protein.** *Acta Crystallographica Section A* 2016, **72:**s247-s248.
135. O'Donnell ST, Ross RP, Stanton C: **The Progress of Multi-Omics Technologies: Determining Function in Lactic Acid Bacteria Using a Systems Level Approach.** *Frontiers in Microbiology* 2020, **10**.
136. Zhang W, Li F, Nie L: **Integrating multiple 'omics' analysis for microbial biology: application and methodologies.** *Microbiology* 2010, **156:**287-301.

137. Becker J, Wittmann C: **From systems biology to metabolically engineered cells—an omics perspective on the development of industrial microbes.** *Current Opinion in Microbiology* 2018, **45:**180-188.
138. Lee JW, Na D, Park JM, Lee J, Choi S, Lee SY: **Systems metabolic engineering of microorganisms for natural and non-natural chemicals.** *Nature Chemical Biology* 2012, **8:**536-546.
139. Shukla PR, Skea J, Calvo Buendia E, Masson -DV, Pörtner H-O, Roberts DC, Zhai P, Slade R, Connors S, van Diemen R, et al: **IPCC, 2019: Climate Change and Land: an IPCC special report on climate change, desertification, land degradation, sustainable land management, food security, and greenhouse gas fluxes in terrestrial ecosystems.** *Cambridge University Press* 2019.
140. Fekete H, Kuramochi T, Roelfsema M, Elzen Md, Forsell N, Höhne N, Luna L, Hans F, Sterl S, Olivier J, et al: **A review of successful climate change mitigation policies in major emitting economies and the potential of global replication.** *Renewable and Sustainable Energy Reviews* 2021, **137:**110602.
141. Rose SK, Kriegler E, Bibas R, Calvin K, Popp A, van Vuuren DP, Weyant J: **Bioenergy in energy transformation and climate management.** *Climatic Change* 2014, **123:**477-493.
142. Klein D, Luderer G, Kriegler E, Strefler J, Bauer N, Leimbach M, Popp A, Dietrich JP, Humpenöder F, Lotze-Campen H, Edenhofer O: **The value of bioenergy in low stabilization scenarios: an assessment using REMIND-MAgPIE.** *Climatic Change* 2014, **123:**705-718.
143. Bauer N, Rose SK, Fujimori S, van Vuuren DP, Weyant J, Wise M, Cui Y, Daioglou V, Gidden MJ, Kato E, et al: **Global energy sector emission reductions and bioenergy use: overview of the bioenergy demand phase of the EMF-33 model comparison.** *Climatic Change* 2020, **163:**1553-1568.
144. Prasad S, Ingle AP: **Chapter 12 - Impacts of sustainable biofuels production from biomass.** In *Sustainable Bioenergy.* Edited by Rai M, Ingle AP: Elsevier; 2019: 327-346
145. Rosegrant MW, Msangi S: **Consensus and Contention in the Food-Versus-Fuel Debate.** *Annual Review of Environment and Resources* 2014, **39:**271-294.
146. Eungrasamee K, Miao R, Incharoensakdi A, Lindblad P, Jantaro S: **Improved lipid production via fatty acid biosynthesis and free fatty acid recycling in engineered *Synechocystis* sp. PCC 6803.** *Biotechnology for biofuels* 2019, **12:**8.
147. Gao Z, Zhao H, Li Z, Tan X, Lu X: **Photosynthetic production of ethanol from carbon dioxide in genetically engineered cyanobacteria.** *Energy & Environmental Science* 2012, **5:**9857-9865.

8. Appendix

Abbreviations

Word	Abbreviation
1-(2-Carboxyphenylamino)-1-deoxy-D-ribulose 5-phosphate	CPADR5P
2-keto-3-deoxy-6-phosphogluconate	KDPG
3-phosphoglycerate	3PG
6-phosphogluconate	6PG
Acetyl coenzyme A	AcCOA
Adenosine diphosphate	ADP
Adenosine triphosphate	ATP
Alanine	ALA
Anthranilate	ANTHR
Arginine	ARG
Aspartate	ASP
Chorismate	CHRM
Cysteine	CYS
dihydroxyacetone phosphate	DHAP
Elementary flux modes	EFM
Embden-Meyerhof-Parnas Pathway	EMP
Entner-Douroroff pathway	ED
Equation	Eq
Erythrose 4-phosphate	E4P
Ferredoxin	Fd
ferredoxin-$NADP^+$-oxidoreductase	FNR
Flavin adenine dinucleotide	FAD(H)
Fructose 1,6-bisphosphate	F16BP
Fructose 6-phosphate	F6P
Fumarate	FUM
Gas chromatography	GC
Glucose	GLC
Glucose 6-phosphate	G6P
Glutamate	GLU
glyceraldehyde 3-phosphate	GAP
Glycine	GLY
Histidine	HIS
Indigo	INDG
Isocitrate	iCIT
Isoleucine	ILE
Isovalerate	ISV
Leucine	LEU
Lysine	LYS
Malate	MAL
Mass distribution vector	MDV
Mass spectrometer	MS
Methionine	MET
Nicotinamide adenine dinucleotide	NAD(H)
Nicotinamide adenine dinucleotide phosphate	NADP(H)
Nuclear magnetic resonance spectroscopy	NMR
Pentose 5-phosphate	P5P
Pentose phosphate pathway	PP
Phenylalanine	PHE

Word	Abbreviation
Phosphoenolpyruvate	PEP
Phosphoketolase	PK
Photo bioreactors	PBR
Photosystem	PS
Phycocyanin	PC
Plastoquinol	QH_2
Plastoquinone	Q
Polhydroxybutyrates	PHB
Pyruvate	PYR
Reaction equation	RXN
Sedoheptulose 1,7-bisphosphate	S17BP
Sedoheptulose 7-phosphate	S7P
Serine	SER
Shikimate	SHKM
Sum of squares residual	SSR
Succinate	SUC
Succinate-semialdehyde	SucA
Threonine	THR
Tricarboxylic acid cycle	TCA
Tryptophane	TRP
Valine	Val
α-ketoglutarate	AKG

List of figures

Table A 1: Slopes resulting from linear regressions for correlations between the logarithms of measured transmission and varying light passages for suspension of *Synechocystis* sp. PCC 6803 in BG11 medium with different optical densities as depicted in Fig. 10 A and B.

OD_{750} [-]	Slope [cm^{-1}]	Deviation [cm^{-1}]	R^2
5.0	-2.03442	0.03661	0.99709
4.5	-1.84769	0.02564	0.99827
4.0	-1.59059	0.01986	0.9986
3.5	-1.34191	0.01658	0.99863
3.0	-1.15266	0.01309	0.99884
2.5	-0.96245	0.00478	0.99978
2.0	-0.77946	0.00536	0.99957
1.5	-0.58504	0.00474	0.99941
1.0	-0.40191	0.00109	0.99993
0.5	-0.22022	0.00516	0.99508
0.0	0	0	0

Model for elementary flux modes

%Core Metabolism
'GLC_ex --> GLC'
'CO2_EX <==> CO2'
'GLC + ATP --> G6P + ADP'
%% oxPP
'G6P + NADP --> PGnat + NADPH'
'PGnat + NADP --> Ru5P + CO2 + NADPH'
%%Entner-Doudoroff
'PGnat --> KDPG'
'KDPG --> PYR + G3P'
%%Glycolysis
'G6P <==> F6P'
'F6P + ATP --> F16BP + ADP'
'F16BP --> F6P + Pi'
'F16BP <==> DHAP + G3P'
'DHAP <==> GAP'
'GAP + Pi + NAD --> G13BP + NADH'
'G13BP + NADPH --> GAP + NADP + Pi'
'G13BP + ADP <==> G3P + ATP'
'G3P <==> PG'
'PG <==> PEP'
'PEP + ADP --> PYR + ATP'
'PYR + NAD --> ACCOA + CO2 + NADH'
%Pentose-Phosphate-Pathway
'X5P <==> Ru5P'
'Ru5P <==> Ri5P'
'Ri5P + X5P <==> S7P + GAP'
'S7P + GAP <==> E4P + F6P'
'E4P + X5P <==> F6P + G3P'
%%Calvin-Benson-Bessham
'Ru5P + ATP --> Ru15BP + ADP'
'Ru15BP + CO2 --> (2) PG'
'DHAP + E4P --> S17BP'
'S17BP --> S7P + Pi'
%%TCA
'ACCOA + OAA --> ICIT'
'ICIT + NADP --> AKG + CO2 + NADPH'
'AKG --> SucA + CO2'
'SucA + NADP --> SUC + NADPH'
'SUC + Q <--> FUM + QH2'
'FUM <--> MAL'
'MAL + NAD <--> OAA + NADH'
'PEP + CO2 --> OAA'
'MAL --> PYR + CO2'
'X5P --> ACCOA + G3P'
'F6P --> ACCOA + E4P'
%N-Metabolism (NO3)
'NO3_ex + ATP --> NO3 + Pi + ADP'
'NO3 + 8 FD_red --> NH3 + 8 FD_ox'
%S-Metabolism (SO4)
'SO4_ex + ATP --> SO4 + ADP + Pi'
'SO4 + 2 ATP --> SO3 + ADP + AMP + Pi + PPi'
'SO3 + 6 FD_red --> SH2 + 6 FD_ox'
%PO4 Metabolism

```
'PPi --> 2 Pi'
'Pi + ATP --> ADP + PPi'
'AMP + ATP --> 2 ADP'
'PO4 --> Pi'
%Photoxynthesis
'2 Phot + Q --> QH2 + 2 H_ex'
'1 Phot + 1 PC_red + FD_ox --> PC_ox + FD_red'
%Electrone transport
'NADH + Q --> NAD + QH2 + 4 H_ex'
'NADH + Q --> NAD + QH2'
'NADPH + Q --> NADP + QH2 + 4 H_ex'
'NADPH + 2 FD_ox <==> NADP + 2 FD_red'
'QH2 + 2 PC_ox --> Q + 2 PC_red + 4 H_ex'
'QH2 --> Q + 2 H_ex'
%ATP-regeneration
'14 H_ex + 3 ADP + 3 Pi --> 3 ATP'
'ATP --> ADP + Pi'
%Externals
'BIOMASS -->'
'--> CO2_EX'
'--> GLC_ex'
'--> NO3_ex'
'--> SO4_ex'
'-->PO4'
'--> Phot'
};
```

Table A 2: Anabolic fluxes for elementary flux mode analysis. Given are anabolic demands for photomixotrophic and heterotrophic growth modes.

Compound	Photomixotrophic [mmol g^{-1}]	Heterotrophic [mmol g^{-1}]
ATP	38.89	39.21
SH_2	0.136	0.136
NH_3	7.14	7.14
G6P	1.228	0.882
NADPH	29.01	27.22
PYR	2.44	+ 2.64
GAP	0.208	0.238
NAD	2.82	2.82
PEP	1.42	1.53
ACCOA	3.96	4.64
Ri5P	0.382	0.399
E4P	0.376	0.406
OAA	1.14	1.23
AKG	0.886	1.04
CO_2	-1.834	-1.834

^{13}C metabolic flux analysis model and results

Table A 3 :Model topology for the estimation of in vivo fluxes for Synechocystis sp. PCC 6803 including reaction stoichiometry, atom transition, and reaction directionality. F = forward only, FR= reversible reaction, B = Biomass.

Number	Stoichiometry	Atom transition	Reaction type
R1	GLC_EX = G6P	abcdef = abcdef	F
R2	CO2_EX = CO2	a = a	FR
R3	G6P = F6P	abcdef = abcdef	F
R4	F6P = F16BP	abcdef = abcdef	FR
R5	F16BP = DHAP + GAP	abcdef = abc + def	FR
R6	DHAP = GAP	abc = cba	FR
R7	GAP = 3PG	abc = abc	FR
R8	3PG = PEP	abc = abc	FR
R9	PEP = PYR	abc = abc	F
R10	G6P = 6PG	abcdef = abcdef	F
R11	6PG = Ru5P + CO2	abcdef = bcdef + a	F
R12	Ru5P = X5P	abcde = abcde	FR
R13	Ru5P = Ri5P	abcde = abcde	FR
R14	Ri5P + X5P = S7P + G3P	abcde + fghij = fgabcde + hij	FR
R15	S7P + G3P = E4P + F6P	abcdefg + hij = defg + abchij	FR
R16	E4P + X5P = F6P + G3P	abcd + efghi = efabcd + ghi	FR
R17	6PG = KDPG	abcdef = abcdef	F
R18	KDPG = PYR + G3P	abcdef = abc + def	F
R19	RuBP + CO2 = 3PG + 3PG	abcde + f = fba + cde	F
R20	DHAP + E4P = S7P	abc + defg = abcdefg	F
R21	PYR = ACCOA + CO2	abc = bc + a	F
R22	ACCOA + OAA = ICIT	ab + cdef = fedbac	F
R23	ICIT = AKG + CO2	abcdef = abcde + f	F
R24	AKG = SucA + CO2	abcde = edcb + a	F
R25	SucA = SUC	abcd = abcd	F
R26	SUC = 0.5 FUM + 0.5 FUM	abcd = 0.5 abcd + 0.5 dcba	FR
R27	FUM = MAL	abcd = abcd	FR
R28	MAL = OAA	abcd = abcd	FR
R29	MAL = PYR + CO2	abc + d = abcd	F
R30	PEP + CO2 = OAA	abcd = abc + d	F
R31	X5P = ACCOA + G3P	abcde = ba + cde	F
R32	F6P = ACCOA + E4P	abcdef = ba + cdef	F
R33	PYR + PYR = VAL + CO2	abc + def = abefc + d	F
R34	PYR + OAA = ILE + CO2	abc + defg = debfgc + a	F
R35	E4P + PEP = SHKM	abcd + efg = efgabcd	F
R36	SHKM + PEP = CHRM	abcdefg + hij = abcdefghij	F
R37	CHRM = PHE + CO2	abcdefghij = hijbcdefg + a	F
R38	CHRM = TYR + CO2	abcdefghij = hijbcdefg + a	F
R39	PYR + PYR = ISV + CO2	abc + def = abefc + d	F
R40	ISV + ACCOA = LEU + CO2	abcde + fg = fgbcde + a	F

R41	CHRM = ANTHR + PYR	abcdefghij = abcdefg + hij	F
R42	ANTHR + Ri5P = CPADP5P	abcdefg + hijkl = abcdefghijkl	F
R43	CPADP5P = INDG + CO2	abcdefghijkl = abcdfghijkl + e	F
R44	INDG = IND + G3P	abcdefghijk = abcdefgh + ijk	F
R45	IND + 3PG = TRP	abcdefgh + ijk = abcdefghkji	F
R46	OAA + PYR = LYS + CO2	abcd + efg = abcdgf + e	F
R47	GLU = PRO	abcde = abcde	F
R48	GLU + CO2 = ARG	abcde + f = abcdef	F
R49	PYR = ALA	abc = abc	F
R50	OAA = ASP	abcd = abcd	F
R51	OAA = THR	abcd = abcd	F
R52	SER = GLY + C1	abc = ab + c	F
R53	SER = CYS	abc = abc	F
R54	3PG = SER	abc = abc	F
R55	AKG = GLU	abcde = abcde	F
R56	ASP + C1 = MET	abcd + e = abcde	F
R57	Ri5P + C1 = HIS	abcde + f = edcbaf	F
R58	C1 = C1X	a = a	F
R59	G6P = G6PB		B
R60	Ri5P = Ri5PB		B
R61	ACCOA = ACCOAB		B
R62	AKG = AKGB		B
R63	3PG = 3PGB		B
R64	ALA = ALAB		B
R65	ARG = ARGB		B
R66	ASP = ASPB		B
R67	CYS = CYSB		B
R68	GLU = GLUB		B
R69	GLY = GLYB		B
R70	ILE = ILEB		B
R71	LEU = LEUB		B
R72	LYS = LYSB		B
R73	PHE = PHEB		B
R74	PRO = PROB		B
R75	SER = SERB		B
R76	THR = THRB		B
R77	TRP = TRPB		B
R78	TYR = TYRB		B
R79	VAL = VALB		B
R80	MET = METB		B
R81	HIS = HISB		B
R82	C1 = C1B		B

Table A 4: Measured and simulated ^{13}C labelling data for the estimation of *in vivo* fluxes for *Synechocystis* sp. PCC 6803 grown with four parallel tracer experiments under photomixotrophic conditions as shown in Figure 4.21. SSR = 583, χ^2 cut-off for 0.05 significance: 615.

Fragment	[1-^{13}C] glucose		[3-^{13}C] glucose		[6 -^{13}C] glucose		[$^{13}C_6$] glucose	
	Meas.	Sim.	Meas.	Sim.	Meas.	Sim.	Meas.	Sim.
Ala_260	0.673	0.677	0.733	0.732	0.703	0.703	0.106	0.098
	0.318	0.315	0.235	0.237	0.291	0.291	0.207	0.217
	0.008	0.009	0.032	0.031	0.006	0.006	0.490	0.482
	0.000	0.000	0.001	0.000	0.000	0.000	0.197	0.203
Ala_232	0.681	0.688	0.745	0.746	0.709	0.711	0.113	0.106
	0.316	0.309	0.228	0.226	0.288	0.286	0.223	0.226
	0.003	0.003	0.027	0.027	0.003	0.003	0.664	0.668
Gly_246	0.967	0.972	0.753	0.766	0.974	0.977	0.154	0.152
	0.033	0.028	0.242	0.231	0.026	0.023	0.625	0.632
	0.000	0.000	0.005	0.004	0.000	0.000	0.221	0.216
Gly_218	0.979	0.988	0.766	0.781	0.984	0.989	0.168	0.164
	0.021	0.012	0.234	0.219	0.016	0.011	0.832	0.836
Val_288	0.464	0.465	0.551	0.546	0.505	0.500	0.027	0.010
	0.420	0.426	0.336	0.343	0.400	0.408	0.053	0.045
	0.110	0.105	0.097	0.096	0.091	0.090	0.153	0.166
	0.004	0.004	0.013	0.014	0.002	0.003	0.252	0.275
	0.001	0.000	0.002	0.001	0.001	0.000	0.376	0.368
	0.001	0.000	0.001	0.000	0.001	0.000	0.139	0.136
Val_260	0.463	0.473	0.553	0.557	0.503	0.506	0.027	0.011
	0.423	0.425	0.337	0.338	0.402	0.407	0.056	0.048
	0.110	0.100	0.095	0.092	0.092	0.086	0.171	0.193
	0.004	0.002	0.013	0.012	0.003	0.002	0.282	0.302
	0.001	0.000	0.002	0.001	0.001	0.000	0.465	0.447
Leu_274	0.337	0.329	0.523	0.523	0.378	0.364	0.003	0.003
	0.429	0.440	0.349	0.351	0.422	0.434	0.025	0.021
	0.199	0.199	0.107	0.107	0.173	0.176	0.092	0.087
	0.034	0.032	0.017	0.017	0.026	0.025	0.219	0.222
	0.001	0.001	0.003	0.001	0.001	0.000	0.336	0.341
	0.001	0.000	0.001	0.000	0.000	0.000	0.326	0.324
Ileu_274	0.451	0.464	0.541	0.549	0.490	0.499	0.026	0.010
	0.423	0.426	0.339	0.341	0.403	0.408	0.054	0.045
	0.117	0.106	0.101	0.095	0.099	0.090	0.164	0.181
	0.006	0.004	0.015	0.013	0.005	0.003	0.269	0.292
	0.001	0.000	0.003	0.001	0.001	0.000	0.436	0.432
	0.002	0.000	0.001	0.000	0.001	0.000	0.052	0.039
Ser_390	0.678	0.677	0.733	0.732	0.707	0.703	0.105	0.098
	0.314	0.315	0.237	0.237	0.289	0.291	0.210	0.217
	0.008	0.009	0.029	0.031	0.005	0.006	0.488	0.482
	0.000	0.000	0.001	0.000	0.000	0.000	0.198	0.203
Ser_362	0.686	0.688	0.745	0.746	0.713	0.711	0.109	0.106
	0.314	0.309	0.232	0.226	0.287	0.286	0.231	0.226

	0.001	0.003	0.024	0.027	0.000	0.003	0.660	0.668
Thr_404	0.666	0.663	0.726	0.720	0.696	0.692	0.098	0.091
	0.321	0.322	0.237	0.245	0.296	0.297	0.197	0.207
	0.011	0.015	0.034	0.034	0.007	0.011	0.461	0.460
	0.001	0.000	0.002	0.001	0.000	0.000	0.226	0.224
	0.001	0.000	0.001	0.000	0.001	0.000	0.018	0.019
Thr_376	0.672	0.674	0.736	0.736	0.700	0.701	0.106	0.098
	0.322	0.316	0.232	0.234	0.295	0.292	0.210	0.216
	0.006	0.009	0.031	0.030	0.004	0.007	0.626	0.627
	0.000	0.000	0.001	0.000	0.000	0.000	0.058	0.058
Phe_336	0.380	0.376	0.188	0.204	0.182	0.179	0.002	0.000
	0.419	0.430	0.444	0.451	0.435	0.457	0.005	0.003
	0.162	0.167	0.255	0.257	0.297	0.296	0.015	0.013
	0.024	0.026	0.082	0.074	0.071	0.065	0.040	0.037
	0.003	0.002	0.016	0.012	0.005	0.004	0.089	0.087
	0.004	0.000	0.006	0.001	0.003	0.000	0.143	0.145
	0.002	0.000	0.002	0.000	0.002	0.000	0.208	0.216
	0.002	0.000	0.002	0.000	0.002	0.000	0.217	0.223
	0.003	0.000	0.003	0.000	0.003	0.000	0.203	0.207
	0.002	0.000	0.002	0.000	0.001	0.000	0.079	0.069
Asp_418	0.674	0.663	0.728	0.720	0.699	0.692	0.109	0.091
	0.314	0.322	0.237	0.245	0.294	0.297	0.202	0.207
	0.011	0.015	0.033	0.034	0.007	0.011	0.456	0.460
	0.000	0.000	0.001	0.001	0.000	0.000	0.217	0.224
	0.000	0.000	0.000	0.000	0.000	0.000	0.017	0.019
Asp_390	0.678	0.674	0.736	0.736	0.702	0.701	0.111	0.098
	0.318	0.316	0.233	0.234	0.295	0.292	0.212	0.216
	0.005	0.009	0.030	0.030	0.003	0.007	0.620	0.627
	0.000	0.000	0.000	0.000	0.000	0.000	0.057	0.058
Glu_432	0.468	0.464	0.553	0.549	0.505	0.499	0.025	0.010
	0.419	0.426	0.336	0.341	0.401	0.408	0.052	0.045
	0.109	0.106	0.097	0.095	0.092	0.090	0.162	0.181
	0.004	0.004	0.013	0.013	0.002	0.003	0.272	0.292
	0.000	0.000	0.002	0.001	0.000	0.000	0.447	0.432
	0.000	0.000	0.000	0.000	0.000	0.000	0.043	0.039
Arg_442	0.468	0.456	0.544	0.542	0.499	0.493	0.029	0.010
	0.412	0.427	0.331	0.344	0.398	0.409	0.058	0.043
	0.109	0.112	0.103	0.099	0.095	0.094	0.167	0.171
	0.006	0.006	0.015	0.015	0.004	0.004	0.259	0.285
	0.001	0.000	0.003	0.001	0.001	0.000	0.423	0.423
	0.002	0.000	0.002	0.000	0.002	0.000	0.060	0.066
	0.002	0.000	0.001	0.000	0.001	0.000	0.003	0.003
Glcn_319	0.817	0.809	0.349	0.374	0.359	0.358	0.064	0.037
	0.171	0.184	0.612	0.591	0.618	0.622	0.092	0.095
	0.011	0.007	0.035	0.034	0.020	0.020	0.164	0.210

	0.001	0.000	0.003	0.001	0.003	0.000	0.177	0.150
	0.000	0.000	0.001	0.000	0.000	0.000	0.503	0.508
Glc_319	0.847	0.843	0.290	0.291	0.278	0.279	0.073	0.029
	0.131	0.152	0.669	0.674	0.692	0.698	0.073	0.073
	0.012	0.006	0.035	0.033	0.023	0.023	0.124	0.163
	0.004	0.000	0.003	0.001	0.004	0.000	0.127	0.117
	0.006	0.000	0.003	0.000	0.004	0.000	0.603	0.619
Rib_307	0.750	0.752	0.792	0.792	0.518	0.522	0.087	0.072
	0.243	0.242	0.183	0.185	0.472	0.468	0.156	0.160
	0.007	0.006	0.024	0.023	0.011	0.010	0.356	0.356
	0.000	0.000	0.001	0.000	0.000	0.000	0.401	0.412
Ala_C2	0.968	0.988	0.785	0.781	0.972	0.989	0.170	0.164
	0.032	0.012	0.215	0.219	0.028	0.011	0.830	0.836
Ala_C3	0.714	0.696	0.944	0.938	0.735	0.719	0.311	0.273
	0.286	0.304	0.056	0.062	0.265	0.281	0.689	0.727
Glu_C2	0.711	0.711	0.964	0.930	0.734	0.733	0.291	0.268
	0.289	0.289	0.036	0.070	0.266	0.267	0.709	0.732
Gly_C2	0.979	0.988	0.783	0.781	0.985	0.989	0.173	0.164
	0.021	0.012	0.218	0.219	0.015	0.011	0.827	0.836
His_C6	0.725	0.696	0.953	0.938	0.752	0.719	0.289	0.273
	0.276	0.304	0.047	0.062	0.249	0.281	0.711	0.727
Ile_C4	0.718	0.711	0.947	0.930	0.746	0.733	0.304	0.268
	0.282	0.289	0.053	0.070	0.255	0.267	0.696	0.732
Ile_C5	0.951	0.981	0.965	0.985	0.969	0.986	0.907	0.916
	0.049	0.019	0.035	0.015	0.031	0.014	0.093	0.084
Leu_C2	0.732	0.696	0.959	0.938	0.752	0.719	0.295	0.273
	0.268	0.304	0.041	0.062	0.248	0.281	0.706	0.727
Leu_C5+C6	0.710	0.696	0.946	0.938	0.737	0.719	0.280	0.273
	0.290	0.304	0.054	0.062	0.263	0.281	0.720	0.727
Lys_C5	0.698	0.696	0.947	0.938	0.714	0.719	0.299	0.273
	0.302	0.304	0.053	0.062	0.286	0.281	0.701	0.727
Lys_C6	1.000	0.988	0.790	0.781	1.000	0.989	0.167	0.164
	0.000	0.012	0.210	0.219	0.000	0.011	0.833	0.836
Pro_C2	0.705	0.711	0.930	0.930	0.730	0.733	0.288	0.268
	0.295	0.289	0.070	0.070	0.270	0.267	0.712	0.732
Pro_C3	1.000	0.973	0.761	0.789	1.000	0.975	0.156	0.170
	0.000	0.027	0.239	0.211	0.000	0.025	0.844	0.830
Pro_C5	1.000	0.988	0.823	0.781	1.000	0.989	0.155	0.164
	0.000	0.012	0.177	0.219	0.000	0.011	0.845	0.836
Ser_C2	0.976	0.988	0.772	0.781	1.000	0.989	0.160	0.164
	0.024	0.012	0.228	0.219	0.000	0.011	0.841	0.836
Thr_C2	1.000	0.973	0.818	0.789	1.000	0.975	0.166	0.170
	0.000	0.027	0.182	0.211	0.000	0.025	0.834	0.830
Thr_C3	0.743	0.711	0.938	0.930	0.768	0.733	0.288	0.268
	0.257	0.289	0.062	0.070	0.232	0.267	0.712	0.732

Thr_C4	0.981	0.981	0.980	0.985	0.985	0.986	0.914	0.916
	0.019	0.019	0.020	0.015	0.015	0.014	0.086	0.084
Val_C3	0.997	0.988	0.777	0.781	0.976	0.989	0.172	0.164
	0.003	0.012	0.223	0.219	0.024	0.011	0.828	0.836
Val_C4	0.718	0.696	0.944	0.938	0.743	0.719	0.296	0.273
	0.282	0.304	0.056	0.062	0.257	0.281	0.704	0.727
Val_C5	0.706	0.696	0.934	0.938	0.756	0.719	0.269	0.273
	0.294	0.304	0.066	0.062	0.244	0.281	0.731	0.727

Table A 5: Measured and simulated ^{13}C labelling data for the estimation of *in vivo* fluxes for Δ*eda* grown with four parallel tracer experiments under photomixotrophic conditions as shown in Figure 4.23. SSR= 394, χ^2 cut-off for 0.05 significance: 431.

Fragment	[1-^{13}C] glucose		[3-^{13}C] glucose		[6 -^{13}C] glucose		[$^{13}C_6$] glucose	
	Meas.	Sim.	Meas.	Sim.		Meas.	Sim.	Meas.
Ala_260	0.526	0.529	0.576	0.572	0.548	0.547	0.112	0.105
	0.347	0.344	0.286	0.291	0.330	0.330	0.201	0.209
	0.099	0.098	0.111	0.110	0.095	0.096	0.443	0.437
	0.028	0.028	0.028	0.027	0.026	0.027	0.244	0.250
Ala_232	0.547	0.551	0.600	0.601	0.568	0.569	0.129	0.119
	0.355	0.352	0.291	0.291	0.338	0.337	0.233	0.233
	0.097	0.097	0.109	0.108	0.094	0.095	0.638	0.648
Gly_246	0.759	0.764	0.604	0.615	0.761	0.764	0.154	0.153
	0.170	0.166	0.304	0.295	0.168	0.166	0.561	0.566
	0.070	0.070	0.092	0.090	0.071	0.070	0.286	0.280
Gly_218	0.828	0.829	0.674	0.686	0.829	0.829	0.185	0.179
	0.173	0.171	0.326	0.314	0.171	0.171	0.815	0.821
Val_288	0.365	0.364	0.437	0.428	0.397	0.389	0.034	0.013
	0.392	0.398	0.334	0.342	0.381	0.389	0.067	0.049
	0.177	0.174	0.161	0.162	0.163	0.163	0.163	0.167
	0.051	0.050	0.052	0.053	0.047	0.047	0.239	0.259
	0.013	0.012	0.014	0.013	0.011	0.011	0.331	0.338
	0.003	0.002	0.003	0.003	0.002	0.002	0.176	0.174
Val_260	0.366	0.369	0.440	0.439	0.397	0.395	0.033	0.015
	0.395	0.400	0.337	0.340	0.383	0.390	0.068	0.054
	0.177	0.172	0.160	0.158	0.163	0.160	0.184	0.202
	0.050	0.048	0.050	0.050	0.046	0.045	0.275	0.298
	0.012	0.011	0.014	0.012	0.011	0.010	0.440	0.431
Leu_274	0.268	0.256	0.414	0.408	0.302	0.285	0.007	0.004
	0.379	0.390	0.340	0.346	0.380	0.391	0.023	0.026
	0.238	0.241	0.167	0.170	0.217	0.224	0.083	0.095
	0.086	0.086	0.058	0.057	0.076	0.077	0.225	0.224
	0.023	0.022	0.016	0.015	0.020	0.020	0.338	0.329
	0.005	0.005	0.004	0.003	0.005	0.004	0.324	0.322
Ileu_274	0.357	0.363	0.429	0.431	0.385	0.388	0.027	0.013
	0.392	0.399	0.336	0.341	0.382	0.390	0.058	0.048

	0.181	0.175	0.163	0.161	0.168	0.164	0.162	0.177
	0.053	0.050	0.053	0.052	0.049	0.047	0.245	0.268
	0.014	0.012	0.015	0.013	0.013	0.011	0.388	0.385
	0.003	0.002	0.004	0.002	0.003	0.002	0.120	0.108
Ser_390	0.463	0.460	0.499	0.497	0.480	0.475	0.099	0.095
	0.351	0.353	0.310	0.311	0.340	0.343	0.199	0.201
	0.139	0.139	0.144	0.145	0.135	0.136	0.426	0.423
	0.047	0.048	0.046	0.046	0.045	0.046	0.276	0.281
Ser_362	0.490	0.488	0.532	0.532	0.507	0.503	0.119	0.114
	0.370	0.369	0.322	0.320	0.356	0.357	0.246	0.236
	0.141	0.143	0.146	0.148	0.137	0.139	0.635	0.650
Thr_404	0.448	0.446	0.490	0.482	0.466	0.461	0.087	0.083
	0.351	0.352	0.304	0.310	0.340	0.342	0.170	0.176
	0.140	0.142	0.145	0.147	0.136	0.139	0.373	0.374
	0.049	0.049	0.047	0.048	0.046	0.047	0.265	0.260
	0.012	0.012	0.013	0.013	0.011	0.011	0.105	0.107
Thr_376	0.458	0.458	0.504	0.501	0.475	0.474	0.098	0.091
	0.356	0.354	0.306	0.310	0.345	0.344	0.190	0.193
	0.138	0.140	0.144	0.144	0.135	0.137	0.516	0.516
	0.048	0.048	0.046	0.046	0.045	0.046	0.197	0.201
Phe_336	0.304	0.293	0.154	0.168	0.147	0.147	0.002	0.001
	0.381	0.389	0.376	0.379	0.363	0.381	0.007	0.004
	0.210	0.217	0.268	0.274	0.304	0.303	0.021	0.017
	0.072	0.076	0.131	0.125	0.129	0.123	0.049	0.044
	0.020	0.020	0.045	0.041	0.038	0.036	0.084	0.094
	0.006	0.004	0.016	0.010	0.011	0.008	0.141	0.146
	0.002	0.001	0.005	0.002	0.003	0.001	0.204	0.205
	0.002	0.000	0.003	0.000	0.002	0.000	0.197	0.208
	0.002	0.000	0.002	0.000	0.002	0.000	0.196	0.192
	0.002	0.000	0.002	0.000	0.002	0.000	0.099	0.090
Asp_418	0.448	0.445	0.489	0.481	0.463	0.460	0.087	0.082
	0.350	0.351	0.303	0.310	0.342	0.341	0.167	0.176
	0.141	0.143	0.147	0.148	0.137	0.140	0.372	0.374
	0.049	0.050	0.048	0.048	0.047	0.048	0.267	0.260
	0.012	0.012	0.013	0.013	0.011	0.011	0.107	0.108
Asp_390	0.456	0.458	0.502	0.500	0.471	0.473	0.094	0.090
	0.357	0.354	0.305	0.309	0.347	0.343	0.184	0.192
	0.139	0.140	0.146	0.145	0.136	0.137	0.521	0.515
	0.048	0.048	0.046	0.046	0.046	0.046	0.202	0.202
Glu_432	0.313	0.310	0.374	0.371	0.335	0.333	0.026	0.011
	0.375	0.379	0.330	0.336	0.369	0.374	0.057	0.044
	0.207	0.205	0.190	0.189	0.196	0.195	0.152	0.162
	0.077	0.077	0.075	0.075	0.073	0.073	0.239	0.258
	0.023	0.023	0.024	0.023	0.021	0.021	0.382	0.377
	0.005	0.005	0.006	0.006	0.005	0.005	0.144	0.148

Arg_442	0.310	0.304	0.367	0.363	0.327	0.327	0.024	0.010
	0.373	0.379	0.327	0.338	0.368	0.374	0.052	0.040
	0.207	0.208	0.193	0.191	0.198	0.198	0.144	0.150
	0.077	0.079	0.077	0.076	0.074	0.074	0.222	0.242
	0.024	0.024	0.026	0.024	0.023	0.022	0.358	0.353
	0.007	0.005	0.008	0.006	0.007	0.005	0.146	0.147
	0.002	0.001	0.003	0.001	0.003	0.001	0.053	0.057
Glcn_319	0.580	0.569	0.252	0.277	0.256	0.268	0.069	0.045
	0.264	0.277	0.494	0.476	0.504	0.494	0.110	0.104
	0.115	0.114	0.167	0.164	0.159	0.158	0.176	0.218
	0.033	0.032	0.071	0.068	0.067	0.067	0.181	0.172
	0.009	0.007	0.016	0.015	0.013	0.014	0.465	0.462
Glc_319	0.595	0.581	0.245	0.246	0.240	0.237	0.076	0.041
	0.257	0.268	0.501	0.500	0.513	0.515	0.104	0.093
	0.112	0.112	0.167	0.168	0.163	0.162	0.162	0.196
	0.029	0.031	0.072	0.071	0.070	0.071	0.156	0.155
	0.007	0.007	0.016	0.015	0.014	0.014	0.502	0.515
Rib_307	0.536	0.534	0.568	0.564	0.382	0.386	0.090	0.080
	0.308	0.309	0.272	0.274	0.423	0.420	0.161	0.163
	0.119	0.120	0.125	0.127	0.141	0.141	0.343	0.344
	0.037	0.037	0.035	0.036	0.054	0.054	0.406	0.414

Table A 6: Measured and simulated ^{13}C labelling data for the estimation of in *vivo fluxes* for ∆*pfkA/pfkB* grown with four parallel tracer experiments under photomixotrophic conditions, as shown in Figure 4.23. SSR = 401, χ^2 cut-off for 0.05 significance: 431.

Fragment	[1-^{13}C] glucose		[3-^{13}C] glucose		[6 -^{13}C] glucose		[$^{13}C_6$] glucose	
	Meas.	Sim.	Meas.	Sim.	Meas.	Meas.	Sim.	Meas.
Ala_260	0.516	0.524	0.571	0.573	0.545	0.545	0.092	0.084
	0.353	0.347	0.291	0.289	0.332	0.332	0.189	0.200
	0.102	0.100	0.111	0.110	0.096	0.096	0.450	0.446
	0.029	0.028	0.028	0.027	0.027	0.027	0.269	0.270
Ala_232	0.543	0.548	0.595	0.596	0.566	0.567	0.108	0.100
	0.359	0.355	0.296	0.294	0.339	0.338	0.225	0.229
	0.098	0.098	0.109	0.110	0.095	0.095	0.667	0.671
Gly_246	0.753	0.761	0.601	0.615	0.759	0.763	0.132	0.133
	0.176	0.169	0.306	0.296	0.170	0.167	0.555	0.564
	0.071	0.070	0.093	0.090	0.071	0.070	0.312	0.303
Gly_218	0.827	0.829	0.672	0.681	0.828	0.829	0.164	0.162
	0.174	0.171	0.328	0.319	0.172	0.171	0.836	0.838
Val_288	0.354	0.358	0.429	0.425	0.392	0.385	0.023	0.009
	0.396	0.399	0.339	0.342	0.383	0.390	0.051	0.039
	0.182	0.177	0.162	0.163	0.165	0.164	0.138	0.145
	0.053	0.051	0.053	0.053	0.047	0.047	0.231	0.256
	0.013	0.012	0.014	0.013	0.011	0.011	0.358	0.357
	0.003	0.002	0.003	0.003	0.002	0.002	0.200	0.193

Val_260	0.360	0.365	0.433	0.432	0.394	0.392	0.025	0.010
	0.396	0.401	0.342	0.342	0.385	0.391	0.057	0.045
	0.180	0.174	0.161	0.161	0.164	0.161	0.166	0.181
	0.051	0.049	0.051	0.052	0.046	0.045	0.277	0.303
	0.013	0.011	0.014	0.013	0.011	0.010	0.475	0.461
Leu_274	0.260	0.253	0.407	0.401	0.297	0.281	0.007	0.003
	0.380	0.390	0.345	0.348	0.381	0.391	0.022	0.019
	0.242	0.243	0.169	0.173	0.220	0.226	0.079	0.080
	0.089	0.087	0.059	0.059	0.078	0.078	0.204	0.208
	0.024	0.023	0.016	0.015	0.020	0.020	0.334	0.337
	0.006	0.005	0.004	0.003	0.005	0.004	0.354	0.353
Ileu_274	0.347	0.357	0.419	0.425	0.384	0.385	0.022	0.009
	0.393	0.400	0.342	0.343	0.382	0.391	0.051	0.038
	0.185	0.178	0.164	0.163	0.168	0.165	0.143	0.154
	0.056	0.051	0.054	0.053	0.050	0.047	0.241	0.267
	0.015	0.012	0.015	0.013	0.013	0.011	0.405	0.404
	0.004	0.002	0.005	0.003	0.004	0.002	0.138	0.128
Ser_390	0.454	0.456	0.496	0.498	0.474	0.473	0.081	0.077
	0.356	0.355	0.312	0.310	0.344	0.344	0.184	0.191
	0.142	0.141	0.145	0.146	0.137	0.137	0.433	0.431
	0.049	0.048	0.047	0.046	0.046	0.046	0.303	0.301
Ser_362	0.485	0.485	0.529	0.528	0.503	0.502	0.099	0.096
	0.373	0.371	0.324	0.323	0.359	0.359	0.232	0.231
	0.142	0.143	0.147	0.150	0.138	0.140	0.669	0.673
Thr_404	0.439	0.441	0.483	0.484	0.462	0.460	0.071	0.064
	0.354	0.354	0.309	0.309	0.342	0.343	0.157	0.164
	0.144	0.144	0.146	0.147	0.138	0.139	0.368	0.372
	0.050	0.050	0.049	0.048	0.047	0.047	0.285	0.281
	0.013	0.012	0.014	0.013	0.012	0.011	0.120	0.118
Thr_376	0.451	0.455	0.498	0.498	0.473	0.472	0.082	0.073
	0.359	0.357	0.311	0.311	0.346	0.345	0.180	0.184
	0.141	0.141	0.145	0.145	0.136	0.137	0.520	0.520
	0.049	0.048	0.047	0.046	0.046	0.046	0.218	0.223
Phe_336	0.291	0.288	0.150	0.161	0.146	0.142	0.003	0.000
	0.379	0.389	0.371	0.378	0.361	0.379	0.006	0.002
	0.216	0.220	0.273	0.277	0.303	0.307	0.022	0.011
	0.076	0.077	0.132	0.128	0.131	0.126	0.042	0.033
	0.022	0.021	0.046	0.043	0.039	0.036	0.084	0.078
	0.007	0.004	0.015	0.011	0.011	0.008	0.132	0.135
	0.003	0.001	0.005	0.002	0.003	0.001	0.195	0.202
	0.002	0.000	0.003	0.000	0.002	0.000	0.209	0.221
	0.003	0.000	0.003	0.000	0.002	0.000	0.202	0.213
	0.002	0.000	0.002	0.000	0.002	0.000	0.104	0.104
Asp_418	0.452	0.440	0.483	0.483	0.460	0.459	0.075	0.064
	0.345	0.353	0.308	0.308	0.342	0.342	0.159	0.164

	0.142	0.144	0.148	0.147	0.139	0.140	0.367	0.372
	0.049	0.050	0.049	0.048	0.047	0.048	0.281	0.281
	0.012	0.012	0.013	0.013	0.011	0.011	0.118	0.119
Asp_390	0.457	0.454	0.497	0.497	0.471	0.472	0.083	0.073
	0.355	0.356	0.310	0.311	0.346	0.344	0.178	0.184
	0.140	0.142	0.146	0.146	0.137	0.138	0.520	0.520
	0.048	0.049	0.047	0.047	0.046	0.046	0.219	0.223
Glu_432	0.327	0.307	0.368	0.365	0.333	0.330	0.022	0.008
	0.367	0.380	0.335	0.337	0.371	0.374	0.050	0.035
	0.203	0.207	0.191	0.191	0.197	0.196	0.139	0.141
	0.076	0.078	0.076	0.076	0.073	0.073	0.236	0.255
	0.023	0.023	0.024	0.024	0.022	0.021	0.393	0.394
	0.005	0.005	0.006	0.006	0.005	0.005	0.159	0.167
Arg_442	0.305	0.299	0.363	0.358	0.330	0.324	0.019	0.007
	0.372	0.379	0.333	0.339	0.368	0.375	0.046	0.031
	0.209	0.211	0.192	0.194	0.198	0.199	0.129	0.126
	0.080	0.080	0.076	0.078	0.074	0.075	0.214	0.233
	0.025	0.024	0.025	0.025	0.022	0.022	0.360	0.362
	0.007	0.006	0.008	0.006	0.006	0.005	0.166	0.174
	0.003	0.001	0.003	0.001	0.002	0.001	0.066	0.068
Glcn_319	0.578	0.568	0.246	0.267	0.253	0.260	0.056	0.033
	0.267	0.277	0.490	0.482	0.502	0.499	0.095	0.092
	0.115	0.115	0.173	0.167	0.161	0.159	0.165	0.209
	0.032	0.033	0.074	0.069	0.070	0.068	0.193	0.182
	0.008	0.007	0.018	0.015	0.015	0.014	0.492	0.483
Glc_319	0.595	0.581	0.218	0.236	0.247	0.230	0.074	0.030
	0.256	0.268	0.515	0.506	0.506	0.521	0.095	0.082
	0.113	0.113	0.174	0.170	0.163	0.164	0.151	0.187
	0.030	0.031	0.076	0.073	0.070	0.072	0.161	0.163
	0.007	0.007	0.017	0.016	0.014	0.014	0.519	0.537
Rib_307	0.534	0.533	0.568	0.567	0.377	0.379	0.078	0.063
	0.308	0.310	0.273	0.272	0.426	0.425	0.152	0.154
	0.121	0.120	0.124	0.126	0.142	0.142	0.342	0.346
	0.037	0.037	0.036	0.035	0.055	0.055	0.428	0.437

Table A 7: Measured and simulated ^{13}C labelling data for the estimation of *in vivo* fluxes for ∆*xfp1/xfp2* grown with four parallel tracer experiments under photomixotrophic conditions, as shown in Figure 4.23. SSR = 415, χ^2 cut-off for 0.05 significance: 430.

Fragment	[1-^{13}C] glucose		[3-^{13}C] glucose		[6 -^{13}C] glucose		[$^{13}C_6$] glucose	
	Meas.	Sim.	Meas.	Sim.	Meas.	Sim.	Meas.	Sim.
Ala_260	0.5293	0.5311	0.5689	0.5620	0.5383	0.5422	0.0983	0.0899
	0.3437	0.3419	0.2972	0.3023	0.3370	0.3341	0.1954	0.2042
	0.0989	0.0990	0.1065	0.1081	0.0973	0.0967	0.4297	0.4290
	0.0281	0.0280	0.0275	0.0276	0.0274	0.0269	0.2766	0.2769
Ala_232	0.5498	0.5570	0.5919	0.5968	0.5591	0.5647	0.1136	0.1065

	0.3527	0.3467	0.3030	0.2977	0.3450	0.3400	0.2311	0.2344
	0.0975	0.0963	0.1051	0.1055	0.0959	0.0953	0.6553	0.6591
Gly_246	0.7590	0.7601	0.5970	0.6016	0.7593	0.7633	0.1410	0.1370
	0.1704	0.1695	0.3098	0.3063	0.1695	0.1667	0.5431	0.5520
	0.0707	0.0704	0.0932	0.0920	0.0712	0.0700	0.3159	0.3110
Gly_218	0.8265	0.8286	0.6659	0.6797	0.8268	0.8292	0.1717	0.1666
	0.1735	0.1714	0.3341	0.3203	0.1732	0.1708	0.8283	0.8334
Val_288	0.3689	0.3689	0.4261	0.4180	0.3853	0.3823	0.0251	0.0100
	0.3914	0.3954	0.3486	0.3520	0.3829	0.3913	0.0570	0.0429
	0.1740	0.1722	0.1583	0.1625	0.1685	0.1659	0.1495	0.1510
	0.0504	0.0500	0.0504	0.0523	0.0485	0.0478	0.2356	0.2572
	0.0126	0.0116	0.0133	0.0128	0.0121	0.0109	0.3331	0.3437
	0.0028	0.0018	0.0033	0.0024	0.0028	0.0017	0.1997	0.1951
Val_260	0.3712	0.3777	0.4294	0.4340	0.3883	0.3888	0.0279	0.0116
	0.3931	0.3968	0.3517	0.3485	0.3842	0.3925	0.0637	0.0488
	0.1737	0.1677	0.1571	0.1568	0.1679	0.1627	0.1783	0.1891
	0.0499	0.0472	0.0491	0.0491	0.0479	0.0457	0.2813	0.3047
	0.0121	0.0107	0.0126	0.0116	0.0117	0.0102	0.4488	0.4458
Leu_274	0.2716	0.2667	0.4090	0.4071	0.2913	0.2782	0.0062	0.0032
	0.3834	0.3907	0.3554	0.3530	0.3806	0.3910	0.0235	0.0217
	0.2348	0.2346	0.1651	0.1680	0.2231	0.2277	0.0775	0.0867
	0.0836	0.0824	0.0535	0.0554	0.0797	0.0789	0.2145	0.2162
	0.0219	0.0214	0.0139	0.0139	0.0206	0.0203	0.3460	0.3358
	0.0047	0.0042	0.0031	0.0027	0.0046	0.0040	0.3322	0.3364
Ileu_274	0.3640	0.3667	0.4212	0.4234	0.3803	0.3792	0.0214	0.0095
	0.3926	0.3958	0.3527	0.3498	0.3826	0.3921	0.0534	0.0413
	0.1768	0.1737	0.1599	0.1607	0.1708	0.1677	0.1536	0.1571
	0.0514	0.0503	0.0502	0.0513	0.0511	0.0483	0.2447	0.2655
	0.0126	0.0116	0.0130	0.0124	0.0124	0.0110	0.3775	0.3842
	0.0026	0.0018	0.0031	0.0023	0.0027	0.0017	0.1494	0.1424
Ser_390	0.4635	0.4623	0.4938	0.4894	0.4704	0.4704	0.0862	0.0821
	0.3506	0.3505	0.3174	0.3192	0.3464	0.3458	0.1910	0.1961
	0.1386	0.1396	0.1426	0.1446	0.1369	0.1374	0.4181	0.4170
	0.0473	0.0476	0.0462	0.0469	0.0463	0.0464	0.3047	0.3049
Ser_362	0.4904	0.4925	0.5247	0.5295	0.4979	0.4992	0.1027	0.1021
	0.3686	0.3658	0.3311	0.3247	0.3628	0.3605	0.2416	0.2363
	0.1410	0.1417	0.1442	0.1458	0.1394	0.1403	0.6557	0.6616
Thr_404	0.4525	0.4429	0.4845	0.4708	0.4598	0.4529	0.0796	0.0663
	0.3481	0.3504	0.3126	0.3195	0.3426	0.3456	0.1653	0.1645
	0.1389	0.1448	0.1422	0.1478	0.1379	0.1416	0.3506	0.3549
	0.0484	0.0500	0.0474	0.0491	0.0477	0.0484	0.2788	0.2849
	0.0121	0.0120	0.0132	0.0128	0.0120	0.0114	0.1257	0.1294
Thr_376	0.4614	0.4585	0.4970	0.4943	0.4693	0.4671	0.0896	0.0769
	0.3532	0.3526	0.3157	0.3162	0.3473	0.3476	0.1876	0.1874
	0.1381	0.1410	0.1414	0.1435	0.1370	0.1387	0.4979	0.4935

	0.0473	0.0479	0.0458	0.0460	0.0465	0.0466	0.2248	0.2422
Phe_336	0.3025	0.2988	0.1511	0.1579	0.1393	0.1399	0.0029	0.0004
	0.3805	0.3876	0.3711	0.3798	0.3589	0.3774	0.0058	0.0028
	0.2082	0.2143	0.2759	0.2817	0.3040	0.3086	0.0203	0.0125
	0.0720	0.0747	0.1284	0.1269	0.1321	0.1274	0.0362	0.0356
	0.0199	0.0198	0.0437	0.0411	0.0393	0.0368	0.0870	0.0812
	0.0061	0.0040	0.0141	0.0102	0.0114	0.0084	0.1304	0.1366
	0.0026	0.0006	0.0048	0.0020	0.0038	0.0014	0.1957	0.2012
	0.0023	0.0001	0.0030	0.0003	0.0028	0.0002	0.2101	0.2191
	0.0037	0.0000	0.0053	0.0000	0.0055	0.0000	0.2065	0.2063
	0.0022	0.0000	0.0028	0.0000	0.0029	0.0000	0.1051	0.1044
Asp_418	0.4472	0.4420	0.4806	0.4698	0.4517	0.4520	0.0718	0.0662
	0.3500	0.3497	0.3117	0.3189	0.3474	0.3450	0.1523	0.1643
	0.1421	0.1454	0.1463	0.1485	0.1408	0.1423	0.3438	0.3546
	0.0492	0.0506	0.0484	0.0497	0.0486	0.0490	0.2942	0.2849
	0.0116	0.0122	0.0130	0.0131	0.0116	0.0117	0.1378	0.1300
Asp_390	0.4579	0.4577	0.4944	0.4934	0.4608	0.4662	0.0788	0.0768
	0.3550	0.3521	0.3145	0.3157	0.3526	0.3470	0.1725	0.1872
	0.1394	0.1417	0.1445	0.1443	0.1392	0.1395	0.5048	0.4934
	0.0477	0.0485	0.0465	0.0466	0.0474	0.0473	0.2439	0.2425
Glu_432	0.3129	0.3147	0.3636	0.3634	0.3229	0.3254	0.0193	0.0085
	0.3756	0.3768	0.3411	0.3431	0.3703	0.3749	0.0459	0.0377
	0.2060	0.2032	0.1907	0.1897	0.2029	0.1982	0.1317	0.1446
	0.0772	0.0770	0.0749	0.0750	0.0759	0.0745	0.2283	0.2546
	0.0230	0.0229	0.0236	0.0231	0.0227	0.0219	0.3892	0.3764
	0.0053	0.0053	0.0060	0.0058	0.0053	0.0050	0.1856	0.1782
Arg_442	0.3151	0.3071	0.3592	0.3549	0.3230	0.3189	0.0188	0.0074
	0.3720	0.3762	0.3395	0.3446	0.3673	0.3749	0.0449	0.0333
	0.2038	0.2074	0.1910	0.1928	0.2018	0.2016	0.1245	0.1281
	0.0763	0.0792	0.0750	0.0768	0.0753	0.0761	0.2061	0.2316
	0.0237	0.0237	0.0245	0.0238	0.0233	0.0224	0.3308	0.3452
	0.0068	0.0054	0.0078	0.0059	0.0068	0.0051	0.1923	0.1826
	0.0023	0.0011	0.0030	0.0012	0.0025	0.0010	0.0826	0.0717
Glcn_319	0.5670	0.5713	0.2451	0.2660	0.2428	0.2595	0.0557	0.0358
	0.2630	0.2746	0.4863	0.4852	0.5017	0.4993	0.0954	0.0951
	0.1243	0.1146	0.1760	0.1651	0.1633	0.1592	0.1634	0.2042
	0.0361	0.0323	0.0746	0.0689	0.0759	0.0682	0.1853	0.1829
	0.0096	0.0072	0.0179	0.0148	0.0163	0.0138	0.5002	0.4820
Glc_319	0.6018	0.5854	0.2187	0.2309	0.2133	0.2253	0.0671	0.0316
	0.2544	0.2646	0.5107	0.5117	0.5261	0.5239	0.1004	0.0839
	0.1095	0.1125	0.1760	0.1692	0.1700	0.1641	0.1639	0.1802
	0.0280	0.0306	0.0774	0.0728	0.0756	0.0721	0.1537	0.1619
	0.0063	0.0069	0.0172	0.0154	0.0150	0.0145	0.5150	0.5424
Rib_307	0.5422	0.5352	0.5685	0.5571	0.3762	0.3836	0.0902	0.0686
	0.3041	0.3078	0.2765	0.2812	0.4278	0.4211	0.1648	0.1599

	0.1177	0.1201	0.1203	0.1256	0.1411	0.1409	0.3304	0.3396
	0.0360	0.0370	0.0347	0.0361	0.0548	0.0545	0.4146	0.4319

Table A 8: *In vivo* fluxes determined for *Synechocystis* sp. PCC 6803 in photomixotrophic growth mode. Fluxes, standard deviations, and boundaries for 95 % confidence intervals were obtained from 250 runs of Monte-Carlo simulation. The resulting flux map is shown in Figure 4.22.

Reaction number	Mean flux [%]	Standard deviation [%]	Lower boundary [%]	Upper boundary [%]
R1	100.00	0.00	100.00	100.00
R2	236.84	7.30	222.52	251.16
R3	63.15	2.14	58.96	67.34
R4	-87.21	8.44	-103.75	-70.66
R5	-87.21	8.44	-103.75	-70.66
R6	-176.90	2.78	-182.35	-171.44
R7	-476.23	6.68	-489.31	-463.14
R8	200.55	3.05	194.57	206.52
R9	129.67	3.70	122.42	136.93
R10	9.30	2.08	5.22	13.37
R11	9.26	2.07	5.19	13.32
R12	-239.76	2.93	-245.50	-234.02
R13	-98.53	1.80	-102.06	-95.01
R14	-115.73	1.49	-118.66	-112.80
R15	-26.04	8.56	-42.82	-9.27
R16	-124.17	1.47	-127.05	-121.29
R17	0.04	0.13	-0.22	0.30
R18	0.04	0.13	-0.22	0.30
R19	347.55	4.35	339.02	356.08
R20	89.69	8.45	73.13	106.25
R21	83.06	4.41	74.41	91.70
R22	31.90	2.02	27.94	35.86
R23	31.90	2.02	27.94	35.86
R24	0.38	0.39	-0.38	1.14
R25	0.38	0.39	-0.38	1.14
R26	0.38	0.39	-0.38	1.14
R27	0.38	0.39	-0.38	1.14
R28	0.38	0.39	-0.38	1.14
R29	0.00	0.00	0.00	0.00
R30	53.70	2.19	49.41	57.99
R31	0.14	0.39	-0.61	0.90
R32	0.14	0.41	-0.66	0.94
R33	5.55	0.58	4.41	6.69
R34	5.18	0.54	4.12	6.24
R35	8.59	0.07	8.46	8.71
R36	8.59	0.07	8.46	8.71
R37	4.07	0.01	4.04	4.10
R38	2.96	0.01	2.93	2.98

R39	10.78	0.89	9.02	12.53
R40	10.78	0.89	9.02	12.53
R41	1.56	0.05	1.46	1.65
R42	1.56	0.05	1.46	1.65
R43	1.56	0.05	1.46	1.65
R44	1.56	0.05	1.46	1.65
R45	1.56	0.05	1.46	1.65
R46	3.47	0.35	2.77	4.16
R47	4.62	0.34	3.96	5.28
R48	4.51	0.34	3.85	5.17
R49	6.91	0.72	5.50	8.33
R50	9.03	0.91	7.26	10.81
R51	4.50	0.46	3.60	5.39
R52	6.15	0.66	4.86	7.45
R53	0.83	0.08	0.69	0.98
R54	11.72	1.19	9.39	14.05
R55	19.41	1.27	16.92	21.91
R56	1.62	0.15	1.32	1.91
R57	1.86	0.07	1.72	1.99
R58	0.79	0.52	-0.22	1.80
R59	27.55	0.48	26.61	28.50
R60	13.78	0.51	12.79	14.78
R61	40.67	3.69	33.44	47.89
R62	12.11	0.90	10.33	13.88
R63	5.05	0.49	4.09	6.02
R64	6.91	0.72	5.50	8.33
R65	4.51	0.34	3.85	5.17
R66	7.42	0.77	5.91	8.92
R67	0.83	0.08	0.69	0.98
R68	10.29	0.80	8.72	11.85
R69	6.15	0.66	4.86	7.45
R70	5.18	0.54	4.12	6.24
R71	10.78	0.89	9.02	12.53
R72	3.47	0.35	2.77	4.16
R73	4.07	0.01	4.04	4.10
R74	4.62	0.34	3.96	5.28
R75	4.73	0.47	3.81	5.66
R76	4.50	0.46	3.60	5.39
R77	1.56	0.05	1.46	1.65
R78	2.96	0.01	2.93	2.98
R79	5.55	0.58	4.41	6.69
R80	1.62	0.15	1.32	1.91
R81	1.86	0.07	1.72	1.99
R82	1.89	0.06	1.78	2.00

Table A 9: *In vivo* fluxes determined for Δ*eda* in photomixotrophic growth mode. Fluxes, standard deviations, and boundaries for 95 % confidence intervals were obtained from 250 runs of Monte-Carlo simulation. The resulting flux map is shown in Figure 4.24.

Reaction number	Mean flux [%]	Standard deviation [%]	Lower boundary [%]	Upper boundary [%]
R1	100.00	0.00	100.00	100.00
R2	263.28	6.27	250.98	275.58
R3	63.44	1.90	59.71	67.18
R4	-101.88	9.99	-121.45	-82.31
R5	-101.88	9.99	-121.45	-82.31
R6	-192.92	3.11	-199.02	-186.82
R7	-514.87	8.06	-530.66	-499.07
R8	197.95	5.00	188.15	207.76
R9	129.44	4.18	121.24	137.63
R10	1.34	1.62	-1.84	4.52
R11	1.34	1.62	-1.84	4.52
R12	-254.75	4.37	-263.32	-246.18
R13	-109.64	2.63	-114.79	-104.48
R14	-124.39	2.21	-128.73	-120.05
R15	-33.35	10.03	-53.00	-13.70
R16	-131.35	2.18	-135.62	-127.08
R17	0.00	0.00	0.00	0.00
R18	0.00	0.00	0.00	0.00
R19	365.72	5.71	354.54	376.91
R20	91.04	10.12	71.21	110.87
R21	81.19	4.05	73.25	89.13
R22	31.91	2.11	27.78	36.04
R23	31.91	2.11	27.78	36.04
R24	1.69	0.57	0.57	2.81
R25	1.69	0.57	0.57	2.81
R26	1.69	0.57	0.57	2.81
R27	1.69	0.57	0.57	2.81
R28	1.69	0.57	0.57	2.81
R29	0.00	0.00	0.00	0.00
R30	53.35	2.48	48.49	58.21
R31	0.99	1.41	-1.78	3.76
R32	0.62	1.01	-1.36	2.60
R33	6.00	0.36	5.31	6.70
R34	5.55	0.32	4.93	6.17
R35	7.58	0.54	6.53	8.64
R36	7.58	0.54	6.53	8.64
R37	3.62	0.31	3.01	4.23
R38	2.63	0.22	2.19	3.07
R39	10.51	0.36	9.80	11.21
R40	10.51	0.36	9.80	11.21
R41	1.33	0.16	1.02	1.64

R42	1.33	0.16	1.02	1.64
R43	1.33	0.16	1.02	1.64
R44	1.33	0.16	1.02	1.64
R45	1.33	0.16	1.02	1.64
R46	3.68	0.22	3.25	4.12
R47	4.27	0.36	3.57	4.97
R48	4.18	0.35	3.50	4.85
R49	7.32	0.54	6.27	8.37
R50	9.31	0.71	7.91	10.70
R51	4.59	0.39	3.83	5.35
R52	6.38	0.47	5.45	7.31
R53	0.84	0.05	0.73	0.94
R54	12.08	0.89	10.33	13.83
R55	18.38	1.34	15.76	21.00
R56	1.64	0.12	1.40	1.87
R57	1.59	0.17	1.26	1.92
R58	1.36	0.47	0.44	2.29
R59	35.22	1.10	33.07	37.37
R60	11.83	1.35	9.19	14.47
R61	40.38	2.62	35.24	45.53
R62	11.84	0.79	10.29	13.38
R63	5.21	0.45	4.33	6.10
R64	7.32	0.54	6.27	8.37
R65	4.18	0.35	3.50	4.85
R66	7.67	0.64	6.43	8.92
R67	0.84	0.05	0.73	0.94
R68	9.94	0.73	8.51	11.36
R69	6.38	0.47	5.45	7.31
R70	5.55	0.32	4.93	6.17
R71	10.51	0.36	9.80	11.21
R72	3.68	0.22	3.25	4.12
R73	3.62	0.31	3.01	4.23
R74	4.27	0.36	3.57	4.97
R75	4.86	0.41	4.06	5.66
R76	4.59	0.39	3.83	5.35
R77	1.33	0.16	1.02	1.64
R78	2.63	0.22	2.19	3.07
R79	6.00	0.36	5.31	6.70
R80	1.64	0.12	1.40	1.87
R81	1.59	0.17	1.26	1.92
R82	1.79	0.04	1.71	1.87

Table A 10: *In vivo* fluxes determined for Δ*pfkA*/*pfkB* in photomixotrophic growth mode. Fluxes, standard deviations, and boundaries for 95 % confidence intervals were obtained from 250 runs of Monte-Carlo simulation. The resulting flux map is shown in Figure 4.25.

Reaction number	Mean flux [%]	Standard deviation [%]	Lower boundary [%]	Upper boundary [%]
R1	100.00	0.00	100.00	100.00
R2	259.20	8.71	242.12	276.28
R3	67.65	2.25	63.24	72.05
R4	-87.28	11.28	-109.38	-65.17
R5	-87.28	11.28	-109.38	-65.17
R6	-190.06	2.50	-194.95	-185.17
R7	-511.52	5.90	-523.08	-499.96
R8	209.90	3.38	203.28	216.52
R9	135.00	4.84	125.52	144.48
R10	5.07	2.20	0.75	9.38
R11	4.93	2.23	0.57	9.29
R12	-257.68	2.62	-262.81	-252.56
R13	-107.65	1.64	-110.87	-104.44
R14	-124.61	1.33	-127.21	-122.01
R15	-21.83	11.01	-43.40	-0.26
R16	-133.09	1.31	-135.65	-130.53
R17	0.14	0.26	-0.38	0.65
R18	0.14	0.26	-0.38	0.65
R19	370.27	3.58	363.25	377.29
R20	102.78	11.04	81.15	124.42
R21	88.07	5.03	78.21	97.94
R22	35.66	1.70	32.33	38.99
R23	35.66	1.70	32.33	38.99
R24	1.15	0.53	0.10	2.20
R25	1.15	0.53	0.10	2.20
R26	1.15	0.53	0.10	2.20
R27	1.15	0.53	0.10	2.20
R28	1.15	0.53	0.10	2.20
R29	0.00	0.00	0.00	0.00
R30	57.93	2.36	53.30	62.56
R31	0.02	0.16	-0.30	0.33
R32	0.00	0.04	-0.08	0.09
R33	5.78	0.70	4.40	7.15
R34	5.49	0.63	4.25	6.73
R35	8.48	0.16	8.17	8.80
R36	8.48	0.16	8.17	8.80
R37	4.03	0.07	3.90	4.15
R38	2.93	0.04	2.84	3.01
R39	10.33	1.23	7.92	12.74
R40	10.33	1.23	7.92	12.74
R41	1.53	0.09	1.36	1.71

R42	1.53	0.09	1.36	1.71
R43	1.53	0.09	1.36	1.71
R44	1.53	0.09	1.36	1.71
R45	1.53	0.09	1.36	1.71
R46	3.66	0.41	2.85	4.46
R47	4.96	0.28	4.41	5.51
R48	4.88	0.27	4.34	5.41
R49	7.23	0.96	5.36	9.10
R50	9.53	1.18	7.21	11.85
R51	4.74	0.60	3.56	5.93
R52	6.43	0.81	4.84	8.02
R53	0.86	0.10	0.68	1.05
R54	12.27	1.52	9.29	15.25
R55	21.16	1.01	19.18	23.14
R56	1.69	0.20	1.29	2.09
R57	1.83	0.11	1.62	2.04
R58	1.03	0.60	-0.14	2.19
R59	27.29	0.37	26.57	28.00
R60	13.59	0.68	12.26	14.92
R61	42.10	3.68	34.89	49.31
R62	13.36	0.64	12.10	14.61
R63	5.32	0.68	4.00	6.65
R64	7.23	0.96	5.36	9.10
R65	4.88	0.27	4.34	5.41
R66	7.84	0.99	5.89	9.78
R67	0.86	0.10	0.68	1.05
R68	11.32	0.52	10.31	12.33
R69	6.43	0.81	4.84	8.02
R70	5.49	0.63	4.25	6.73
R71	10.33	1.23	7.92	12.74
R72	3.66	0.41	2.85	4.46
R73	4.03	0.07	3.90	4.15
R74	4.96	0.28	4.41	5.51
R75	4.97	0.63	3.74	6.21
R76	4.74	0.60	3.56	5.93
R77	1.53	0.09	1.36	1.71
R78	2.93	0.04	2.84	3.01
R79	5.78	0.70	4.40	7.15
R80	1.69	0.20	1.29	2.09
R81	1.83	0.11	1.62	2.04
R82	1.88	0.04	1.80	1.96

Table A 11: *In vivo* fluxes determined for Δ*xfp1*/*xfp2* in photomixotrophic growth mode. Fluxes, standard deviations, and boundaries for 95 % confidence intervals were obtained from 250 runs of Monte-Carlo simulation. The resulting flux map is shown in Figure 4.26

Reaction number	Mean flux [%]	Standard deviation [%]	Lower boundary [%]	Upper boundary [%]
R1	100.00	0.00	100.00	100.00
R2	255.85	6.76	242.59	269.11
R3	68.01	2.10	63.90	72.13
R4	-91.14	4.55	-100.05	-82.22
R5	-91.14	4.55	-100.05	-82.22
R6	-193.96	2.80	-199.46	-188.47
R7	-520.23	7.15	-534.24	-506.21
R8	216.55	2.17	212.29	220.81
R9	143.95	2.04	139.95	147.95
R10	5.35	2.08	1.27	9.43
R11	4.68	2.17	0.42	8.93
R12	-261.98	3.68	-269.18	-254.77
R13	-110.84	2.00	-114.76	-106.92
R14	-127.48	1.96	-131.33	-123.64
R15	-24.66	4.37	-33.22	-16.10
R16	-134.49	1.77	-137.97	-131.02
R17	0.67	0.58	-0.46	1.81
R18	0.67	0.58	-0.46	1.81
R19	377.49	4.57	368.54	386.44
R20	102.83	4.54	93.94	111.72
R21	93.27	1.29	90.75	95.79
R22	37.92	0.85	36.26	39.58
R23	37.92	0.85	36.26	39.58
R24	3.39	0.59	2.22	4.55
R25	3.39	0.59	2.22	4.55
R26	3.38	0.59	2.22	4.55
R27	3.39	0.59	2.22	4.55
R28	3.39	0.59	2.22	4.55
R29	0.00	0.00	0.00	0.00
R30	58.59	1.55	55.54	61.63
R31	0.00	0.00	0.00	0.00
R32	0.00	0.00	0.00	0.00
R33	6.48	0.28	5.94	7.02
R34	6.03	0.22	5.60	6.46
R35	7.01	0.67	5.69	8.33
R36	7.01	0.67	5.69	8.33
R37	3.18	0.40	2.40	3.96
R38	2.31	0.28	1.76	2.86
R39	11.17	0.10	10.97	11.37
R40	11.17	0.10	10.97	11.37
R41	1.52	0.01	1.50	1.53

R42	1.52	0.01	1.50	1.53
R43	1.52	0.01	1.50	1.53
R44	1.52	0.01	1.50	1.53
R45	1.52	0.01	1.50	1.53
R46	4.00	0.16	3.70	4.31
R47	4.97	0.13	4.71	5.22
R48	4.89	0.09	4.70	5.07
R49	7.54	0.81	5.95	9.12
R50	9.38	0.88	7.66	11.10
R51	4.64	0.45	3.75	5.53
R52	6.14	0.61	4.95	7.34
R53	0.82	0.07	0.69	0.95
R54	11.64	1.06	9.56	13.72
R55	21.17	0.40	20.38	21.96
R56	1.64	0.15	1.36	1.93
R57	1.79	0.07	1.65	1.94
R58	0.87	0.55	-0.21	1.95
R59	26.64	0.27	26.10	27.17
R60	13.34	0.45	12.45	14.22
R61	44.18	0.74	42.74	45.63
R62	13.36	0.24	12.89	13.84
R63	5.05	0.50	4.06	6.03
R64	7.54	0.81	5.95	9.12
R65	4.89	0.09	4.70	5.07
R66	7.74	0.78	6.20	9.27
R67	0.82	0.07	0.69	0.95
R68	11.32	0.23	10.87	11.76
R69	6.14	0.61	4.95	7.34
R70	6.03	0.22	5.60	6.46
R71	11.17	0.10	10.97	11.37
R72	4.00	0.16	3.70	4.31
R73	3.18	0.40	2.40	3.96
R74	4.97	0.13	4.71	5.22
R75	4.68	0.45	3.79	5.57
R76	4.64	0.45	3.75	5.53
R77	1.52	0.01	1.50	1.53
R78	2.31	0.28	1.76	2.86
R79	6.48	0.28	5.94	7.02
R80	1.64	0.15	1.36	1.93
R81	1.79	0.07	1.65	1.94
R82	1.84	0.07	1.70	1.98

Table A 12: Measured and simulated ^{13}C labelling data for the estimation of *in vivo* fluxes for heterotrophic growth of *Synechocystis* sp. PCC 6803 with three parallel tracer experiments, as shown in Figure 4.29.

Fragment	[1-^{13}C]		[6-^{13}C]		50 % (N/N) [$^{13}C_6$]	
	Meas.	Sim.	Meas.	Sim.	Meas.	Sim.
ala_260	0.690	0.703	0.198	0.188	0.357	0.333
	0.213	0.205	0.599	0.611	0.168	0.165
	0.081	0.077	0.147	0.145	0.152	0.165
	0.016	0.014	0.056	0.056	0.323	0.337
ala232	0.757	0.734	0.219	0.213	0.419	0.389
	0.172	0.193	0.637	0.645	0.144	0.171
	0.071	0.073	0.144	0.143	0.437	0.439
gly_246	0.739	0.749	0.745	0.743	0.406	0.367
	0.187	0.179	0.179	0.184	0.215	0.210
	0.075	0.072	0.076	0.073	0.379	0.424
gly_218	0.826	0.823	0.822	0.821	0.475	0.456
	0.174	0.177	0.178	0.179	0.525	0.544
val_288	0.636	0.656	0.056	0.048	0.161	0.141
	0.247	0.236	0.295	0.293	0.115	0.105
	0.091	0.086	0.473	0.483	0.228	0.228
	0.021	0.018	0.125	0.125	0.223	0.230
	0.004	0.003	0.043	0.044	0.125	0.135
	0.001	0.000	0.007	0.007	0.147	0.161
val_260	0.721	0.677	0.058	0.052	0.193	0.163
	0.190	0.224	0.302	0.305	0.092	0.112
	0.074	0.080	0.476	0.484	0.381	0.364
	0.013	0.016	0.122	0.118	0.128	0.154
	0.002	0.003	0.042	0.041	0.206	0.207
leu_274	0.720	0.648	0.022	0.019	0.101	0.080
	0.190	0.243	0.137	0.142	0.135	0.135
	0.075	0.086	0.356	0.368	0.236	0.233
	0.012	0.019	0.362	0.353	0.244	0.253
	0.002	0.003	0.093	0.090	0.164	0.177
	0.000	0.000	0.030	0.029	0.119	0.122
ser_390	0.601	0.612	0.181	0.164	0.317	0.307
	0.253	0.247	0.543	0.555	0.198	0.184
	0.115	0.112	0.192	0.196	0.171	0.153
	0.030	0.029	0.084	0.085	0.314	0.356
ser362	0.664	0.645	0.202	0.192	0.366	0.360
	0.229	0.245	0.595	0.603	0.203	0.201
	0.106	0.110	0.203	0.205	0.431	0.439
thr_404	0.560	0.567	0.164	0.154	0.269	0.241
	0.273	0.271	0.528	0.529	0.190	0.183
	0.122	0.120	0.201	0.206	0.144	0.143
	0.036	0.034	0.086	0.088	0.275	0.299
	0.009	0.008	0.021	0.022	0.123	0.134

phe_336	0.549	0.577	0.013	0.009	0.048	0.032
	0.289	0.282	0.088	0.093	0.066	0.054
	0.113	0.106	0.303	0.314	0.093	0.083
	0.031	0.028	0.400	0.400	0.148	0.139
	0.007	0.006	0.124	0.132	0.151	0.153
	0.003	0.001	0.044	0.042	0.151	0.156
	0.001	0.000	0.010	0.008	0.145	0.156
	0.001	0.000	0.006	0.001	0.093	0.107
	0.003	0.000	0.009	0.000	0.064	0.072
	0.002	0.000	0.005	0.000	0.041	0.049
asp_418	0.556	0.565	0.163	0.154	0.268	0.241
	0.275	0.270	0.524	0.528	0.191	0.183
	0.124	0.121	0.203	0.206	0.145	0.144
	0.036	0.035	0.088	0.089	0.273	0.299
	0.009	0.008	0.021	0.022	0.122	0.134
glut_432	0.523	0.541	0.049	0.043	0.132	0.118
	0.292	0.283	0.262	0.257	0.125	0.114
	0.133	0.127	0.433	0.439	0.291	0.294
	0.041	0.038	0.169	0.173	0.190	0.192
	0.010	0.009	0.069	0.070	0.185	0.199
	0.002	0.002	0.017	0.017	0.077	0.082
glcn_319	0.584	0.616	0.116	0.137	0.205	0.183
	0.247	0.241	0.581	0.557	0.227	0.220
	0.125	0.109	0.195	0.199	0.131	0.141
	0.034	0.027	0.089	0.087	0.209	0.214
	0.010	0.006	0.020	0.020	0.228	0.242
glc_319	0.585	0.625	0.112	0.116	0.237	0.215
	0.258	0.235	0.562	0.577	0.215	0.205
	0.120	0.108	0.207	0.199	0.125	0.129
	0.031	0.026	0.098	0.089	0.182	0.185
	0.007	0.006	0.021	0.020	0.240	0.267
rib_307	0.648	0.651	0.160	0.160	0.343	0.325
	0.226	0.221	0.586	0.585	0.162	0.168
	0.103	0.104	0.173	0.174	0.156	0.142
	0.024	0.024	0.080	0.081	0.339	0.365

Table A 13: Measured and simulated ^{13}C labelling data for the estimation of *in vivo* fluxes for heterotrophic growth of Δ*eda* with three parallel tracer experiments, as shown in Figure 4.32.

Fragment	[1-1^{3}C]		[6-^{13}C]		50 % (N/N) [$^{13}C_{6]}$	
	Meas.	Sim.	Meas.	Sim.	Meas.	Sim.
ala_260	0.699	0.703	0.164	0.188	0.379	0.333
	0.207	0.205	0.627	0.611	0.154	0.165
	0.079	0.077	0.150	0.145	0.130	0.165
	0.016	0.014	0.059	0.056	0.337	0.337
ala232	0.726	0.734	0.180	0.213	0.411	0.389
	0.197	0.193	0.671	0.645	0.166	0.171
	0.077	0.073	0.149	0.143	0.423	0.439
gly_246	0.737	0.749	0.748	0.743	0.420	0.367
	0.187	0.179	0.178	0.184	0.192	0.210
	0.076	0.072	0.074	0.073	0.388	0.424
gly_218	0.820	0.823	0.822	0.821	0.483	0.456
	0.180	0.177	0.178	0.179	0.517	0.544
val_288	0.652	0.656	0.049	0.048	0.181	0.141
	0.235	0.236	0.244	0.293	0.105	0.105
	0.087	0.086	0.519	0.483	0.225	0.228
	0.020	0.018	0.132	0.125	0.222	0.230
	0.004	0.003	0.048	0.044	0.111	0.135
	0.001	0.000	0.008	0.007	0.154	0.161
val_260	0.659	0.677	0.050	0.052	0.189	0.163
	0.229	0.224	0.249	0.305	0.111	0.112
	0.086	0.080	0.523	0.484	0.362	0.364
	0.020	0.016	0.131	0.118	0.144	0.154
	0.006	0.003	0.047	0.041	0.194	0.207
leu_274	0.634	0.648	0.025	0.019	0.104	0.080
	0.244	0.243	0.097	0.142	0.141	0.135
	0.090	0.086	0.313	0.368	0.237	0.233
	0.024	0.019	0.424	0.353	0.242	0.253
	0.006	0.003	0.104	0.090	0.164	0.177
	0.003	0.000	0.036	0.029	0.112	0.122
ser_390	0.609	0.612	0.158	0.164	0.325	0.307
	0.248	0.247	0.559	0.555	0.193	0.184
	0.113	0.112	0.196	0.196	0.162	0.153
	0.030	0.029	0.087	0.085	0.320	0.356
ser362	0.638	0.645	0.174	0.192	0.353	0.360
	0.247	0.245	0.617	0.603	0.233	0.201
	0.115	0.110	0.209	0.205	0.415	0.439
thr_404	0.566	0.567	0.140	0.154	0.271	0.241
	0.269	0.271	0.543	0.529	0.192	0.183
	0.121	0.120	0.205	0.206	0.131	0.143
	0.035	0.034	0.090	0.088	0.271	0.299
	0.009	0.008	0.022	0.022	0.134	0.134

phe_336	0.544	0.577	0.020	0.009	0.058	0.032
	0.267	0.282	0.065	0.093	0.069	0.054
	0.115	0.106	0.256	0.314	0.091	0.083
	0.033	0.028	0.449	0.400	0.148	0.139
	0.010	0.006	0.134	0.132	0.144	0.153
	0.009	0.001	0.051	0.042	0.144	0.156
	0.005	0.000	0.011	0.008	0.142	0.156
	0.007	0.000	0.005	0.001	0.091	0.107
	0.005	0.000	0.005	0.000	0.066	0.072
	0.004	0.000	0.004	0.000	0.047	0.049
asp_418	0.565	0.565	0.135	0.154	0.268	0.241
	0.269	0.270	0.544	0.528	0.194	0.183
	0.122	0.121	0.207	0.206	0.133	0.144
	0.035	0.035	0.092	0.089	0.271	0.299
	0.009	0.008	0.022	0.022	0.135	0.134
glut_432	0.539	0.541	0.040	0.043	0.135	0.118
	0.282	0.283	0.215	0.257	0.121	0.114
	0.127	0.127	0.470	0.439	0.286	0.294
	0.039	0.038	0.180	0.173	0.190	0.192
	0.010	0.009	0.076	0.070	0.184	0.199
	0.003	0.002	0.019	0.017	0.084	0.082
glcn_319	0.605	0.616	0.091	0.137	0.219	0.183
	0.248	0.241	0.604	0.557	0.228	0.220
	0.112	0.109	0.195	0.199	0.115	0.141
	0.029	0.027	0.091	0.087	0.202	0.214
	0.007	0.006	0.020	0.020	0.235	0.242
glc_319	0.586	0.625	0.080	0.116	0.250	0.215
	0.256	0.235	0.587	0.577	0.209	0.205
	0.121	0.108	0.210	0.199	0.106	0.129
	0.031	0.026	0.102	0.089	0.173	0.185
	0.007	0.006	0.022	0.020	0.262	0.267
rib_307	0.653	0.651	0.130	0.160	0.367	0.325
	0.224	0.221	0.609	0.585	0.148	0.168
	0.101	0.104	0.177	0.174	0.124	0.142
	0.023	0.024	0.083	0.081	0.361	0.365

Table 9: *In vivo* fluxes determined for *Synechocystis* sp. PCC 6803 in heterotrophic growth mode. Fluxes, standard deviations, and boundaries for 95 % confidence intervals were obtained from 250 runs of Monte-Carlo simulation. The resulting flux map is shown in Figure 4.30.

Reaction number	Mean flux [%]	Standard deviation [%]	Lower boundary [%]	Upper boundary [%]
R1	100.00	0.00	100.00	100.00
R2	413.20	6.07	413.15	413.25
R3	-286.45	8.20	-286.52	-286.39
R4	-33.05	2.71	-33.07	-33.03
R5	-33.05	2.71	-33.07	-33.03
R6	-34.16	2.72	-34.18	-34.13
R7	59.20	2.71	59.18	59.23
R8	54.08	2.67	54.06	54.10
R9	17.81	11.66	17.71	17.90
R10	384.64	8.20	384.57	384.70
R11	384.48	8.21	384.41	384.54
R12	253.62	5.52	253.58	253.67
R13	130.85	2.71	130.83	130.88
R14	127.25	2.78	127.23	127.28
R15	127.25	2.78	127.23	127.28
R16	126.17	2.78	126.14	126.19
R17	0.16	0.26	0.16	0.16
R18	0.16	0.26	0.16	0.16
R19	0.00	0.00	0.00	0.00
R20	0.00	0.00	0.00	0.00
R21	29.28	2.51	29.26	29.30
R22	3.83	0.24	3.83	3.83
R23	3.83	0.24	3.83	3.83
R24	0.01	0.02	0.01	0.01
R25	0.01	0.02	0.01	0.01
R26	0.01	0.02	0.01	0.01
R27	0.01	0.02	0.01	0.01
R28	-22.20	11.56	-22.29	-22.11
R29	22.21	11.56	22.12	22.30
R30	34.07	11.59	33.98	34.16
R31	0.21	0.51	0.20	0.21
R32	0.01	0.02	0.01	0.01
R33	1.29	0.13	1.28	1.29
R34	1.09	0.11	1.09	1.09
R35	1.10	0.07	1.10	1.10
R36	1.10	0.07	1.10	1.10
R37	0.56	0.06	0.56	0.56
R38	0.37	0.04	0.37	0.37
R39	1.99	0.19	1.98	1.99

R40	1.99	0.19	1.98	1.99
R41	0.17	0.02	0.17	0.17
R42	0.17	0.02	0.17	0.17
R43	0.17	0.02	0.17	0.17
R44	0.17	0.02	0.17	0.17
R45	0.17	0.02	0.17	0.17
R46	0.68	0.07	0.68	0.68
R47	1.03	0.10	1.03	1.03
R48	0.66	0.07	0.66	0.66
R49	2.46	0.25	2.46	2.47
R50	5.22	0.51	5.21	5.22
R51	1.05	0.11	1.05	1.06
R52	3.49	0.32	3.48	3.49
R53	0.00	0.00	0.00	0.00
R54	4.95	0.35	4.95	4.96
R55	3.83	0.24	3.82	3.83
R56	0.00	0.00	0.00	0.00
R57	0.00	0.00	0.00	0.00
R58	1.14	0.41	1.13	1.14
R59	1.82	0.18	1.82	1.82
R60	3.43	0.34	3.43	3.43
R61	23.68	2.47	23.66	23.70
R62	0.00	0.00	0.00	0.00
R63	1.70	0.16	1.69	1.70
R64	2.46	0.25	2.46	2.47
R65	0.66	0.07	0.66	0.66
R66	5.22	0.51	5.21	5.22
R67	0.00	0.00	0.00	0.00
R68	2.14	0.21	2.14	2.14
R69	3.49	0.32	3.48	3.49
R70	1.09	0.11	1.09	1.09
R71	1.99	0.19	1.98	1.99
R72	0.68	0.07	0.68	0.68
R73	0.56	0.06	0.56	0.56
R74	1.03	0.10	1.03	1.03
R75	1.47	0.14	1.47	1.47
R76	1.05	0.11	1.05	1.06
R77	0.17	0.02	0.17	0.17
R78	0.37	0.04	0.37	0.37
R79	1.29	0.13	1.28	1.29
R80	0.00	0.00	0.00	0.00
R81	0.00	0.00	0.00	0.00
R82	2.35	0.25	2.35	2.35

Table 10: *In vivo* fluxes determined for Δ*eda* in heterotrophic growth mode. Fluxes, standard deviations, and boundaries for 95 % confidence intervals were obtained from 250 runs of Monte-Carlo simulation. The resulting flux map is shown in Figure 4.33.

Reaction number	Mean flux [%]	Standard deviation [%]	Lower boundary [%]	Upper boundary [%]
R1	100.00	0.00	100.00	100.00
R2	445.86	4.47	445.82	445.89
R3	-322.32	4.91	-322.36	-322.28
R4	-44.11	1.57	-44.12	-44.09
R5	-44.11	1.57	-44.12	-44.09
R6	-45.01	1.54	-45.02	-44.99
R7	49.58	1.37	49.57	49.59
R8	45.44	1.25	45.43	45.45
R9	20.62	9.67	20.55	20.70
R10	420.85	4.96	420.81	420.89
R11	420.85	4.96	420.81	420.89
R12	278.34	3.41	278.31	278.37
R13	142.51	1.55	142.50	142.52
R14	139.55	1.66	139.54	139.57
R15	139.55	1.66	139.54	139.57
R16	138.69	1.72	138.68	138.71
R17	0.00	0.00	0.00	0.00
R18	0.00	0.00	0.00	0.00
R19	0.00	0.00	0.00	0.00
R20	0.00	0.00	0.00	0.00
R21	24.87	0.74	24.87	24.88
R22	3.46	0.40	3.46	3.46
R23	3.46	0.40	3.46	3.46
R24	0.30	0.40	0.30	0.30
R25	0.30	0.40	0.30	0.30
R26	0.30	0.40	0.30	0.30
R27	0.30	0.40	0.30	0.30
R28	-12.94	9.68	-13.02	-12.86
R29	13.24	9.74	13.16	13.32
R30	23.02	9.74	22.94	23.10
R31	0.09	0.19	0.09	0.09
R32	0.04	0.08	0.04	0.04
R33	1.06	0.04	1.06	1.06
R34	0.90	0.03	0.90	0.90
R35	0.90	0.03	0.90	0.90
R36	0.90	0.03	0.90	0.90
R37	0.46	0.02	0.45	0.46
R38	0.30	0.01	0.30	0.30
R39	1.65	0.05	1.65	1.65
R40	1.65	0.05	1.65	1.65

R41	0.14	0.00	0.14	0.14
R42	0.14	0.00	0.14	0.14
R43	0.14	0.00	0.14	0.14
R44	0.14	0.00	0.14	0.14
R45	0.14	0.00	0.14	0.14
R46	0.55	0.02	0.55	0.55
R47	0.83	0.03	0.83	0.83
R48	0.55	0.02	0.55	0.55
R49	2.03	0.07	2.03	2.04
R50	4.31	0.15	4.31	4.31
R51	0.86	0.03	0.86	0.86
R52	2.80	0.09	2.80	2.80
R53	0.00	0.00	0.00	0.00
R54	4.00	0.14	4.00	4.00
R55	3.16	0.09	3.16	3.16
R56	0.00	0.00	0.00	0.00
R57	0.00	0.00	0.00	0.00
R58	1.01	0.09	1.01	1.01
R59	1.47	0.08	1.47	1.47
R60	2.81	0.14	2.81	2.81
R61	19.89	0.42	19.89	19.90
R62	0.00	0.00	0.00	0.00
R63	1.37	0.01	1.37	1.37
R64	2.03	0.07	2.03	2.04
R65	0.55	0.02	0.55	0.55
R66	4.31	0.15	4.31	4.31
R67	0.00	0.00	0.00	0.00
R68	1.78	0.05	1.78	1.78
R69	2.80	0.09	2.80	2.80
R70	0.90	0.03	0.90	0.90
R71	1.65	0.05	1.65	1.65
R72	0.55	0.02	0.55	0.55
R73	0.46	0.02	0.45	0.46
R74	0.83	0.03	0.83	0.83
R75	1.20	0.05	1.20	1.20
R76	0.86	0.03	0.86	0.86
R77	0.14	0.00	0.14	0.14
R78	0.30	0.01	0.30	0.30
R79	1.06	0.04	1.06	1.06
R80	0.00	0.00	0.00	0.00
R81	0.00	0.00	0.00	0.00
R82	1.79	0.01	1.79	1.79